Fuel Composition and Performance Analysis of Endothermically Heated Fuels for Pulse Detonation Engines

Thesis

Christopher A Stevens, Contractor, USAF

AFIT/GAE/ENY/09-M21

DEPARTMENT OF THE AIR FORCE
AIR UNIVERSITY

AIR FORCE INSTITUTE OF TECHNOLOGY

Wright-Patterson Air Force Base, Ohio

APPROVED FOR PUBLIC RELEASE DISTRIBUTION UNLIMITED

The views expressed in this thesis are those of the author and do not reflect the official policy or position of the United States Air Force, Department of Defense, or the United States Government.

AFIT/GAE/ENY/09-M21

FUEL COMPOSITION AND PERFORMANCE ANALYSIS OF ENDOTHERMICALLY HEATED FUELS FOR PULSE DETONATION ENGINES

THESIS

Presented to the Faculty

Department of Aeronautics and Astronautics

Graduate School of Engineering and Management

Air Force Institute of Technology

Air University

Air Education and Training Command

In Partial Fulfillment of the Requirements for the

Degree of Master of Science in Aeronautical Engineering

Christopher A Stevens, B.S.

Contractor, USAF

March 2009

APPROVED FOR PUBLIC RELEASE; DISTRIBUTION UNLIMITED

AFIT/GAE/ENY/06-M21

FUEL COMPOSITION AND PERFORMANCE ANALYSIS OF ENDOTHERMICALLY HEATED FUELS FOR PULSE DETONATION ENGINES

Christopher A Stevens, B.S.
Contractor, USAF

Approved:

_____/SIGNED/_____	20 Mar 2009__
Paul I. King (Chairman)	Date
_____/SIGNED/_____	20 Mar 2009__
Richard D. Branam, LtCol, Usaf (Member)	Date
_____/SIGNED/_____	20 Mar 2009__
Mark F. Reeder (Member)	Date

Abstract

Waste heat from a pulse detonation engine (PDE) was extracted via concentric, counter flow heat exchangers to produce supercritical pyrolytic conditions for JP-7 and JP-8 fuels. A sampling system and method was utilized to collect samples of reacted fuel to be extracted during steady state operation. Samples were collected over a range of heat exchanger exit temperatures from 820 K (1016 °F) to 940 K (1232 °F) and for two sets of heat exchangers, one set coated with zeolite catalyst and one set left uncoated. Variation in fuel mass flow rate required the calculation of heat addition as an alternate to heat exchanger exit temperature as the independent variable when comparing fuel decomposition and engine performance. Offline chemical analysis of liquid and vapor portions of each sample indicated fuel decomposition via pyrolytic pathways. The analyses showed the formation of hydrogen, unsaturated hydrocarbons (aromatics and alkenes), and smaller alkanes in both fuels. The high thermal stability and low aromatic content of neat JP-7 resulted in the formation of more gaseous products and fewer poly-aromatic compounds than was produced by JP-8. The additional concentrations of lighter hydrocarbons reduced the ignition times by an average of 15.6%, and the reduced poly-aromatic concentrations decreased the bulk carbon deposits formed during pyrolysis by 92.5% on average.

Acknowledgements

I would like to thank my thesis advisor, Dr. Paul King for the opportunity to perform this rewarding work, and for the constant support, and innumerable hours of advice. Thank you also to my committee members, LtCol Richard Branam and Dr Mark Reeder for helping me refine the presentation of my work.

It was a privilege to work with Dr. Fred Schauer who offered me the opportunity to work in the Pulsed Detonation Research Facility. I am grateful for you ongoing support of my work. I would also like to thank Dr. John Hoke who was instrumental in making sure that I had the knowledge and oversight necessary to conduct safe and accurate experiments in the lab. I also want to thank Curt Rice and Capt. Jon Gilbert who were a big help in the setup and execution of my experiments. I would also like to thank Dave Baker and Dwight Fox for their excellent workmanship.

The guidance of Dr. Matt Dewitt was instrumental in the completion of the chemical analyses that are the key to this research. His teaching allowed me to understand the chemical mechanisms of pyrolysis and to analyze gaseous samples on my own. Thank you also to Linda Shafer for the time and expertise needed to analyze the liquid samples.

Finally I would like to thank my parents and sister for their perpetual support and understanding, and for allowing me to live under their roof while working my way through school.

Table of Contents

List of Figures

Page

List of Tables

Page

List of Symbols

Acronyms

AFIT	= Air Force Institute of Techology
AFRL	= Air Force Research Laboratory
FF	= Fill fraction
FID	= Flame ionization detector
FN	= Flow number
GC	= Gas chromatograph
GC-MS	= Gas chromatograph/mass spectrometry
HLPC	= High performance liquid chromatography
NPT	= National pipe thread
PAH	= Polycyclic aromatic hydrocarbon
PDE	= Pulse detonation engine
PF	= Purge fraction
SI	= International system of units
TCD	= Thermal conductivity detector
USAF	= United States Air Force

Symbols – [] denotes SI units and {} denotes English units

A	= area [m^2] {ft^2}
B	= bias limit
C_p	= constant pressure specific heat [J/(kg*K)] {BTU/(lbm*°R)}
D	= diameter [m] {ft}
E	= energy [J} {Btu}
freq	= frequency [Hz]
h	= specific enthalpy [J/g] {BTU/lbm}
H	= enthalpy [J/g] {BTU/lbm}
L	= length [m] {ft}
m_dot	= mass flow rate [g/s] {lbm/s}
M	= Mach number
n	= moles
N	= number of individual readings
n_c	= number of carbon atoms
P	= pressure [atm] {psi}
P_s	= precision limit
q_dot	= specific heat transfer rate [W/(g*s)] {BTU/(lbm*s)}
Q_dot	= heat transfer rate
R	= universal gas constant [J/(mol*K)] {(ft^3*psi*lbm)/mol*°R}
S_x	= sample standard deviation
T	= temperature [K] {°F}
t	= time [s]
u	= velocity [m/s] {ft/s}
U	= uncertainty
V	= volume [m^3] {ft^3}

X = measured variable of interest

Symbols (continued) – [] denotes SI units and {} denotes English units

X_bar = sample mean
Y = mass fraction
# = number of

Greek Symbols – [] denotes SI units and {} denotes English units

χ = mole fraction
λ = cell size [mm] {in}
ρ = density [g/ml] {lbm/ft^3}
ϕ = equivalence ratio

Subscripts

ex = exit
fuel = fuel
gas = gas
i = individual
in = inlet
initiation = initiation
L-G = liquid-to-gas
liq = liquid
sam = sample
tube = tube

FUEL COMPOSITION AND PERFORMANCE ANALYSIS OF ENDOTHERMICALLY HEATED FUELS FOR PULSE DETONATION ENGINES

I. Introduction

Motivation

As Pulse Detonation Engines PDE technology continues to mature, there is a need to be able to operate these engines on fuels that have high energy density and are relatively safe to handle. The United States Air Force uses JP-8 as the predominant fuel in aircraft. It has both a high energy density (42.8 MJ/L) and a high flash point (38 °C). It is also a liquid fuel that does not need to be stored under pressure or refrigeration. For these reasons JP-8 is an attractive fuel for PDE's. However, JP-8 is a poor fuel choice for PDE's when compared with hydrogen or ethylene. Both of these gasses have lower ignition times resulting in better performance during the initiation of the detonations that drive a PDE.

One method to improve the performance of JP-8 or other hydrocarbon fuels is to alter the chemistry of the fuel via endothermic reactions (Edwards, 2003:1098-1104). In these reactions, the high molecular weight compounds that make up liquid hydrocarbon fuels break down into lighter hydrocarbons, hydrogen, and carbon. Recent work with JP-8 has shown that a 30% reduction in ignition time can be achieved when the fuel is heated endothermically (Nagley, 2008, 75-80).

While the performance improvements for JP-8 have been characterized, it is not known whether other fuels such as JP-7 will perform any better. It would be a great advantage to know the properties of a raw or "neat" fuel that produce the best results after heating. Also, an expensive catalytic coating was applied to the heat exchangers used to

heat the fuel in the JP-8 experiments. It is unknown what effect the coating had on the endothermic reactions in the fuel. The elimination of such a coating would reduce the cost of the fuel heating system if it is not necessary.

Problem Statement

When liquid hydrocarbon fuels are heated to an adequate temperature, known as the endothermic limit, chemical reactions begin to break down the fuel (Helfrich, 2007:3). These endothermic reactions are known as cracking (Huang 2002:2). During cracking, high molecular weight compounds thermally decompose into lower molecular weight aromatics, alkenes, and alkanes (Edwards, 2006:4,5). These lighter molecular weight hydrocarbons are shown to have lower initiation energy and there are substantial benefits in PDE performance (Schauer, 2005:2), (Nagley 2008:81). It is not known what effects initial fuel composition has on the endothermic breakdown and PDE performance or how much influence the presence of a catalyst has on the reactions.

This research will expand upon the previous work of investigating the break down and performance improvements measured in endothermically heated JP-8 by investigating the performance of a high thermal stability fuel (JP-7). Also the effect of the catalyst coating used to promote endothermic reaction of the fuel will be quantified by constructing a physically identical set of heat exchangers which lack the catalyst coating. As in the past the final fuel composition and ignition times will be the measurements by which performance is judged.

Research Objectives

The foremost goal of this research is to produce two comparisons. The first is a comparison between a petroleum distillate fuel (JP-8) and a high thermal stability fuel (JP-7). The change in chemical makeup of the fuels will determine what fuel properties favor the production of chemical species that improve PDE performance. The analyses of collected samples of stressed fuel will show if there is any benefit to the use of high thermal stability fuels in PDE's with endothermic fuel heating systems.

The second primary goal of this research is to quantify the effect of the proprietary zeolite catalyst coating used in previous experiments with JP-8. To quantify the effects of the coating, a second pair of heat exchanger tubes needs to be constructed. While identical in physical dimension and construction to the original heat exchangers, the new heat exchangers lack the zeolite coating. By repeating the endothermic experiments conducted with the zeolite coated heat exchangers and collecting new samples of the stressed fuel, the effect of the coating can be quantified.

An opportunity arose while working on this research to explore the use of a fuel seeded catalyst. The palladium catalyst was intended to enhance the performance of PDE's without the need to heat the fuel past the endothermic threshold. The seeded catalyst experiment utilized JP-4 as the carrier for the catalyst. In order to activate the catalyst the fuel temperature must be raised to at least 360 °C (680 °F). This is accomplished by flowing the fuel through one of the two thrust tube heat exchangers. If the catalyst can produce significant performance improvements it will have several benefits over endothermic heating including reduced heat loads and the elimination of carbon deposits.

Units

The PDE community uses both the International System of units (SI) and the English system. Both sets of units are presented where practical, and where it would not be practical, only the SI units are listed.

Organization

Chapter I introduces the motivation and focus of this research. It includes the problem statement defining the research and the goals that are to be achieved. Chapter II presents the background and theory necessary to explore both the operation and performance of a PDE as well as the endothermic reactions that the fuel endures during heating. The Pulse Detonation Research Facility (PDRF), the research engine, and the specialized apparatus needed to heat the fuel and collect samples is discussed in Chapter III. Also the test procedures and collection methods are described. In Chapter IV, the methods used to collect and analyze PDE engine data are explained along with the equipment and methods used to analyze the gas and liquid samples collected during testing. Chapter V lists the results of the chemical and performance analyses and discusses the findings. Finally, Chapter VI draws conclusions from the results, and makes recommendations for the next step in the study of endothermic fuel heating for PDE's.

II. Background and Theory

Overview

In order to effectively study how endothermically reacted fuels affect the operation of a pulse detonation engine it is important to understand the theory behind detonation. It is also necessary to be familiar with the effects that fuel composition has on detonation, and to understand how initial fuel composition influences the products of endothermic reactions. This chapter introduces the theory that governs the operation of PDE coupled with an endothermic fuel heating system. The chapter is broken into sections that describe the process of how a detonation forms and propagates within a PDE and the chemical processes that occur when fuel is heated above the endothermic threshold.

The development of a detonation, the structure of an ongoing detonation, and the operating cycle of a PDE are all important pieces in understanding the performance of a PDE. Because, the initiation energies of fuel/air mixtures is on the order of 10^5 J (94.8 Btu) (Schauer 2005:1), a detonation cannot be directly initiated by the spark ignition system employed by the research PDE. Instead the spark is used to initiate a deflagration which then transitions to a detonation through the used of a deflagration to detonation transition (DDT) device. By reducing the time required to complete this ignition and transition process, the cycle frequency of the engine can be increased raising the thrust of the engine.

In order to predict the possible improvements in performance that can be gained by endothermic heating, it is necessary to understand the chemical reaction pathways that the fuel follows during pyrolysis. To that end the chemical pathways are explained in this

chapter as well as the expected changes to hydrocarbon fuels that follow these pathways. It is also necessary to understand the composition of the different raw fuels (JP-4, JP-7, and JP-8) that were used in experiments. By looking at the composition of the neat fuels, and specifically the differences between them, it is possible to pick out the characteristics that are key to the production of favorable species during thermal decomposition.

Detonation Wave Development

The basic principle of pulse detonation engines is that detonation waves produce the thrust. A detonation is defined as a traveling shock wave coupled with a combustion zone (Turns 2000:598). Because the initiation energies of hydrocarbon/air mixtures is on the order of 10^5 J (98.4 Btu), it is impractical to directly initiate the detonation. Instead, a low energy spark is used to ignite the fuel/air mixture at the closed end of a thrust tube. The deflagration formed travels down the tube as it increases in speed. The deflagration propagates by heat transfer from the flame to adjacent fuel/air mixture. As the deflagration travels down the tube, it encounters a Shchelkin-type spiral. The spiral causes a concentration of heat and pressure that initiates a detonation. Energy is released rapidly as the detonation propagates down the tube at high speed, and thrust is produced by the mass ejected from the tube as the detonation propagates down the tube and from the blow down of the high pressure products.

One-Dimensional Detonation Analysis

Detonation and deflagration are characterized by the changes in density (ρ), pressure (P), temperature (T), and velocity (u) produced. Figure 1 shows a schematic view of the stationary flame front, and Table 1 compares the changes in these properties associated with the two phenomena.

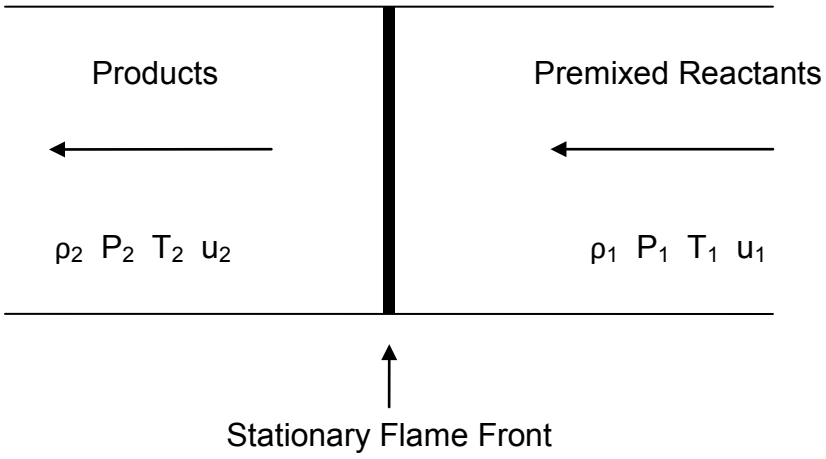

Figure 1. Schematic of stationary flame front

Table 1. Typical detonation and deflagration Mach numbers and ratios across a stationary flame front (Kuo, 2005:357)

	Detonation	Deflagration
u_1/a_1	5 – 10	0.0001 – 0.03
u_2/u_1	0.4 – 0.7 (Deceleration)	4 – 6 (Acceleration)
P_2/P_1	13 – 55 (Compression)	≈ 0.98 (Slight Expansion)
T_2/T_1	8 – 21 (Heat Addition)	4 – 16 (Heat Addition)
ρ_2/ρ_1	1.7 – 2.6	0.006 – 0.25

Subscript one (1) denotes upstream conditions, and subscript two (2) denotes downstream conditions of a stationary wave. Deflagration is characterized by low flame speed, acceleration of products, and smaller increases in pressure, temperature, and density. Detonation is characterized by a high flame speed with the products moving slower than the wave. There are much larger increases in pressure, temperature and density. Deflagrations propagate at subsonic speeds while detonations propagate at supersonic speeds. Realistically, the structure of a detonation is complex and three dimensional. Insight can still be gained from a 1-d analysis. The same assumptions used to analyze stationary 1-d normal shocks are applied.

- One-dimensional steady flow
- Constant area duct
- Ideal gas behavior before and after the shock
- Constant and equal specific heats
- Negligible body forces
- Adiabatic conditions

For the stationary deflagration, the velocities are relative to the flame front traveling through the channel. The 1-d steady conservation of mass, momentum and energy equations as well as the ideal gas equation can be applied (Eq. 1, 2, 3, and 4 respectively).

$$\rho_1 u_1 = \rho_2 u_2 \tag{1}$$

$$P_1 + \rho_1 u_1^2 = P_2 + \rho_2 u_2^2 \tag{2}$$

$$C_P T_1 + \frac{u_1^2}{2} + q = C_P T_2 + \frac{u_2^2}{2} \tag{3}$$

$$P = \rho R T \tag{4}$$

In the conservation equations, ρ is density, u is velocity, P is pressure, Cp is specific heat, q is the heat of combustion, and R is the universal gas constant (Kuo 2005:358). The speed of sound (a) is defined in Eq. 5.

$$a = \sqrt{\gamma RT} = \sqrt{\gamma P/\rho} \tag{5}$$

In Eq. 5, γ is the ratio of specific heats, R is specific gas constant, T is the static temperature, P is the static pressure, and ρ is the static density. Combining the speed of sound equation with conservation of mass (Eq. 1) and momentum (Eq. 2) yields the Rayleigh relation (Eq. 6) (Kuo 2005:359).

$$\gamma M_1^2 = \left(\frac{P_2}{P_1} - 1\right) \Big/ \left(1 - \frac{\rho_1}{\rho_2}\right) \tag{6}$$

Note that in Eq. 6, M is the Mach number defined as $M = u/a$. The Rayleigh relationship represents lines that obey both continuity and conservation of momentum. The slope of the Rayleigh lines measures mass flux. The Rankine-Hugoniot relation is given in Eq. 7 and results from satisfying the energy equation (Eq. 4) in addition to the continuity equation (Eq. 1) and momentum equation (Eq. 2).

$$\frac{\gamma}{\gamma - 1}\left(\frac{P_2}{\rho_2} - \frac{P_1}{\rho_1}\right) - \frac{1}{2}(P_2 - P_1)\left(\frac{1}{\rho_1} + \frac{1}{\rho_2}\right) = q \tag{7}$$

If the initial conditions (P_1, ρ_1, and q) are given, all possible values of P_2 and ρ_2 can be calculated, and q is the heat of combustion using the Rankine-Hugoniot relation. Fig 2 plots a generic Hugoniot curve with Rayleigh lines.

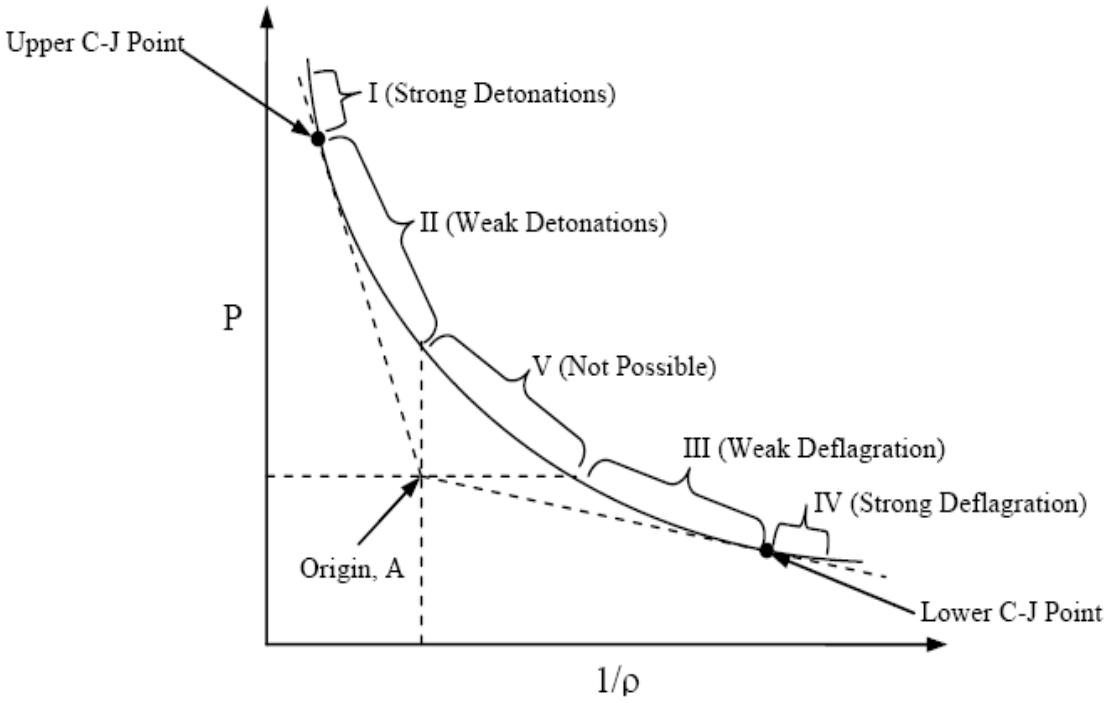

Figure 2. Hugoniot curve with Rayleigh lines (Kuo, 2005)

A pair of tangent Rayleigh lines and a pair of intersecting lines form four points on the curve dividing the curve into five sections. Two critical points are formed by the tangent Rayleigh lines and are termed the Chapman-Jouguet (C-J) points. The other two critical points are formed by the intersections of the horizontal and vertical Rayleigh lines with the Hugoniot curve. The vertical and horizontal Rayleigh lines represent the limit of infinite mass flux, and zero mass flux respectively (Turns, 2000:603). Due to continuity, the region between these two points on the Hugoniot curves is a physical impossibility. (Region V) The strong deflagrations predicted by region IV have never been experimentally observed. The gas velocity relative to the flame front would have to be accelerated from subsonic to supersonic (Kuo, 2005:364). Detonations in Region II are weak. Weak detonations are not possible for liquid hydrocarbons because the chemical

kinetics of liquid hydrocarbons are too slow to allow weak detonation. (Helfrich, 2006:11). In Region II, the pressure of the products must be less than that of the upper C-J point. The only regions left are Region I and Region III. These are the regions of interest to PDE research.

Region I is where strong detonations occur, and Region III is where weak deflagration occurs. In region I, a strong detonation will tend to move down the curve to the upper C-J point. Detonations propagating at this point are stable and travel at the Chapman-Jouguet wave speed. The weak deflagrations of region III are also of interest because flames in this region are what transition into detonations (Turns, 2000:598). The wave speed of the upper C-J point is the measure by which a detonation is judged to have occurred. The upper C-J speed for liquid hydrocarbon air mixtures used in PDE's is about 1800 m/s (5906 ft/s), and the lower C-J wave speed is approximately 500 m/s (1640 ft/s) (Helfrich 2006:12).

Detonation Wave Structure and Initiation Energy

While the one-dimensional analysis yields a tool to distinguish detonation from deflagration, it is also important to understand the structure of a detonation and how it is affected by fuel composition. The Zeldovich, von Neumann, Döring (ZND) Model introduces three zones of a detonation wave (Fig. 3). The first zone consists of a shock wave with the characteristic rises in temperature, pressure, and density. Chemistry is frozen in this zone because of the narrow width of the shockwave. The shock wave is only a few mean free paths thick (Turns, 2000:613). In the second zone, known as the induction zone, thermodynamic properties change little. In the induction zone, ideal gas

relationship can be used to for analysis. The final zone is the reaction zone. It is characterized by high reaction rate, sharp increases in temperature, and decreases in pressure and density. The reaction zone concludes when the chemical reaction reaches equilibrium.

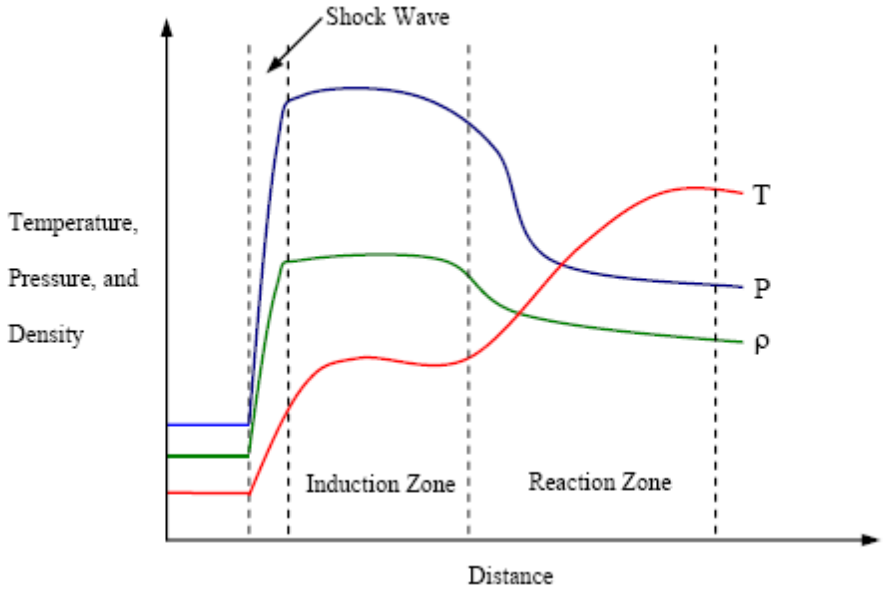

Figure 3. Plot of temperature (T), pressure (P), and density (ρ) changes across a ZND detonation wave (Slack, 2006:17)

The ZND model of detonation aids in the understanding of a detonation, but it does not address the effects of different fuels on the detonation. Detonations like those that occur in a PDE travel through long narrow channels. Therefore, a two dimensional model will more accurately capture the behavior of the detonation (Fickett, 1979:998). A fully developed detonation wave propagating from left to right is shown in Fig 4.

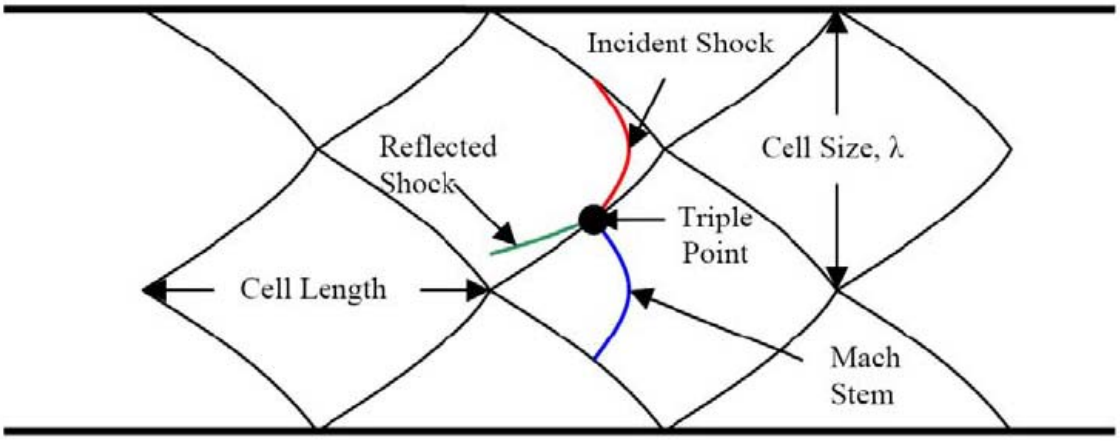

Figure 4. Sketch of a two-dimensional detonation wave confined to a long narrow passage (Helfrich, 2006:15)

Experimental observation has shown that there are several shock fronts interacting in the traveling detonation wave. The point where a Mach stem, an incident shock, and the reflected shock interact is termed the triple point. As the detonation propagates, a fish scale pattern is formed by the triple shock interaction. This pattern was captured by smoke foil tracings in experiments. The width of the "fish scales" is termed the cell size λ.

The cell size is important to this work because, it is proportional to the energy required to directly initiate detonation ($E_{initiation}$), and is a function of the fuel used (Tucker, 2005:25). The relationship between cell size and initiation energy is described in Fig. 5.

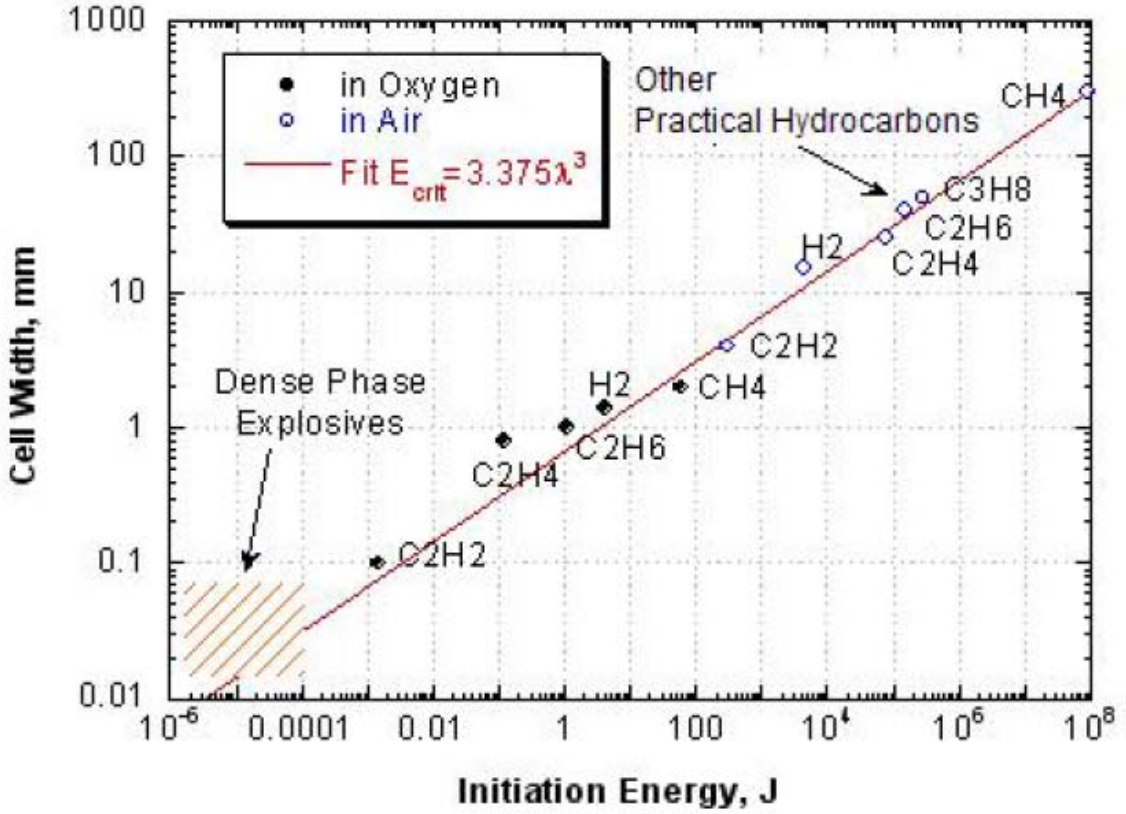

Figure 5.Cell size of various stoichiometric fuel-oxidizer mixtures as a function of initiation energy (Kaneshige, 1997), (Schauer, 2005:2)

The label "Other Practical Hydrocarbons" refers to liquid hydrocarbon fuels such as JP-4, JP-7, and JP-8. The least squares trend line represents a relation ship between initiation energy and cell size given analytically by Eq. 8

$$E_{initiation} = 3.375 \cdot \lambda^3 \tag{8}$$

Note that Eq. 8 only applies to equivalence ratios of unity. The trend was validated by experiment and shows that unsaturated hydrocarbons such as ethylene (C_2H_4) and acetylene (C_2H_2) were more detonable than fully saturated hydrocarbons (hydrocarbons that have no double or triple bonds) such as methane (CH_4) and propane (C_3H_8) or higher molecular weight hydrocarbons like JP-8 and JP-10 (Kaneshige, 1997) (Knystautas,

1984:23-37). It has been shown that thermal cracking of practical hydrocarbons produces partially saturated hydrocarbons. Thermal cracking of fuels was shown to improve the detonability of fuel air mixtures in PDE's. So far, research has only been done with cracking JP-8. In this work, that research will be expanded to include investigations of JP-4 and JP-7. This work also investigates the influence of various methods of enhancing the cracking process via catalysts.

Pulse Detonation Engine Operating Cycle

In order to apply the correlation between fuel composition and initiation energy to a PDE, it is necessary to describe the operation cycle of a PDE. The PDE cycle consists of three phases: fill, fire, and purge (Fig 6). In Fig. 6, the three phases are timed equally for illustration. They regularly vary greatly with the design of a particular engine. The times shown will be discussed later. While the length of the fill and purge phases are controlled by valve timing and the pressure upstream of the valves, the fire phase is governed by the length of time needed to complete the ignition, transition, detonation, and blowdown processes. The total length of the fire phase is the limiting factor on the cycle frequency of a PDE. It is important to understand each portion of this phase in addition to the other phases of the cycle.

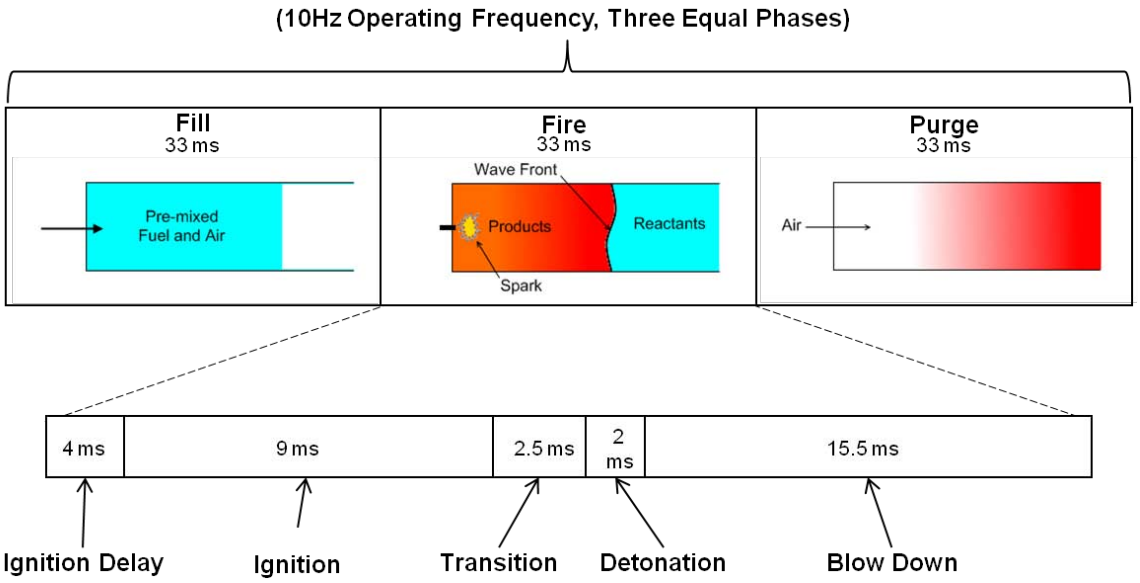

Figure 6. PDE operating cycle with detail of fire phase (Times are representative of neat JP-8)

The cycle begins with the fill phase where the thrust tube is filled with fuel/air mixture to be used in the detonation. The mixture enters the thrust tube through valves at the closed end of the tube. The ratio of the volume of mixture to the volume of the tube is the fill fraction (FF). The fill fraction usually ranges between 0.8 and 1.2. When FF is less than 0.8 there is not enough charge in the tube for the transition to detonation to take place. At FF greater than 1 more fuel/air mixture is forced into the tube than will fit. this results on over flow that cannot provide thrust to the engine. It was necessary to run the engine at fill fractions greater than unity during startup as the fuel nozzles were over sized to provide extra run time before clogging. The engine was run at fill fractions as low as 0.74 in order to achieve the maximum temperature of the fuel in the heat exchangers.

The PDE cycle continues with the fire phase. As shown in Fig. 6, there are five stages of the fire phase. The first stage is the ignition delay. It is the time that passes

between the closing of the intake valves and the discharge of the spark into the fuel/air mix. For this work ignition delays of 4 ms we used. This time is just long enough to prevent backfire of the tube into the intake manifold. The next stage of the fire phase is ignition. The ignition time is the time that passes between the spark and a head pressure rise greater than 5000 psi/s. This rate of pressure rise marks the onset of deflagration. Ignition is a very large portion of the fire phase, and it is for that reason that reductions in ignition time have the potential to greatly shorten the fire phase. Deflagration to Detonation Transition (DDT) time is the time needed for the deflagration produced in the ignition stage to "trip" and become a detonation. This transition is usually accomplished with some type of obstacle. In this work a Shchelkin-type spiral was the used as the obstacle. The Shchelkin-type spiral is a proven and effective obstacle, but fuel composition also affects the time required for the transition. There is not as much opportunity for improvement as there is with ignition times. The experiments performed with JP-8 did not record DDT times so there is not data to compare. The final portion of the fire phase is blow down. After the transition, time is needed for the detonation wave to propagate down the tube and for the hot, high pressure products to escape the thrust tube. The tube "blows down" until the pressure inside the tube equalizes with the ambient pressure outside the tube. This is the portion of the PDE cycle where thrust is produced.

The final phase of the PDE cycle is the purge phase. In this phase another set of valves open, and a measured volume of air is injected into the thrust tube. The air forces the detonation products out of the tube, and absorbs some of the heat generated. The volume of air is determined by the purge fraction (PF) which is the ratio of the air volume

to the total tube volume. Some adjustment of the PF can be used to control the temperature of the tube walls.

The frequency with which the PDE cycle can be repeated within a thrust tube has a direct impact on the performance of the engine. Since each cycle of the tube produces a fixed quantity of thrust, increased cycle frequency proportional to the static thrust of the engine. The goal of this work is not to quantify thrust directly, but instead to quantify the reductions in ignition time and DDT time that will increase cycle frequency. The limiting factor in the cycle frequency is the amount of time it takes to complete the fire phase of the cycle. As the frequency increases less time is available to complete each phase of the cycle. The times shown in Fig. 6 are accurate for a PDE operating at 10 Hz with neat JP-8 as the fuel. Each phase is allotted an equal 33.3 ms. This is far more time than is needed for the fill and purge phases so there is no concern that either will not be completed before starting the next phase. As previously discussed, an ignition delay of 4 ms was used to allow the fill valves to completely close before the spark. To fill in the example, an ignition time of 9 ms, and a DDT time of 2.5 ms are used, and 2 ms was allowed for the detonation to travel down the tube. These are representative of a JP-8 air mixture. The blow down is allotted the rest of the fire phase (15.5 ms). The actual time require for the pressure to drop to within 5% of atmospheric pressure is about 2 ms. The total time required for the fire phase is the sum of the ignition time, DDT time, the time required for the detonation to travel down the tube, and the blow down time. In the example the total is approximately 18 ms. Keeping with the assumption that the fill, fire, and purge phases are equally times, the maximum operation frequency of the engine is limited to 19 Hz. Any reduction in ignition time or DDT time would raise this limit.

Thermal decomposition or cracking of fuel is one method that has been shown to reduce ignition times in JP-8. The more reacted or "stressed" the fuel is prior to detonation the shorter the ignition times tend to be. It would be useful to know the characteristics of a fuel that make it a good candidate for cracking. Also it would help to know if the cracking process can be enhanced through the use of a catalyst coating the walls of the heat exchangers where the fuel is heated. This knowledge would be the key to choosing a fuel for PDE's and for designing the fuel cracking system.

Altering Fuels by Pyrolytic Thermal Decomposition

Liquid hydrocarbon fuels are the practical choice for fuels in aircraft. They have high energy densities requiring less storage space, and are already produced in large quantities for gas turbines and internal combustion engines. JP-8 is the standard fuel used by the United States Air Force, and it was used in earlier experiments for this reason. Alternate fuels such as hydrogen, ethane, ethylene, and acetylene have lower initiation energies, but they introduce scalability challenges and explosion hazards (Galligan, 2005:7). Pyrolysis is an option that allows fuel to be stored as a liquid hydrocarbon, and then altered to improve performance prior to detonation. Previous research (Helfrich. 2007:2) has shown that the waste heat from PDE thrust tubes produces temperatures that cause cracking via zeolite coated heat exchangers.

Pyrolysis is defined as the chemical decomposition of organic compounds by heating without oxidation. This process is endothermic, requires significant heat input, and progresses by free radical reaction chemistry (Ford, 1986:240). At temperatures above the endothermic threshold, (~811 K (1000° F) for JP-8) the fuel will undergo

thermal and/or catalytic cracking reactions (Nagley, 2008:18). The cracking reactions cause a shift in the molecular weight distribution of the fuel, and follow the free radical chain mechanism. The free radical chain mechanism can be outlined as three types of reactions: initiation, propagation, and termination.

Initiation:

Pyrolysis begins with an initiation reaction where a molecule undergoes bond fission, and produces free radicals. Free radicals are molecular species that have unpaired electrons. The heating required to break the bond depends on the bond dissociation energy. Because alkanes make up most of the fuel, and alkane carbon-carbon single bonds are the weakest, alkanes are some of the first species to react (Edwards, 2003:1104). Eq. 9 shows a generic free radical initiation reaction.

$$R_i - R_j \longrightarrow R_i - CH_2 - CH_2 \cdot + \cdot R_k \tag{9}$$

Free radicals are denoted by the "•", and R with subscripts i, j, or k denotes an alkane. The free radicals generated by initiation reactions drive the rest of the reactions.

Propagation:

Immediately following the generation of free radicals, there is a variety of possible pathways for propagation. These pathways fall into four categories: hydrogen abstraction, β-scission, intramolecular hydrogen shift, and molecular addition (Rice, 1933:3035-3040; Kossiakoff, 193:590-595). Hydrogen abstraction occurs when a free radical removes a hydrogen atom from another molecule. The molecule losing a hydrogen then becomes a free radical. Eq. 10 is an example of a hydrogen abstraction reaction.

$$R_i \cdot + R_i - CH_2 - CH_2 - R_j \longrightarrow R_iH + R_i - \dot{C}H - CH_2 - R_j \tag{10}$$

A β-scission reaction occurs when scission takes place at the bond located in the β position of a molecule. For reference, Fig. 7 shows the location of the α, β, and γ bonds relative to the free radical.

Bond Location

$$R_i - \dot{C}H \underset{\alpha}{-} CH_2 \underset{\beta}{-} CH_2 \underset{\gamma}{-} R_j$$

Figure 7. Location α, β, and γ bonds relative to free radical (Dewitt, 2007:15)

The result of β-scission is an alkene with the double bond in α position (α-olefin) or ethylene. Eq. 11 is an example of a β-scission reaction.

$$R_i - \dot{C}H - CH_2 - R_j \longrightarrow R_i - CH = CH_2 + \cdot R_j \qquad (11)$$

The next reaction type is intramolecular hydrogen shift. During this type of reaction, a hydrogen atom shifts position within the molecule (Eq. 12).

$$R_i \cdot \longrightarrow CH_3 - CH_2 - CH_2 - CH_2 - \dot{C}H - R_j \qquad (12)$$

The hydrogen usually shifts from position 1 to position 5 or 6 where position 1 is on the terminal carbon, position 2 is on the next carbon in the chain and so on. Fig. 8 illustrates a shift from position 1 to position 5.

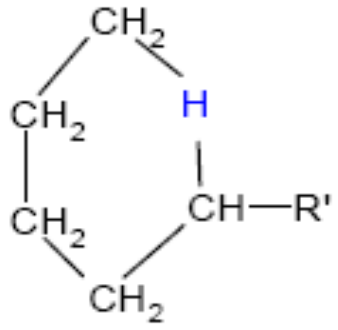

Figure 8, Intramolecular hydrogen transfer propagation reaction (DeWitt, 2007:16)

Molecular addition is the final type of propagation reaction. It becomes important at higher degrees of reaction. During molecular addition, two or more molecules form bonds that reduce overall bond multiplicity. At a high degree of reaction, the result is polycyclic aromatic hydrocarbon (PAH) formation. PAH's are a precursor to bulk deposit formation discussed later.

Termination:

Pyrolysis terminates through two different mechanisms. The first is coupling or recombination where two free radicals combine to form a larger molecule as shown in Eq. 13.

$$R_i \cdot + \cdot R_j \longrightarrow R_i - R_k \tag{13}$$

The second mechanism is disproportionation, and occurs when a hydrogen is abstracted from one free radical leaving an alkene. The hydrogen then attaches to another free radical yielding a stable molecule. A generic disproportionation reaction is shown in Eq. 14.

$$R_i \cdot + \cdot R_j \longrightarrow R_i - CH = CH_2 + H - R_j \tag{14}$$

In both termination mechanisms, the free radical is consumed ending the reaction with the formation of stable species.

Applying the free radical reaction pathways discussed earlier, some predictions can be made about the stressed hydrocarbon fuels produced by pyrolysis. Figure 9 lays out the chemical pathways that any hydrocarbon will follow during pyrolysis.

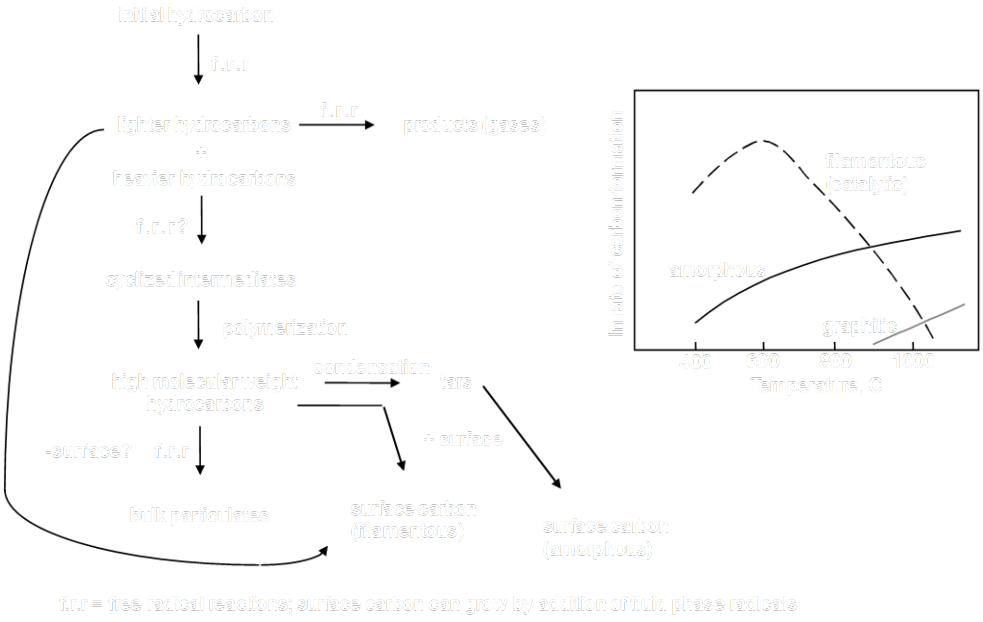

Figure 9. Reaction pathways followed during pyrolysis (Edwards, 2003:1103)

The important factors controlling the reactions are what species are present in the raw fuel, the amount of heat added to the fuel, and what if any catalysts are present during the reaction. Initial fuel composition is controlled through selection of the raw hydrocarbon fuel.

JP-7 was selected for testing because it is more saturated, has fewer double and triple bonds, than JP-8 and because it has a very low concentration of aromatic compounds. Low aromatic concentration has been shown to reduce the formation of oxidative coking. Aromatic compounds are also the precursor to the formation of bulk deposits. Both types of deposits are harmful to fuel systems as they collect on the walls of fuel passages and restrict flow. A highly saturated, fuel such a JP-7, will decompose more than an unsaturated fuel under similar heating. Saturated molecules, especially longer ones have more bond sites where bond fission can occur than unsaturated molecules. The additional free radicals created will result in the creation of more light hydrocarbons.

Heat addition is controlled by the operating conditions of the PDE. A high operating frequency will increase the number of detonations per second increasing the waste heat available for cracking. Increased fill fraction results in more energy release per detonation also increasing the waste heat. Reducing the purge fraction will prevent the waste heat from being convected out of the tubes. Insulating the outside of the thrust tubes will also increase the operating temperature.

Catalysts can be used to alter the chemical pathways during pyrolysis. This work investigates the effects of three different catalyst configurations: a zeolite catalyst bonded to the heat exchanger wall, a palladium catalyst suspended in the raw fuel, and a control with neither catalyst. The motivation for using a catalyst is the possibility of improvement in selective production of desired species with low initiation energies, increased pyrolytic reaction rate, reduction in bulk deposits, and shorter ignition times. Additional production of ethylene or acetylene, for example, would reduce ignition times more than pyrolysis without the catalyst. Figure 9 shows that the initial free radical

reactions will produce lighter hydrocarbons and gaseous products through free radical reactions (f.r.r.).

A convenient measure of the extent of decomposition of the fuel is the ratio of the mass of the gaseous products to the mass of the initial fuel sample. The liquid-to-gas conversion ratio (m_{gas}/m_{fuel}) is important to the study of fuel for PDE's because the gaseous products are expected to have lower initiation energies than the liquids. The production of lighter hydrocarbons suggests that the initial hydrocarbons are decomposed into lighter intermediate hydrocarbons. As the free radicals continue to react with the hydrocarbon products, cyclized intermediates such as cycloalkanes, and aromatics can form. Further reaction leads to the formation of multi-ring aromatics known as polycyclic aromatic hydrocarbons (PAH's) and eventually solid carbon deposits. As PAH production increases so does the production of bulk carbon deposits.

Properties of JP-4, JP-7, and JP-8

In previous work, (Nagley, 2008;17) JP-8 was the fuel of choice for cracking. It is important to the military operation of PDE's because it is the predominant fuel used by the United States Air Force. It has a high flash point and energy density making it both safe to work with and efficient to store. Hydrogen, ethylene, and other light fuels are often used in PDE research, but they are more difficult to use operationally, requiring pressurized tanks or cryogenic cooling and extreme care in handling. However, there may be other fuels or catalysts that offer better performance in PDE's.

This work looks at two additional fuels, JP-7 and JP-4, and two catalysts, zeolite wall coating, and fuel born palladium. The characteristic properties of each fuel tested are listed in Table 2.

Table 2. Characteristics and properties of JP-8, JP-7 and JP-4 (Edwards, 2003:1095)

Property	JP-8 Characteristics	JP-7 Characteristics	JP-4 Characteristics
Approximate Formula	$C_{11}H_{21}$	$C_{12}H_{25}$	$C_{8.5}H_{17}$
H/C Ratio	1.91	2.08	2.00
Critical Temperature K (°F)	683.2 (770)	672.04 (751)	598(620)
Critical Pressure atm (psia)	23 (340)	20.75 (305)	30.5(450)
Specific Gravity @ 298K (77° F)	0.81	0.79	0.81
Average Composition vol%			
Paraffins (Alkanes)	45	65	59
Napthenes (Cycloalkanes)	35	32	29
Aromatics	18	0.1	10
Olefins (Alkenes)	2		2

JP-4 is a 50-50 mix of kerosene and gasoline. This mix gives JP-4 a lower freezing point than pure kerosenes. For this reason it was often used in cold climates. JP-4 was the standard USAF jet fuel until 1996 when it was replaced by JP-8. JP-4 was selected for the seeded catalyst experiments because of its lowhigh vapor pressure. The low vapor pressure allows JP-4 to evaporate more quickly than the other fuels.

JP-7 is not distilled from crude oil like JP-8, but is blended from special stocks for high operating temperatures, and high thermal stability. The term thermal stability is used to refer to the tendency of a fuel to form low temperature oxidative coke, not high temperature pyrolytic coke. Oxidative coke forms through reactions between the fuel and dissolved oxygen. The growth of oxidative deposits is slower in a fuel with a smaller concentration of aromatic compounds. Pyrolytic coke forms as a result of thermal cracking. JP-7 was developed for the SR-71 Blackbird, and was used to internally cool

engine parts. Chemically it is more saturated than JP-8 , and specifically has a very low aromatic content < 0.1%.

This work also quantifies the improvements gained from the use of palladium and zeolite catalysts. Palladium was used as a fuel born catalyst. Zeolite was used as a wall coating within the heat exchangers. Zeolite is made from a silica-alumina structure, but the catalytic agent is proprietary information. Any use of a catalyst should increase the rate of cracking as the fuel is heated and improve performance. This work compares both composition of the catalyst, zeolite vs. palladium, and application, fuel born vs. wall coating.

Coke Formation

The adverse result of any pyrolytic fuel system is the formation of carbon deposits. At temperatures below 644 K (700 °F) deposits form due to auto-oxidation of the fuel. Dissolved oxygen in the fuel reacts with the fuel to produce thermal-oxidative deposits. These deposits will form on the surfaces of a fuel system and continue to grow until all of the dissolved oxygen is consumed. Auto-oxidative coking can be mitigated by removing the dissolved oxygen from fuel before it is heated. The oxygen removal process is known as sparging. To carry away the oxygen, pure nitrogen is bubbled through the fuel in a vented container.

During cracking, the deposits formed are the result of the free radical reactions that produced the desired light hydrocarbons. The recombination of intermediate aromatics and cycloalkanes produces graphite sheets the precipitate out of the fuel as bulk deposits. Because the deposits are formed from reaction of the fuel itself, much

larger quantities of carbon are produced. In earlier experiments, formation of these deposits was a limiting factor because the deposits clogged fuel filters after a few minutes of operation.

Experiments in Thermal and Catalytic Cracking

Based on the free radical reaction pathways, it is expected that pyrolysis will cause a large shift in overall fuel composition. The unknowns for this experiment are extent of reaction and identification of the compounds in the reacted fuel. Most of the previous work has examined either changes in fuel composition due to cracking or performance improvement of PDE's using heated fuel. However, only one work so far (Nagley, 2008) has measured both performance and composition from the same tests.

It is useful first to examine some of the work that studied fuel composition. One such study (Huang, 2440:290) flowed JP-7 through a stainless steel tube heated to 700 K (800° F). Sparged, JP-7 was preheated to 600 K (620°F), and then pumped through a 0.01397 m (0.55 in.) ID stainless steel tube inside a resistive heater. As the fuel flowed through the tube, it was cracked by the heat and underwent pyrolysis. The experiment closely controlled the exit temperature of the fuel, and the residence time of the fuel inside the heated tube. The flow rate of the fuel controlled its residence time, and the outlet temperature was controlled by varying the power supplied to the heater. After exiting the heater, the fuel was cooled and then a portion was collected for offline analysis. The gaseous products were quantified using a Gas Chromatograph/Mass Spectrometer (GC/MS), and the liquids we quantified using a combination of GC/MS and High Precision Liquid Chromatography (HPLC). The resulting "stressed" fuel showed a

shift to lower molecular weight compounds, as well as the production of gaseous species (Fig. 10)

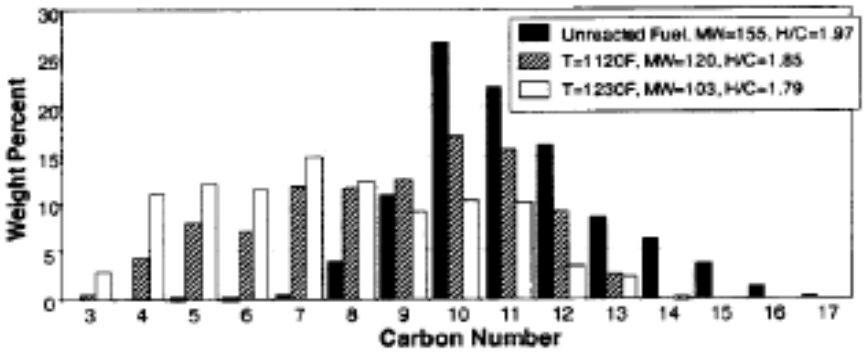

Figure 10. Molecular weight distribution of JP-8+100 as well as liquid products after thermal and catalytic cracking (Huang, 2004:290)

The results were consistent with the expected free radical reaction pathways. The study did not explore the effects of the cracked fuel on PDE performance. It also was not limited by the waste heat production of the PDE. For these reasons the results are only of limited use.

Other studies using JP-8+100, Jet-A, and S-8 (a synthetic Fischer-Tropsch fuel) all reported production of gasses and reduced molecular weights (Edwards 2006) (Helfrich, 2006) (Nagley, 2008). It was found in these studies that increasing the saturation of fuel (raising the H/C ratio) and reducing the amount of cyclic hydrocarbons resulted in higher liquid-to-gas conversions. Work that has studied PDE performance improvements tracked ignition time and DDT time (Helfrich, 2007) (Nagley, 2008). The first work available utilizing waste heat to raise fuel temperatures achieved maximum fuel temperatures of 900 K (1160 °F) with JP-8 (Helfrich, 2007:6,8). As the maximum

fuel temperature increased from 800 K (960 °F) to 900 K (1160 °F), the ignition times dropped by 20% (Fig. 11)

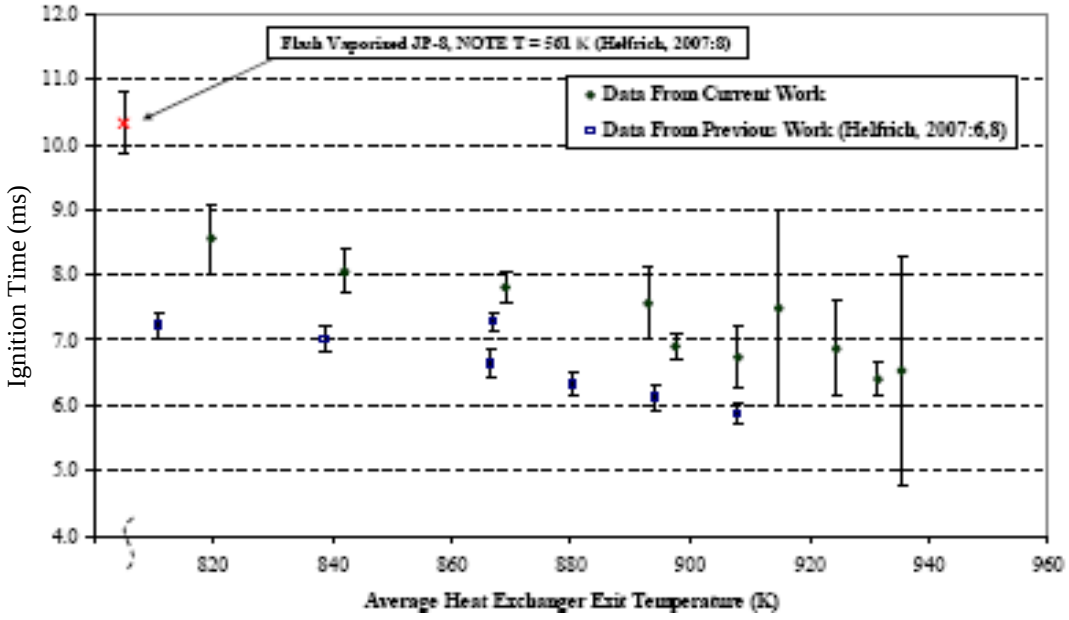

Figure 11. Ignition times as a function of heat exchanger exit temperature for ϕ ≈ 1 (Nagley, 2007:77)

The study did not measure the change in fuel composition during cracking. It also used a different fuel (JP-8+100) than the studies that measure changes in composition. While the two branches of cracking experiments, and performance experiments each produced useful insight, a set of experiments was needed that included both composition and performance measurements.

Knowing the composition of fuel that was injected into the engine after cracking and measuring the resulting performance improvements would yield an overall performance of the initial fuel being tested. The most recent work on fuel cracking for PDE's developed a method to collect both composition and performance data (Nagley, 2008:42). Concentric double tube heat exchangers were used to heat JP-8 using waste

heat from a PDE. The inner tube served as the thrust tube for the PDE, and fuel was heated in the annular space between the inner and outer tubes. The thrust tube heat exchangers were coated with a zeolite catalyst to increase the rate of decomposition. Samples of the cracked fuel were then collected and analyzed to determine liquid-to-gas conversion, and PAH concentration. The experiments performed using these heat exchangers have demonstrated that JP-8 could be cracked at temperatures up to 920 K (1196 °F).

The resulting cracked JP-8 had liquid-to-gas conversion ratios of 30% (Fig. 12), and a 20% reduction in ignition times (Fig 11)

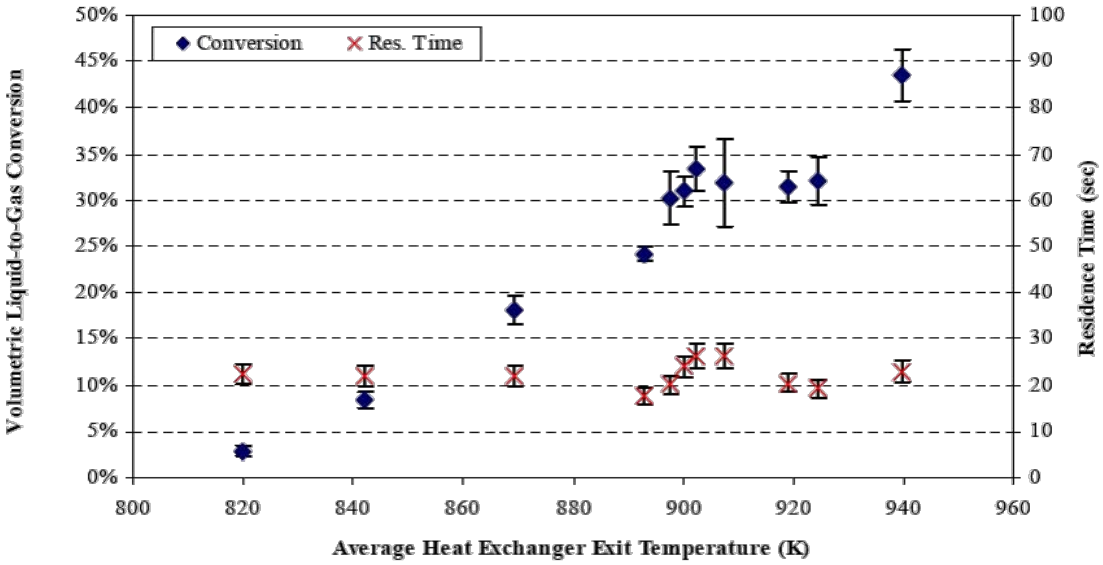

Figure 12. Liquid-to-gas conversion ratios of thermally cracked JP-8 (Nagley, 2008:65)

The same zeolite coated tubes are used in this work to make a comparison between JP-8 and JP-7, and an identical set of tubes made without a catalyst coating are used for fuel born catalyst tests, and for catalyst free baseline data.

III. Experimental Setup and Instrumentation

Pulse Detonation Research Facility

Experiments for this work were carried out at the Pulse Detonation Research Facility located in D-Bay of Building 71A, Wright-Patterson Air Force Base, Ohio (D-Bay). While everyday operations and testing are contractor managed, D-Bay is an element of the Air Force Research Laboratory Propulsion Directorate, Turbine Engine Division, Combustion Sciences Branch (AFRL/RZTC).

D-bay consists of four main areas. They are the test cell, the control room, the fuel room, the compressor room. The facility was built in order to test conventional turbine engines. As a result, the explosion proof 21,200 m^3 (748,670 ft^3) test cell is surrounded by a minimum of 0.61 m (2 ft) of reinforced concrete to protect personnel during testing. The cell contains a turbine engine test stand capable of supporting 267,000 N (60,024 lbf) thrust experiments. To accurately measure the much smaller amount of pulsed thrust produced by the research PDE, a damped thrust stand was mounted on top of the turbine thrust stand. The PDE research engine is mounted to the damped thrust stand.
An exhaust tunnel directly downstream of the thrust stands collects the exhaust from experiments and vents them to the atmosphere.

The control room is located next to the test cell and contains all the equipment needed to remotely operate the engine and record data from experiments. Closed circuit cameras provide visual monitoring of the fuel room and the test cell. The PDE is controlled from two stations, the control panel and the control computer. The control panel contains solid state switches and controls that supply power to various facility

components. It serves as a redundant control for many of the valves operated by the control computer. Deactivating a system on the control panel cuts the power to that system causing it to automatically shut down regardless of the control computer input. The panel also includes controls for the exhaust tunnel vent fan, and the testing warning light which do not have computer controls. The control computer is loaded with *LabVIEW*® control software that manages fuel and air flow control inputs as well as spark timing. The control computer also allows monitoring and control of several operating parameters in real time. It also functions as a low speed (Hz and kHz) data acquisition system. Some of the parameters typically recorded are air and fuel flow rate, engine cycle frequency, and thermocouple outputs. High speed data is recorded from a third station, the data collection computer. The data collection computer is loaded with a *LabVIEW*® program that is capable of recording data at sampling speeds up to 5 MHz from up to 16 channels. This allows for measurement of detonation wave speeds, and tube head pressure. Data must be analyzed post-run; however, the software allows some limited analysis often used to ensure the correct function of sensors before testing.

Air Supply System

Compressors supply the air needed for the purge and fill cycles of the PDE. Three Ingersoll-Rand Pac Air Compressors (Model# PA 300V) are located in the compressor room (Fig. 13)

Figure 13. Photographs of one air compressor, and the receiver tank located in the compressor room (Helfrich, 2007:42)

Each is rated at 6.9 atm (100 psi) and is capable of producing 40 m^3/min (1412 ft^3). Compressed air is stored in a 4.5 m^3 (195 ft^3) receiver tank (Serial # 10894, Buckeye Fabrication Co.). Air flows from the receiver tank to the test cell and is routed underneath the PDE test stand. There, the air is split between the fill and purge streams. The major components of the air supply system past this point are shown in Fig. 14

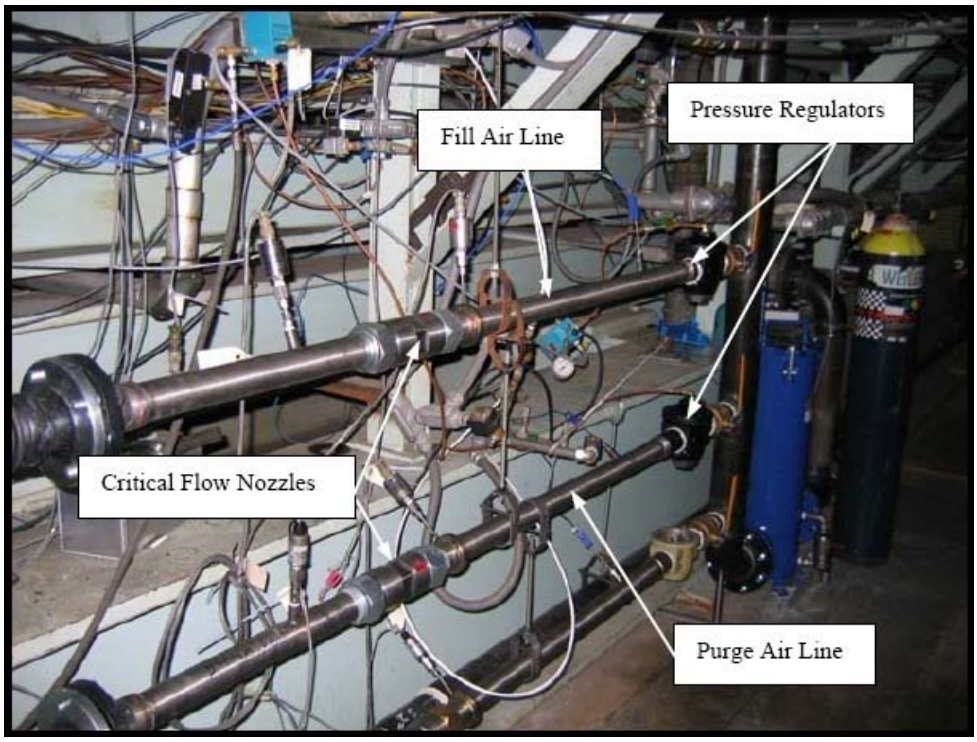

Figure 14. Air supply lines and major components of air supply system (Nagley, 2008:32)

Pressure regulators (Tescom Electro-pneumatic PID Controller, Model #ER 1200) manage the pressure in each stream. The temperature of the air is monitored by T-type thermocouples. Mass flow rates are determined using critical flow nozzles and pressures measured by transducers. For the experiments in this work, a 12.55 mm (0.494 in) nozzle was used in the fill line, and a 10.03 mm (0.395 in) nozzle was used in the purge line.

The fill air is routed to the damped thrust stand where it is heated and mixed with fuel before entering the fill manifold and the tubes. The air is heated by a Chromalox Circulation heater (Part Number: 053-550870-187). The temperature of the air is monitored and controlled by the control computer. The user sets a desired upper temperature limit by selecting the amperage applied to the heater's controller (Chromalox Model #2104) on the control panel. The controller interprets the current as a temperature

and applies power to the heater in order to maintain that temperature. After the heater, the fill air passes an array of fuel spray nozzles mounted on two spray bars. Up to five nozzles can be installed in each spray bar to mix fuel with the air. The fuel air mix then enters the fill manifold and travels to the PDE head. A restrictor plate at the entrance of the manifold, and valves at the exit prevent the flow of fuel/air mixture through head positions that do not have tubes allowing any tube arrangement.

Air Mass Flow Control

Control over the mass flow of air in the purge and fill stream is achieved by varying the pressure of the air upstream of the critical flow nozzles. The *LabVIEW®* program on the control calculates the mass flow using Eq. 15.

$$\dot{m} = \frac{(\#_{tubes})(freq)(V_{tube})(FF)(P)}{R_{air}T} \tag{15}$$

In Eq. 15, $\#_{tubes}$ is the number of tubes used in an experiment, *freq* is the operating frequency of the engine, V_{tube} is the volume of one tube, *FF* is the fill fraction, *P* is the measured air pressure in the fill or purge line, R_{air} is the specific gas constant of air (287.1 J/kg-K or 1716 ft^2/s^2-°R), and *T* is the air temperature. The user must input $\#_{tubes}$, *freq*, V_{tube}, *FF*. Then the computer obtains *P* and *T* from the transducers and thermocouples in the air lines, and calculates mass flow. The computer then compares the result with the desired mass flow, and adjusts the Tescom regulators to meet the appropriate pressure drop across the critical flow nozzle. Pressure transducers monitor the pressure drop across the nozzles and allow the computer to close the loop on the control system.

Fuel Deoxygenating System

As the fuel is heated beyond 436 K (325 °F), the auto-oxidation process discussed in Chapter II causes the formation of carbon deposits. While this process does not alter the fuel chemistry, the deposits restrict fuel flow. Research has shown that removing the dissolved oxygen from the fuel prevents this process from occurring (Panzenhagen, 2004:3-13). Nitrogen sparging was used to remove the dissolved oxygen from fuel. In the sparging process nitrogen is bubbled through the liquid fuel prior to testing. The nitrogen bubbles absorb the dissolved oxygen in the fuel and carry it away through a vent. Figure 15 is a photo of the sparging system used for this research. The major components of the sparging system are labeled.

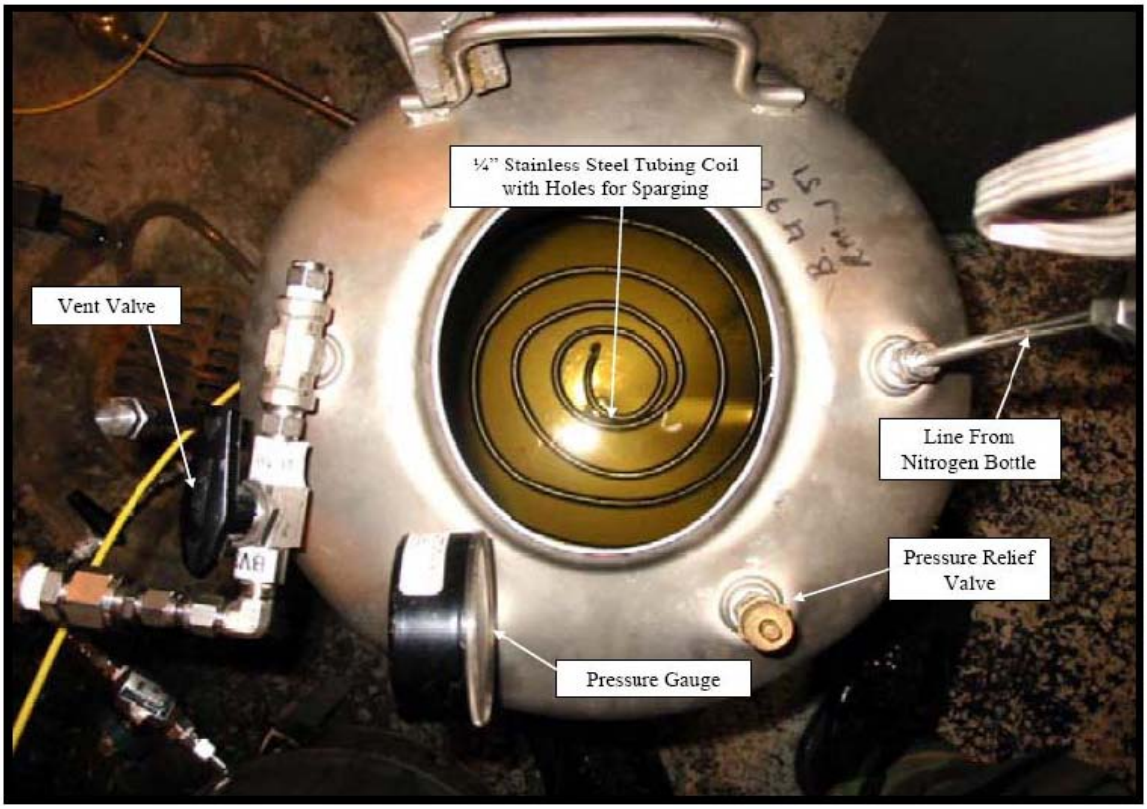

Figure 15. Fuel sparging system showing fuel storage tank with nitrogen sparging tube coiled at tank bottom (Nagley, 2008:34)

To prepare the fuel for testing, raw fuel was transferred into the 41.6 L (11 gal) stainless steel and the tank was sealed. The vent was opened to the facility's ventilation system allowing oxygen and expended nitrogen to escape. Nitrogen was then forced into the perforated coil at the bottom of the tank from a regulated pressurized nitrogen bottle. The regulator was adjusted manually until bubbling could be heard clearly through the walls of the tank. The fuel was allowed to sparge for at least four hours. Then the vent was closed and the fuel tank was pressurized to prevent air from bringing more oxygen into the tank.

Liquid Fuel Feed System

Feed of liquid fuel to the test stand is controlled through the *LabVIEW*® software on the control computer and delivered by a feed system that uses pressurized nitrogen as a pressure source. A schematic of the fuel transfer and delivery processes is shown in Fig. 16, and the actual components are labeled in Fig. 17

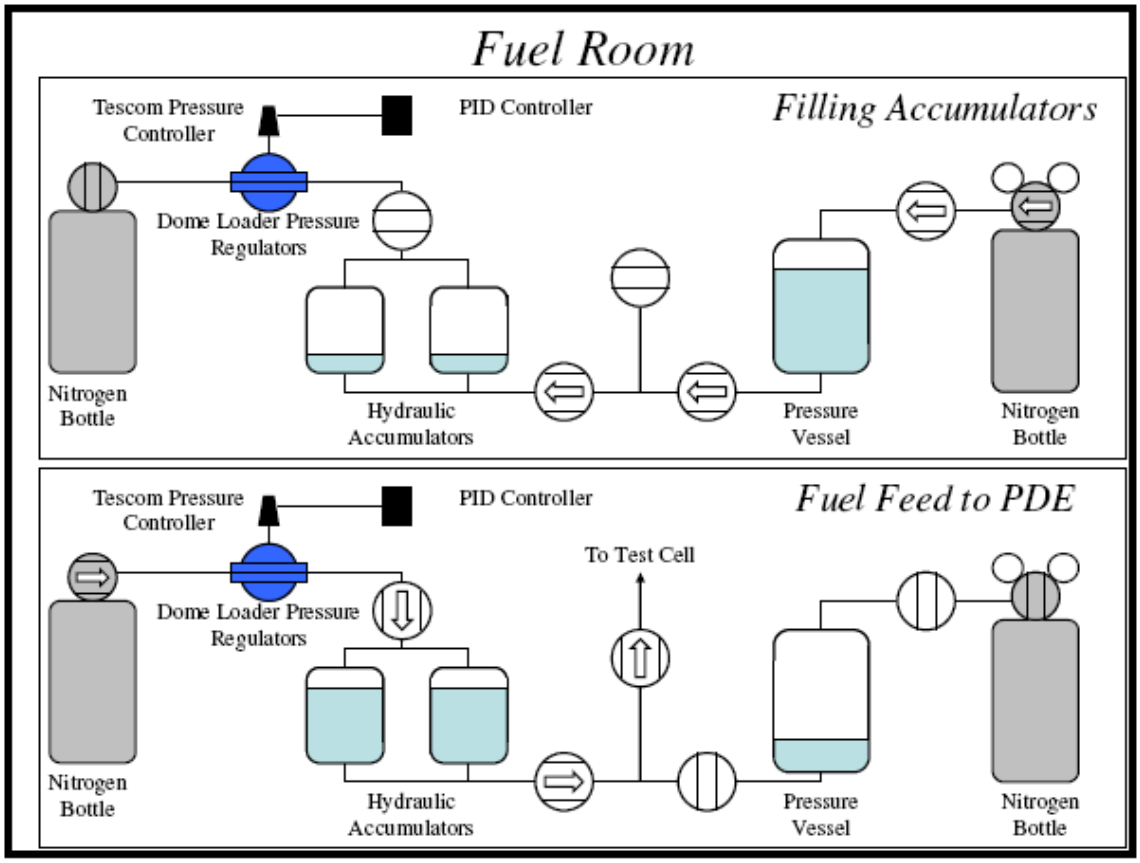

Figure 16. Schematic diagram illustrating the valve settings during accumulator filling and fuel feed to PDE. (Helfrich, 2006:47)

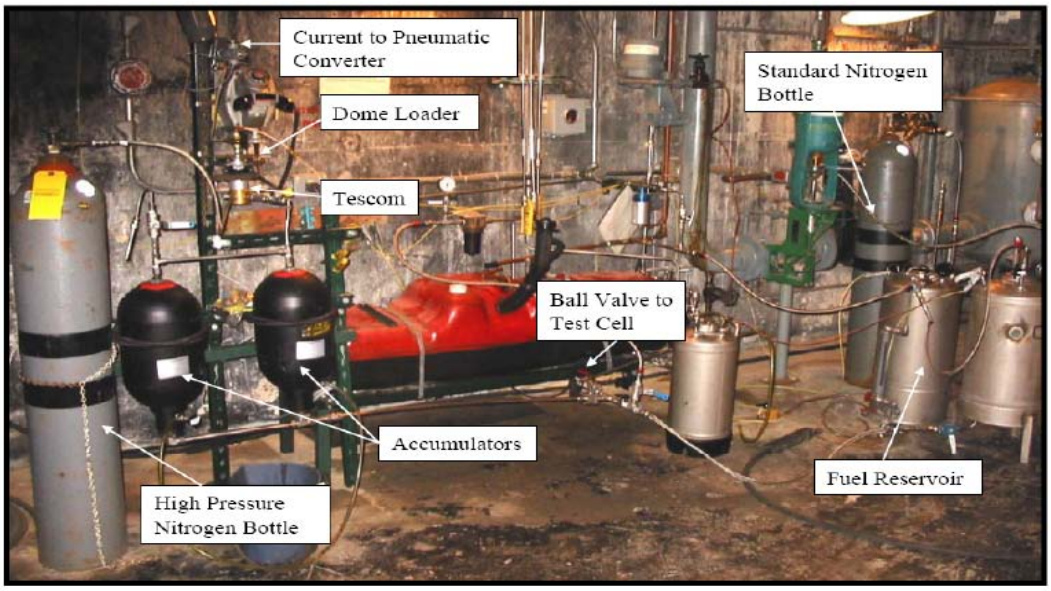

Figure 17. Photograph of liquid fuel supply system located in fuel room (Helfrich, 2006:46)

After dissolved oxygen is removed from the fuel it is transferred via sealed fuel line to two 9.5 L (2.5 gal) Greer hydraulic accumulators (Model #30A-2½A), shown in Fig. 17 They are the only supply of fuel to the PDE during operation, which limits the running time of the engine to about 20 min on two tubes. Fuel in the accumulators is separated from the pressurized nitrogen by rubber bladders, and they have maximum operating pressures of 204.14 atm (3,000 psi). A valve isolates the sparging tank from the accumulators when they are full, and other valves are opened to allow fuel to flow to the PDE. A pair of high pressure nitrogen bottles supply pressure and are regulated by a Tescom dome loader type regulator. From the accumulators the fuel flows to the test cell.

Out in the test cell, the fuel flows to a Flow Technologies turbine flow meter (Model #FT4-8AEU2-LEAT5). During initial priming of the fuel lines, air pockets can be trapped in the lines. These air pockets can damage the flow meter so it is plumbed in parallel with a by pass line. Two valves allow selection of either the flow meter or the

bypass circuit. Once all the air has been purged, the flow meter is engaged for experiments. A thermocouple measures the fuel temperature just downstream of the flow meter. The control computer uses the temperature measurement to compensate for density changes when calculating fuel mass flow. After the thermocouple, the fuel passes through the last chance valve (LCV). The LCV is used to start fuel delivery at the beginning of a test, and to shut off fuel flow at the end. The LCV is the last valve that is controlled by the computer before the PDE test stand. Downstream of the LCV the fuel passes through the fuel heating and sampling systems which will be discussed in detail later.

After heating and sampling the fuel that is not collected is injected into the fill air stream through a set of Delevan flow nozzles like the one shown in Fig. 18.

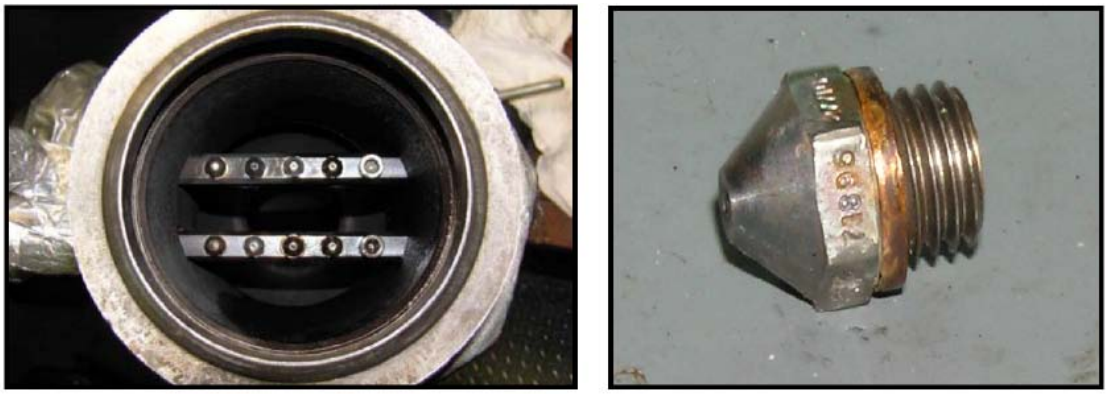

Figure 18. Photographs of air manifold with spray bars (left) and a Delevan flow nozzle (right) (Helfrich, 2006:48)

The nozzles are screwed into the previously mentioned spray bars upstream of the fill manifold. A variety of flow numbers is available so that coarse adjustments to the mass flow of the fuel can be made by selecting the right nozzle(s). Identifying the correct flow numbers was done by trial and error. The total flow number of the nozzles in the sprary

bar ranged between 5 and 10, and the flow number in the sample nozzle was between 1 and 2. Fine adjustment of the mass flow is achieved through the accumulator pressure.

Ignition System

Fuel air mixtures in the thrust tubes are ignited using an off the shelf automotive ignition system. A 12 VDC MSD Digital DIS-4 ignition system supplies the energy for spark discharges. The ignition system is controlled by the *LabVIEW®* program on the control computer. The position of the camshaft driving the valves on the engine is measured by a BEI optical encoder (Model #H25). The encoder relays the camshaft position to the control computer, and the computer calculates the timing of the fill valves. The user inputs an ignition delay, and the computer sends a spark signal at the appropriate number of milliseconds after the fill valves close. The spark signal is transmitted to the MSD ignition system by an ignition relay box. During each ignition event four 105-115 mJ discharges totaling 420-460 mJ are deposited in each tube by a modified automotive spark plug.

Pulse Detonation Research Engine

The valve trains of the research PDE are built from the head of a modified General Motors Quad Four engine. The head is a 16 valve, dual overhead cam design with separate camshafts for intake and exhaust. There are four valves per cylinder two for intake and two for exhaust. Figure 19 shows the head with the tubes removed so the valves are visible.

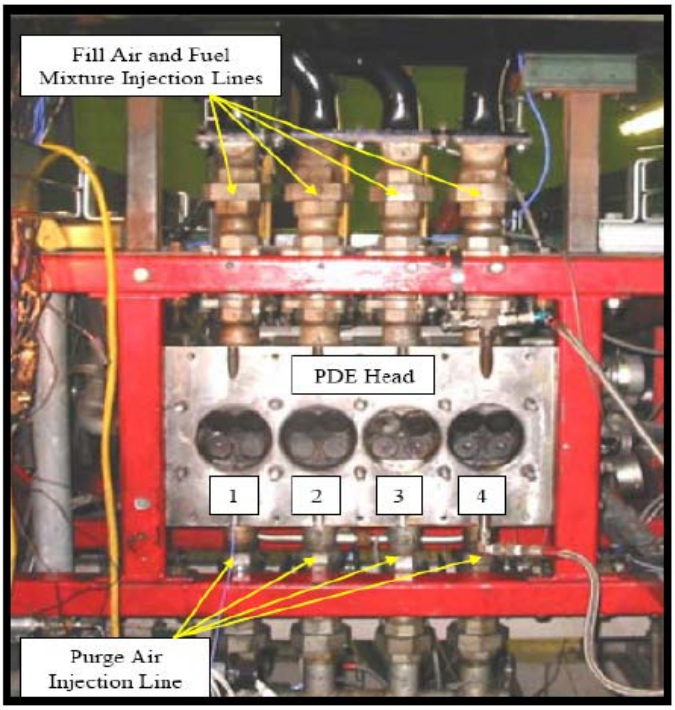

Figure 19. Photograph of PDE head with fill and purge lines labeled

The tube positions are also labeled. The firing order of the engine is 1-3-4-2. The head also has convenient passages for lubrication and water cooling. Both the fill and purge streams are delivered through the head. The fill stream passes through the intake valves and the purge passes through the exhaust valves. The camshafts are both driven by a variable speed Baldor electric motor (Model #M4102T). The motor speed is controlled by the control computer. The cams and valves are lubricated with automotive oil supplied by a Viking electric oil pump (Model #FH432). Cooling water is circulated by a 1.5 hp Teel electric water pump (Model #9HN01), and cooled via radiator and fan with test cell air. During operation of the engine the entire PDE cycle is driven by the speed of the Baldor electric motor. The fill and purge valves are driven by a cogged belt from the motor. The optical encoder signals the beginning of the cycle, also known as Zero-pulse or Z-pulse, when it senses a target mounted on one of the camshaft pulleys. The control

computer uses the Z-pulse frequency to calculate the ignition timing. Two fill valves open to admit fuel/air mixture into to thrust tube. Once the valves close and the ignition delay passes, the ignition system discharges igniting the mixture. Finally, the two purge valves open to expel the exhaust, and the cycle begins again.

Each experiment used two detonation tubes either in positions one and four or in positions two and three. Using two tubes use less fuel than four reducing the fuel demand and allowing longer runs before depleting the accumulators. Ball valves in between the manifold and the head prevent the flow of fuel/air mixture or purge air through positions lacking tubes. The ball valves are visible in Fig. 19.

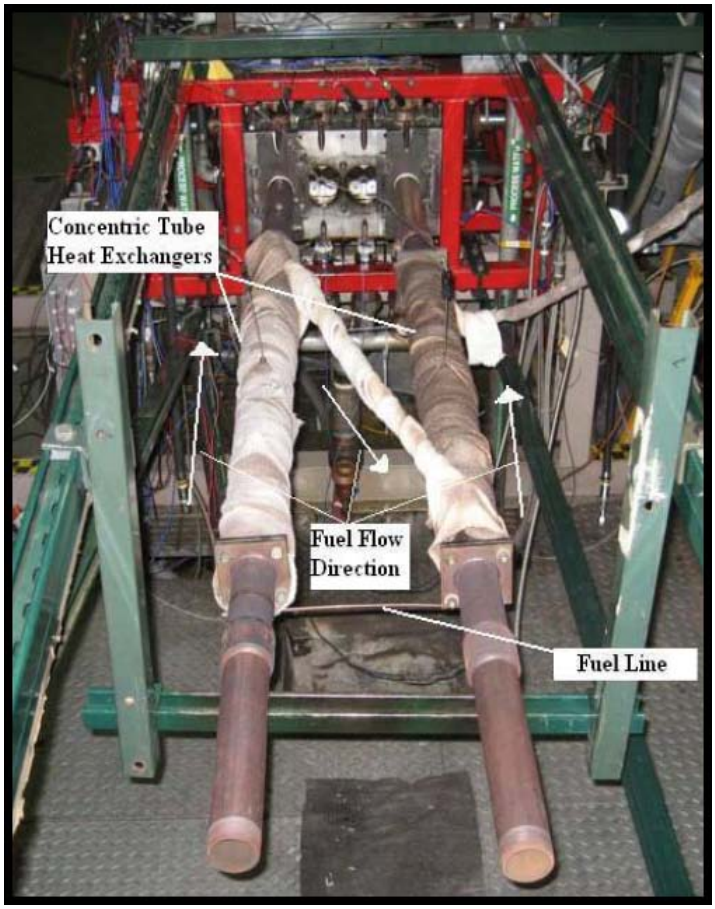

Figure 20. Photograph of the PDE with heat exchanger thrust tubes installed in positions 1 and 4

Figure 20 shows the tubes in positions one and four. This was the configuration for the experiments with JP-8 in catalyst coated tubes. Figure 21 shows the tubes in positions two and three.

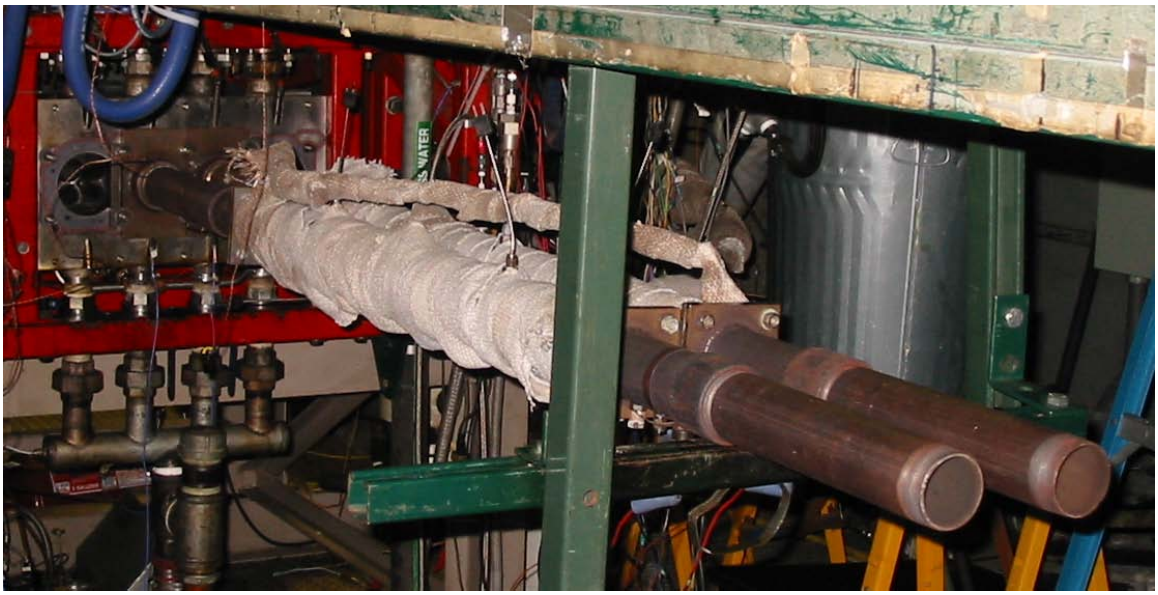

Figure 21. Photograph of the PDE with heat exchanger thrust tubes installed in positions 2 and 3

A two tube setup also reduces fluctuations in equivalence ratio that occur in single tube operation. When the engine operates on one tube, the air in the fill stream does not move for most of the cycle. However, the fuel flows constantly. This causes large fluctuations in the equivalence ratio of the fuel/air mixture. The phenomenon also occurs when two tubes are positioned in head positions that are adjacent in the firing order. For this reason when the valves in positions one and four were fouled prior to beginning the JP-7 runs with catalyst coated heat exchangers the setup was switched to positions two and three for the remainder of the experiments.

The detonation tubes are fabricated from inconel and include heat exchangers to heat fuel. Each tube is 1.91 m (6.27 ft) in length and contains a 1.22 m (4.00 ft) reinforced Shchelkin-type spiral to enable DDT. The thrust tubes are assembled from four pieces, a mounting plate, a standoff section, a heat exchanger section, and a tail section. The mounting plate mates with the head and is threaded with a 2” NPT pipe thread for attaching tube sections. The plates also hold the Shchelkin-type spirals in place. The standoff section provides enough separation between the head and the heat exchanger so that the fuel lines can be attached, and adapts from the thread of the mounting plate to the flanged connection on the heat exchangers. The standoffs are 0.33 m (13 in) long.

The next section of the thrust tubes is the heat exchangers. Each heat exchanger consists of a central passage for the detonation, and an annular passage for fuel to flow through. Two 3/8” Swage-lock fittings connect to fuel lines, and three ¼” Swage-lock fittings allow thermocouples to be inserted to measure intermediate fuel temperatures. The heat exchangers are 0.91 m (36 in) long and have flanged connections. The last part of a completed tube is the tail section. It is bolted to the end of the heat exchanger and is approximately 0.25 m (10 in) long. The tube assembly is supported at the tail section by a cross member to prevent excessive stress on the head bolts. An automotive head gasket was used to seal between the mounting plates and the head, and the assemblies, with spirals, were mounted to the head with nuts and washers. The fully assembled engine is shown in Fig. 20 with tubes in positions one and four.

Fuel Heating System

The fuel heating system centers around two pairs of inconel heat exchangers. The first pair was developed in earlier work (Helfrich, 2007), and all parts of the tubes that come in contact with fuel have been coated with a zeolite catalyst in a silica-alumina binder (sol-gel). The catalytic agent in zeolite is proprietary information. The second pair is the same except that the catalyst coating on the interior of the fuel passages was omitted so that the performance of the catalyst could be determined. The heat exchangers are a concentric double tube design. Figure 21 shows one of the heat exchangers.

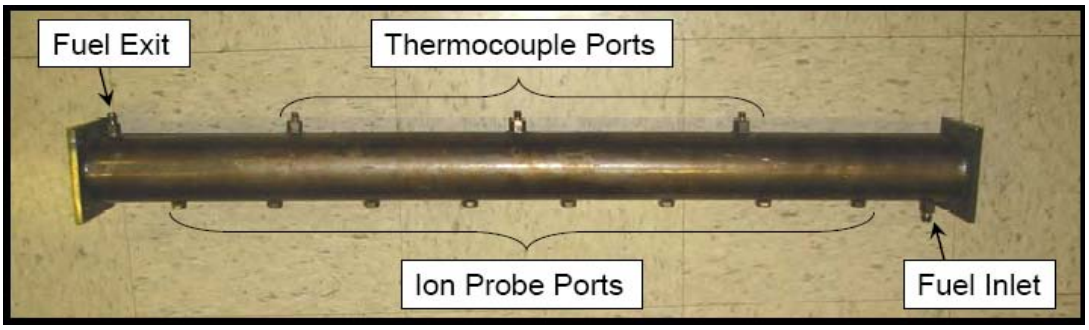

Figure 22. Photograph of the heat exchanger section of a thrust tube

Each heat exchanger was constructed on an inner 2 in Inconel 625 schedule 10 pipe and an outer 2 ½ in Inconel 600 schedule 40 pipe 0.91 m (36 in) in length. The pipes were welded concentrically on to 10.16 cm (4 in) square plates at each end. Three 3.25 mm (0.128 in) diameter ports were drilled through the outer tube, and 1/8" Swage-lock connectors were welded over the ports for thermocouples. Two more 6.35 mm (0.25 in) diameter ports were drilled, and ¼" Swage-lock connectors were welded over the ports for fuel line connections. Eight ports were drilled through both tubes, sealed with welds and threaded for ion probes. Detonation events transpire inside the inner tube, and fuel flows through the annular space between the inner and outer tubes. The heat generated by

the detonations raises the temperature of the fuel causing it to undergo pyrolysis. To increase the fuel temperatures further, the tubes and hot fuel lines were wrapped with high temperature cloth tape insulation.

As shown in Fig 23, during testing fuel, flows from the liquid fuel supply line into solid stainless steel fuel lines that can withstand the high temperatures near the heat exchangers. The fuel then flows through one heat exchanger counter the direction of the detonation wave. It then flows through a crossover line to the tail of the other heat exchanger. After passing through both heat exchangers, the fuel travels through another solid fuel line toward the spray bars. Along the way, it passes through a 7 micron filter (Fig #) to remove any contaminants which could clog the spray nozzles, and a small portion of the fuel is split off into the sampling system.

Sample Collection System

A recent work by Eric Nagley developed a reliable apparatus to collect samples of reacted fuel during operation of the PDE (Nagley, 2008:42). Figure 22 is a schematic drawing of the sampling system.

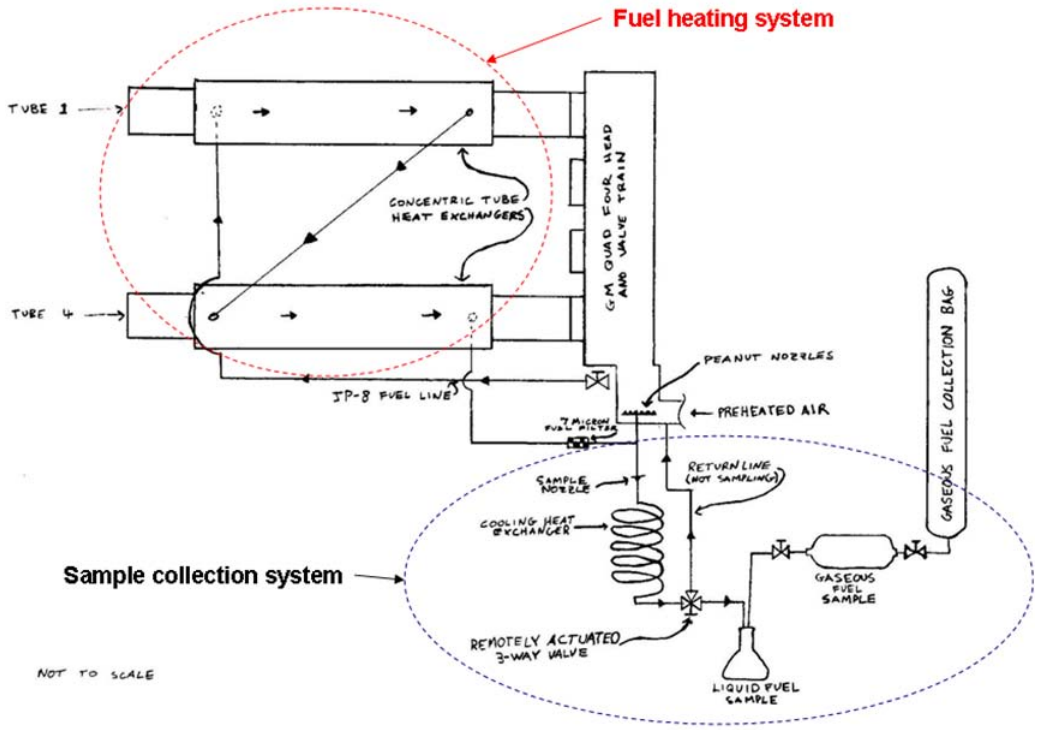

Figure 23. Sample collection system schematic

A portion of the reacted fuel is split off of the main fuel feed line downstream of the 7 micron filter and passed through a nozzle. The flow number of the nozzle determines the portion of fuel that split off from the main stream. Selection of the sample nozzle flow number (FN) in relation to the total flow number of the nozzles used in the spray bar allows control of the sample flow. The flow number of a nozzle is defined by Eq. 16.(Bartok, 1991:552:553)

$$FN = \frac{\dot{m}_{fuel}}{\sqrt{\Delta P_{fuel}}} \sqrt{\frac{\rho_{cal}}{\rho_{fuel}}} \tag{16}$$

The equation is specific to the English unit system, and requires the following units.

- mass flow rate of fuel ($\dot{m}_{fuel}$): lbm/s
- pressure drop across the nozzle (Δp_{fuel}): psi

The density of calibration fluid (ρ_{cal} = 760kg/m^3) and the density of the fuel (ρ_{fuel}) can be any consistent units as long as both are the same unit. During testing the density of fuel was equal for the sample nozzle and the spray bar nozzles, and the pressure drop across all the nozzles was the same. This was verified by measurement of the pressure drop in the previous work (Nagley, 2008:43). Because of these two facts, the ratio of the flow number of the sample nozzle to the total flow number of all the nozzles was the portion of fuel sent to the collection system.

Typically a sample nozzle flow number was selected that resulted in 10% of the total mass flow passing through the sample collection system. It was discovered in experiments that even though the fuel was filtered it was still at sufficiently high temperature for cracking to continue as the fuel flowed through the nozzles. This resulted in the build up of carbon deposits within all of the Delevan nozzles. The mass flow of fuel was monitored throughout experiments and held steady by hand adjustment of the accumulator pressure. When sufficient mass flow could no longer be sustained the nozzles were removed and cleaned. This did not address the relative amount of restriction in the sample nozzle compared with the spray bar nozzles. It was assumed that as the nozzles became restricted the maintained they same proportional mass flows.

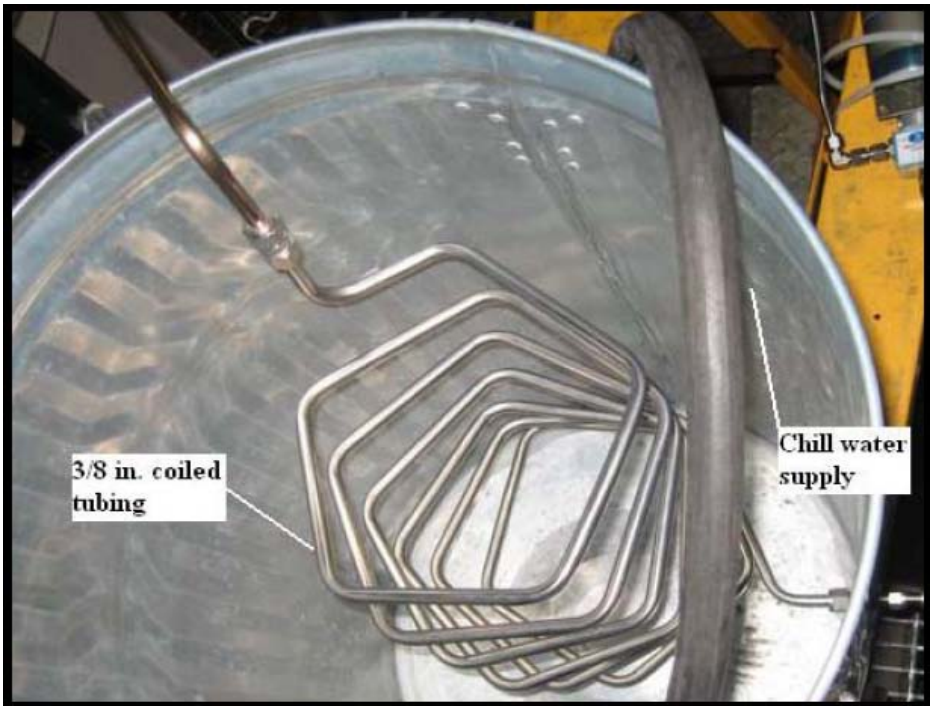

Figure 24. Photograph of interior of cooling water bath

After passing through the metering nozzle, the fuel entered a cooling water bath (Fig. 23). The fuel was cooled by the water stopping the chemical reactions in the fuel, and reducing the temperature to avoid damage to the rest of the sample collection system. Once the fuel was cooled it flowed to a pneumatic valve that selected one of two paths. The first path injected the fuel into the air manifold approximately 0.46 m (18 in) upstream of the spray bars. This was the bypass setting because it bypassed the collection flask and gas cylinder. This setting was used from the start of testing until the heat exchangers reached the desired temperature. The second setting allowed fuel to flow into the liquid collection flask (Fig. 25), the gas sample cylinder (Fig. 26), and the collection bag (Fig. 27). This setting was the collection setting and was used to collect fuel samples.

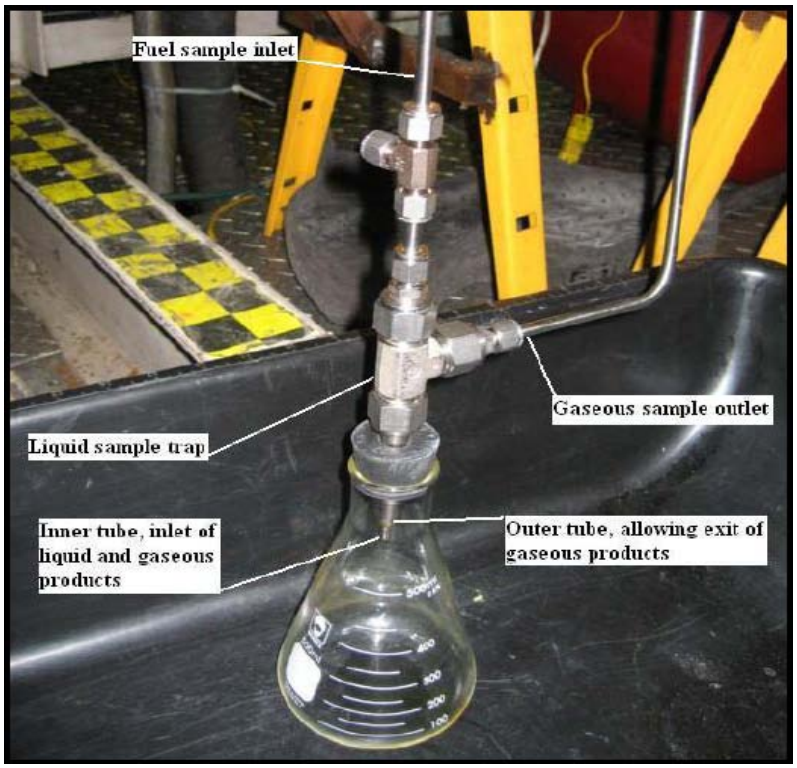

Figure 25. Sample collection flask

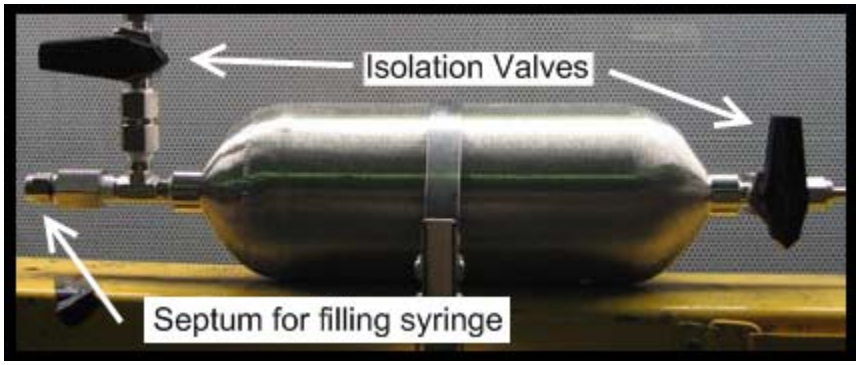

Figure 26. Gas sample cylinder

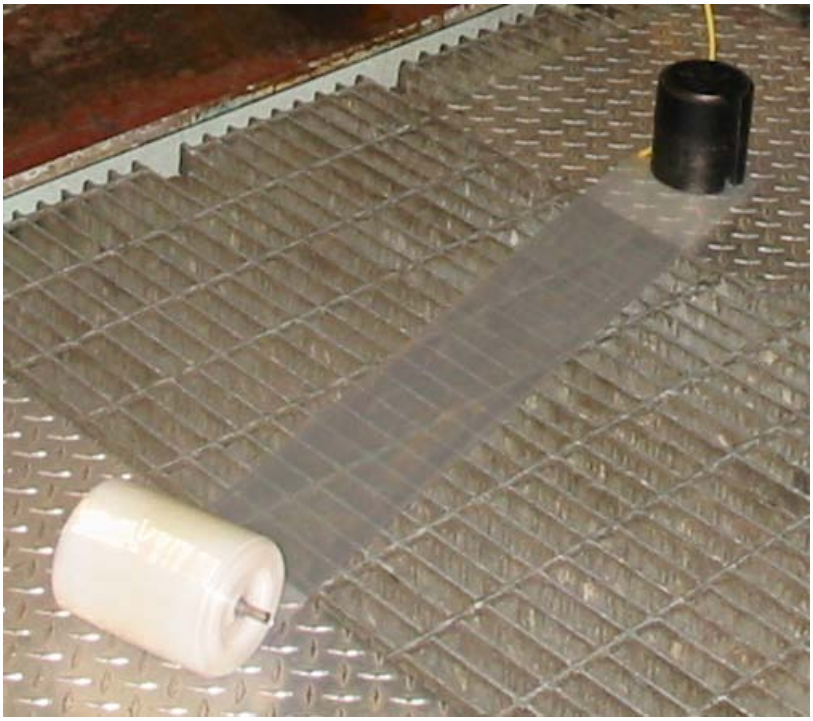

Figure 27. Gas collection bag

PDE Instrumentation

In order to duplicate the testing conditions in Nagley's JP-8 tests, the same instrumentation was used. Pressure transducers were placed at the head of each tube to measure the head pressure in the tubes. 1/16 in. J-type thermocouples were inserted into the fuel flow at five locations to measure temperatures. One was placed at the exit of the first heat exchanger in series, and one was placed at the entrance and exit of the second heat exchanger. The fourth thermocouple was placed where the fuel flow splits between the sample and spray bar streams roughly an inch upstream of the spray bar. The final thermocouple was placed downstream of the cooling water bath to ensure the fuel was cooled sufficiently to avoid damaging the components downstream. The maximum fuel temperature was taken to be that recorded at the exit of the heat exchangers.

Two ion probes were installed in the tail sections of each heat exchanger for measuring wave speed. The distance from the head to each ion probe is needed to determine the wave speed. The distances were measured and are recorded in Table 3.

Table 3. Ion probe locations

Experiment	JP-7 (Coated Tubes)	JP-7 and JP-8 (Uncoated Tubes)	JP-4 (Uncoated Tubes)
Ion Probe Locations (inches from head of tube)	Tube 2	Tube 2	Tube 3
	45	41	21
	53	45	25
	Tube 3	Tube 3	29
	45	41	33
	54	45	37
			41
			45

Test Procedure

Each test was run following the same procedures, and each resulted in a single pair of gas and liquid fuel samples. Prior to testing, the engine, fuel, and auxiliary equipment were prepared for a run. At least four hours before testing the fuel that would be used was transferred in to the sparging tank and the dissolved oxygen was removed. After sparging, a portion of the fuel was transferred to the accumulators, and enough fuel was flowed through the fuel lines to force out the residual fuel in the lines and any bubbles that could damage the flow meter. The lines were purged up to the LCV. Beyond the valve, the fuel lines were dry at the beginning of each test due to evaporation of the remaining fuel after the pervious test. The air compressor was started, and the air lines were bled for about 30 seconds to flush out any collected water or scale. The cooling water, and lube oil pumps were energized and the flows were checked to ensure good supply.

At this point the test cell was cleared of personnel, and the door was closed enabling fuel flow. The electric drive motor was energized allowing computer control. In the control room the fill fraction, purge fraction, tube volume, number of tubes, operating frequency, and critical flow air nozzle sizes were entered into the *LabVIEW®* program on the control computer. The engine was brought up to operating frequency, and air was flowed through the engine. The intake air heater was energized, and the air temperature was allowed to rise above 387 K (220° F). At this point the accumulators were pressurized and the igniters were energized.

Once the engine was prepped and the air was up to temperature, the test began. The LCV was opened flowing fuel into the engine and the air and fuel flow were adjusted until the mixture began to detonate. As the detonations began to warm the thrust tube heat exchangers, the fuel pressure was raised to keep the fuel from boiling in the heat exchangers. When the fuel boils, it produces an undesirable periodic variation in the flow of fuel into the rig. Careful monitoring of the fuel flow rate ensured that the fuel was not allowed to boil before reaching super critical pressure. The engine continued to operate until the fuel reached the desired heat exchanger exit temperature.

With the engine operating at the desired test point, a sample was collected. To collect a sample, the sample valve was opened remotely diverting fuel exiting the water bath into the sampling apparatus. Liquid was collected in the flask and gas passed through the gas cylinder into the collection bag causing it to unroll. While sampling, several high speed data sweeps were collected to measure ignition times, and wave speeds. Sampling was continued until the bag ran out of room to unroll, or until about 200 mL of liquid was collected whichever came first. Then the sampling valve was

closed, and the fuel flow and ignition were halted shutting down the engine and making it safe to enter the test cell. Out in the test cell, the volume of liquid collected, length of unrolled bag, and sampling duration were recorded. The gas sample cylinder was sealed and removed from the collection system, and the liquid was transferred into vials for storage and analysis.

After a successful test it was necessary to partly disassemble the rig to prepare for another test. Once the heat exchangers cooled to the point where work could begin, the reset began with the removal of both fuel filter bodies. The filters were replaced, and any carbon was removed from the filter bodies. The section of the fill air line containing the spray bar was removed and the nozzles were replaced with clean nozzles. The nozzle body containing the sample nozzle was also removed, and that nozzle was cleaned as well. The heat exchanger tubes were flushed with fuel to remove any residue, and the filter bodies, spray bar, and sample nozzle were reinstalled. The gas collection bag was deflated, and rolled back into its starting position. Next, a fresh gas sample cylinder was installed, and the sample collection flask was rinsed with acetone to remove any residue and dried before it was reattached to the rig. Finally, more fuel was transferred to the accumulators from the sparging tank. At this point heating of the fill air could resume in preparation for another test to begin.

IV. Data Analysis

Overview

The analysis of each experiment had two goals. The first was to examine the effect of catalysts and raw fuel composition on the stressed fuel collected. The

composition of the stressed fuel was determined through off line chemical analysis of the liquid and gas samples at the Air Force Research Laboratory, fuels branch (AFRL/RZTG). The fuel composition was the measure by which the different fuels and catalysts were compared. It was necessary to know the fuel composition in order to determine the heat added to the fuel by the heat exchangers, and to quantify the production of chemical species that are favorable to detonation. The second goal was to characterize the effect of stressed fuel composition on PDE performance. PDE performance is determined by a combination of data from the low speed and high speed data collection systems. Low speed data was collected throughout each run by the control computer, and sweeps of high speed data were collected by the high speed computer during sampling, Analysis of the high speed data yielded ignition times and wave speeds, while the low speed data provided fuel temperatures, pressures, and flow rates. Ignition times are important to reducing the length of the fire phase of the PDE cycle, while wave speeds tell whether the transition to detonation is successful.

Data Acquisition

The *LabVIEW*® control software is capable of collecting low speed (Hz to kHz) data. All thermocouple temperature readings, fuel flow measurements, air flow measurements, equivalence ratio, and selected pressure transducers were recorded by this system. The system performs calculations to determine equivalence ratio and mass flow rates, automatically reducing the amount of work that needs to be done later. The compiled data were organized in a Microsoft Excel® document after each day of testing. The high speed computer was used to collect detonation data from within the trust tubes.

The computer runs a *LabVIEW*® application titled *OnLineWavespeed* that collects up to 16 channels of data at scan rates in the MHz range. For all of the tests conducted with sampling, eight channels of data were recorded.

Channel 1: Spark discharge in tube 2
Channel 2: Head pressure in tube 2
Channel 3: Spark discharge in tube 3
Channel 4: Head pressure in tube 3
Channel 5: Ion probe located 41” from the head of tube 2
Channel 6: Ion probe located 45” from the head of tube 2
Channel 7: Ion probe located 41” from the head of tube 3
Channel 8: Ion probe located 45” from the head of tube 3

For the tests involving palladium catalysts seeded in JP-4, eleven channels were recorded

Channel 1: Spark discharge in tube 2
Channel 2: Head pressure in tube 2
Channel 3: Spark discharge in tube 3
Channel 4: Head pressure in tube 3
Channel 5: Ion probe located 21” from the head of tube 3
Channel 6: Ion probe located 25” from the head of tube 3
Channel 7: Ion probe located 29” from the head of tube 3
Channel 8: Ion probe located 33” from the head of tube 3
Channel 9: Ion probe located 37” from the head of tube 3
Channel 10: Ion probe located 41” from the head of tube 3
Channel 11: Ion probe located 45” from the head of tube 3

The software was initially set up to scan at a master scan rate 1,000,000 scans per second for 0.5 second intervals. This produced 500,000 data points per channel when triggered. The data was saved as approximately 20 megabits of binary data including a curve fit necessary to convert the data from binary to floating point values. The data had to be converted from binary to text so that it could be analyzed.

High Speed Data Reduction

A software tool was used to convert the raw binary output from *OnLineWavespeed* to floating point values. The program is named *PTFinder*, It is a C++® program that was developed specifically for the output of *OnLineWavespeed*. *PTFinder* separates the data into combustion events using the spark trace to signal a new event. The program analyzes each event to determine ignition times. Ignition time is defined as the time that passes between the discharge of spark energy, and the beginning of head pressure increase due to deflagration. The spark discharge occurs when the spark signal goes from high (~5V DC) to low (~0 VDC). For all experiments, a rate of pressure increase greater than 340.2 atm/s (5,000 psi/s) marked the beginning of deflagration. The slope of the head pressure trace was calculated for the rate of pressure increase.

To reduce the substantial high frequency noise in the pressure signals, the signal was passed through the Savitzky-Golay digital finite response filter (Parker. 2003:1). The fourth order, 401 point filter removed the high frequency noise with out distorting the shape of the pressure trace. *PTFinder* then calculated the slope of the pressure trace using linear regression of 1000 point sections. The slope was calculated starting from the beginning of a combustion event until the pressure rise exceeded 340.2 atm/s (5000 psi/s). The point in time at the center of the 1,000 point section that met the pressure threshold value was taken to be the time when ignition occurred. Figure 28 shows an example of the spark and pressure traces taken during experiments. The calculated ignition time has been overlaid on the graph.

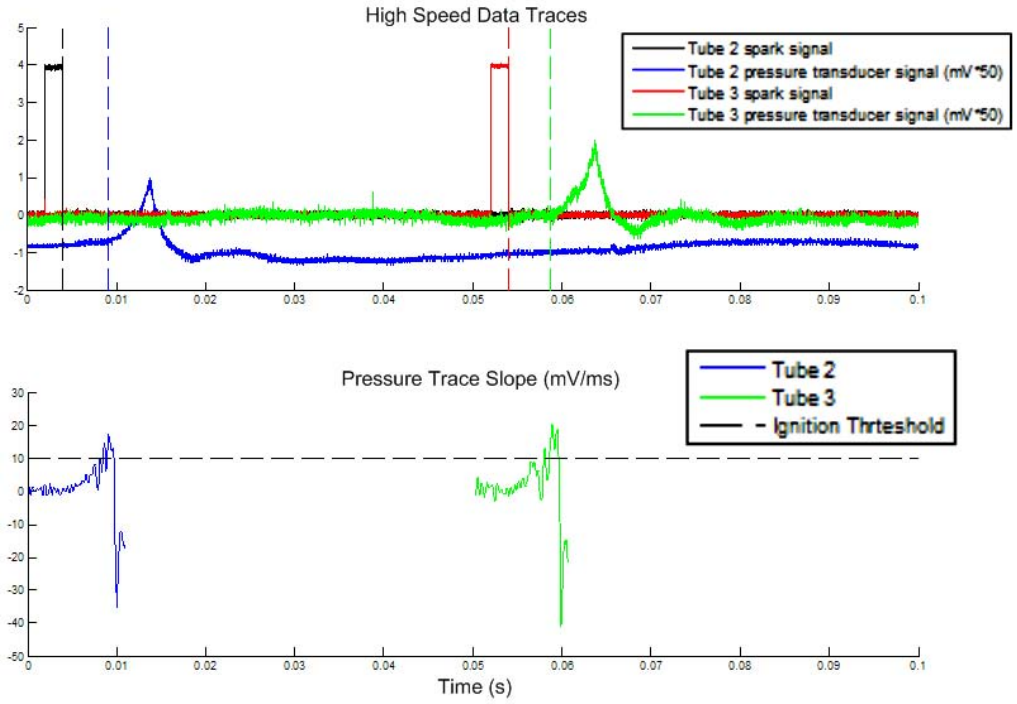

Figure 28. Sample of high speed spark and pressure traces

Gaseous Sample Analysis

The liquid and gas samples collected during testing were analyzed off-line. The volume of each gas sample was measured by measuring the length of the sample bag that unrolled during collection. The bag has a constant, circular cross-section with a diameter of 8.6 cm (3.39 in). The volume of gas collected was obtained by multiplying the length that the bag unrolled by its cross-sectional area. Analysis of the chemical composition of the gas collected in the sample cylinder was performed at the Air Force Research Laboratory, fuels branch (AFRL/RZTG). The samples were analyzed using an Agilent model 6890 gas chromatograph equipped with a thermal conductivity detector (TCD) and

a flame ionization detector (FID). Hydrogen was quantified using the TCD, and hydrocarbons were measured with the FID.

The gas chromatograph functions by retaining different compounds for different lengths of time depending on the volatility of the compound. A portion of the collected gas sample is injected into a column that retains the compounds. The chemicals exit the column in order of decreasing volatility. The length of time that a specific chemical compound remains in the column is referred to as its retention time. Hydrogen was quantified first with a 0.1 mL injection of the gaseous sample. After traveling through the column the hydrogen passed through the TCD. The TCD compares the thermal conductivity of the sample passing though it to the known thermal conductivity of the gas used to carry the injection. In this case, the carrier gas was argon. The TCD outputs a signal corresponding to the difference in thermal conductivity. Figure 29 shows an example of a TCD trace.

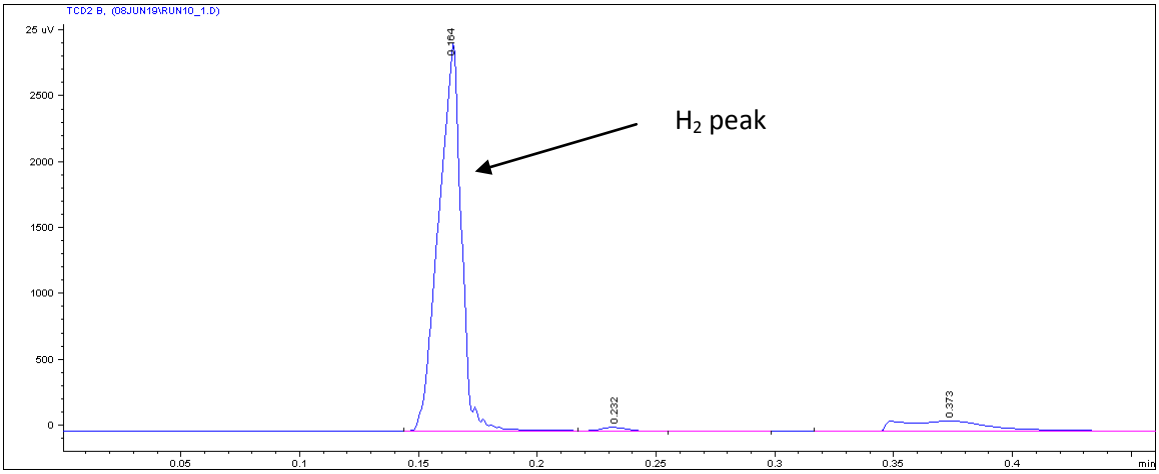

Figure 29. Sample TCD Trace

This signal was integrated to find area and translated to a hydrogen quantity through a calibration curve. The calibration curve was determined by injecting calibration gas with

known concentrations of hydrogen, and recording the TCD response. After the hydrogen, the hydrocarbons were quantified using the FID. A 10 μL portion of the gas sample was injected into the GC. After being separated by the column, each component of the sample was passed on to the FID. A mixture of hydrogen and air was added to the sample and ignited ionizing the carbon and producing electrons (Littlewood, 1970). The FID detected the reduction in resistance between two electrodes due to the ionization, and produced a signal. This signal consists of a multitude of peaks with each one corresponding to a specific hydrocarbon based on retention time as shown in Fig 30 (Cooper, 2003:4). The signal was integrated over each peak to measure the quantities of each component of the sample.

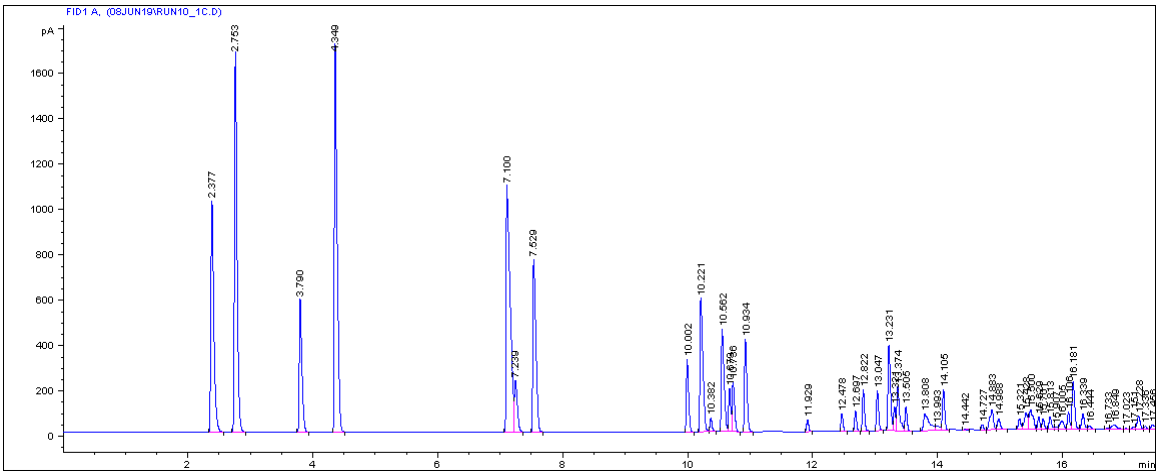

Figure 30. FID hydrocarbon trace

The quantities of the hydrocarbons were not determined with a calibration curve like the hydrogen. In order to identify a specific compound, the retention time of that compound must be known. Over 90 percent of the compounds present in the gas samples could be identified by their respective retention times. The remaining compounds were assumed to be C_6 hydrocarbons and were approximated as n-hexane throughout the

analysis. Standards of known composition were employed to provide a reference for the retention times of known compounds. The FID response for each compound was compared based on carbon number. The area of a peak on the FID signal is proportional to the number of carbon ions that pass through the detector. The GC integrated the FID signal to calculated the area of each peak ($Area_i$) and the total area. The ratio of the area of an individual peak to the total area was proportional to the product of the mole fraction χ_i and carbon number $n_{C,i}$ of that compound, shown in Eq 16.

$$\frac{Area_i}{\sum_i Area_i} \propto \frac{n_{C_i}}{\sum_i n_{C_i}} = \chi_i \tag{16}$$

Liquid Sample Analysis

The liquid portions of the collected samples were analyzed using two different techniques. Gas chromatography-mass spectrometry (GC-MS) was used to quantify a wide range of hydrocarbons including alkanes, alkenes, and multi-ring (three or more) aromatic compounds. An Agilent model 6890 gas chromatograph coupled with an Agilent model 5973 mass spectrometer was used to perform the analysis. Similar to the GC techniques used for the gas samples, the GC-MS separates the components of the liquid sample by volatility. However, the liquid sample must be diluted with hexanes before injection. Upon emerging from the column, the components pass through a detector which records an area that is used to quantify them. After the detector, the compound continues on to the MS where the compound is fragmented into characteristic ions, and the spectrometer determines the identity of the compound based on the number and type of fragments produced.

High Performance Liquid Chromatography (HPLC) was the second method used to quantify compounds in the liquid samples. The American Society for Testing Materials (ASTM) method D6379 was used with an Agilent model 1100 to perform the analyses. As in the GC-MS the liquid samples were diluted in hexanes before analysis. The HPLC also uses columns to separate compounds by volatility. HPLC was used to determine quantities of one and two ring aromatic compounds.

Calculated Percentage of Liquid Converted to Gas

Because the breakdown of hydrocarbons during pyrolysis results in the formation of lighter hydrocarbon species, one way to measure the extent of pyrolysis in the fuel is to measure the percent of fuel that was converted into gaseous species. Because buildup of deposits in the fuel system causes variation in the flow number of the nozzles, the mass flow rate of the fuel was unknown. It was necessary to determine the mass of both the liquid and gas portions of the sample. The sum of the masses of the liquid and gas was the total mass of the sample, and the liquid-to-gas conversion was the ratio of the gas portion to the total mass. The mass of the liquid was calculated by measuring the density of a small amount of the collected liquid and multiplying by the total collected volume. The density was calculated by measuring the mass of one milliliter of the liquid sample. The mass of the gas was calculated using a combination of the ideal gas law and the results of the GC analysis. The total number of moles of gas was determined from the ideal gas law (Eq. 17)

$$n_{vap} = \frac{PV}{RT} \tag{17}$$

The temperature (T) and pressure (P) in Eq. 17 are the ambient temperature and pressure at the time the volume of the collection bag was measured. V is the measured volume, and R is the universal gas constant (8.314 J/(mol*K) or 10.732 (ft^3*psi* lb)/(mol*°R)). Then, through Eq. 18, the number of moles of each component of the gas was calculated using the mole fractions found by the GC.

$$n_i = \chi_i MW_i \tag{18}$$

Next, the number of moles of each component was multiplied by molecular weight to give the mass of that component. The total mass of the gas was the sum of masses of all the individual components using Eq. 19.

$$m_{vap} = \sum n_i \, MW_i \tag{19}$$

Calculation of Heat Addition

Initially in the analysis of pyrolysis of fuel by PDE waste heat it was assumed that the mass flow rate of fuel through the thrust tube heat exchangers would be constant (Nagley, 2008:66). Utilizing this assumption, the break down of the fuel was compared to the heat exchanger exit temperature. The result was data that exhibited non-linear variation that corresponded to the different calculated residence times for the fuel. In this work, exit temperature has been abandoned in favor of a better measure of the amount of energy transferred to the fuel. As long as the composition of the raw fuel going into the heat exchangers and the stressed fuel exiting are known, a control volume can be drawn to include all of the fuel that is within the heat exchangers, and an energy balance can be calculated (Eq. 20).

$$\Delta h = \sum_{i=1}^{n} \chi_{out_i} C_{p_i}(T_{out}) \, T_{out} - \sum_{i=1}^{n} \chi_{in_i} C_{p_i}(T_{in}) \, T_{in} \tag{20}$$

The temperature of the fuel entering the heat exchangers is the ambient temperature of the test cell during testing (T_{in}).The exit temperature of the fuel (T_{out}) was measured via thermocouple. The mole fractions of the components of the fuel (χ_i) were determined by the GC, GC-MS, and HPLC techniques previously mentioned. The specific heats of the components ($C_{p,i}$) were taken from National Institute of Standards and Technology (NIST) webbook online reference, and from Thermodynamic Research Center (TRC) tabulated data. The specific heats of compounds are functions of temperature, and a fourth order polynomial fit of the tabulated data (Eq. 21) was used to estimate the specific heat at the measured temperatures. The result of Eq. 20 is the change in enthalpy of the fuel in J/g.

$$C_{Pi}(T) = a \cdot T^4 + b \cdot T^3 + c \cdot T^2 + d \cdot T + e \qquad (21)$$

The chemical analyses of the fuel samples yielded mole fractions for the 117 different chemical species and groups of species listed in Table 4.

Table 4. Chemical species included in heat addition calculation

Hydrogen	Benzene	Nonene_1	Pyrene
Methane	methyl_Hexane	n_Nonane	benz_a_Anthracene
Ethane	Cyclohexene	Nonene	Chrysene
Ethylene	dimethyl_Cyclopentane	C3_Alkylbenzenes	benzo_b_Fluoranthene
n_Propane	methyl_Hexene_a	Decene_1	benzo_k_Fluoranthene
Propylene	Heptene_1	trimethyl_Benzene_1_2_4	benzo_a_Pyrene
iso_Butane	n_Heptane	C3_Alkylbenzenes_2	indeno_1_2_3_cd_Pyrene
n_Butane	dimethyl_Cyclopentene	Indane	dibenz_a_h_Anthracene
trans_2_Butene	Heptene	C4_Alkylbenzenes	benzo_g_h_i_Perylene
Butene_1	Heptene_a	Butylbenzene	methyl_Octane_3_2
iso_Butylene	methyl_Cyclohexane	C4_Alkylbenzenes_2	n_Nonane_2
cis_2_Butene	ethyl_Cyclopentane	C4_Alkylbenzenes_3	dimethyl_Octane
iso_C5	methyl_Cyclohexene	Undecene_1	methyl_Nonane_2
n_Pentane	ethyl_Cyclopentene	C5_Alkylbenzenes	n_Decane
Butadiene	Octene	Pentylbenzene	butyl_Cyclohexane

Table 4. Chemical species included in heat addition calculation (continued)

Methylenes	methyl_Heptane	C5_Alkylbenzenes_2	trans_Decalin
Pentene_1	Toluene	Tetralin	methyl_Decane_2
Gaseous Hexane	methyl_Cyclohexene_a	Naphthalene	methyl_Decane_3
Propene	dimethyl_Cyclohexane	Dodecene_1	n_Undecane
methyl_Propene	Octene_1	methyl_Naphthalene_2	n_Dodecane
methyl_Butane	dimethyl_Cyclohexene	methyl_Naphthalene_1	n_Tridecane
Pentene_1	n_Octane	dimethyl_Naphthalenes	methyl_Tridecane
n_Pentane_a	Octene_a	dimethyl_Naphthalene_1_3	n_Tetradecane
Hexene_1	dimethyl_Cyclohexene_a	dimethyl_Naphthalenes_2	methyl_Tetradecane
n_Hexane	ethyl_Cyclohexene	Acenaphthylene	n_Pentadecane
Hexene	Ethylbenzene	Acenaphthene	n_Hexadecane
methyl_Cyclopentene	p_Xylene	Fluorene	n_Heptadecane
methyl_Cyclopentane	m_Xylene	Phenanthrene	
methyl_Cyclopentene_a	methyl_Octane_3	Anthracene	
methyl_Hexene	o_Xylene	Fluoranthene	

The chemical species listed account for part of the total mass of the samples. Table 5 shows what percent of the total mass is accounted for in each sample. This is the major weakness in the heat addition analysis. Because the total mass fraction of all the measured species (those listed in Table 4) varies so widely across the samples there is not a constant correlation between the heat added to the measured species and the heat added to the whole mixture.

Figure 31 shows that $\chi_{measured}$ increases with heat addition, and the correlation is nearly linear. This suggests that the list of chemical species favors species with lighter molecular weights and does not account for many of the heavier liquid species present.

Table 5. Mass accounting in heat addition calculation

Fuel	Heat Addition (J/g)	Mass accounted for at T_{exit}
JP-8	0 (Neat)	36.6%
Coated Heat Exchangers	1866	67.4%
(Samples Collected by	1667	62.2%
Nagley)	2036	74.1%
	2038	73.8%
	879	40.1%
	1413	55.8%
	1028	44.3%
	2049	73.3%
	2067	71.4%
	2045	71.9%
	2637	87.7%
JP-7	0 (Neat)	26.8%
Coated Heat Exchangers	955	39.6%
	986	40.4%
	1190	46.9%
	1136	44.8%
	1212	48.6%
	1028	41.8%
	1013	41.7%
	941	39.2%
	1392	53.4%
	1506	57.0%

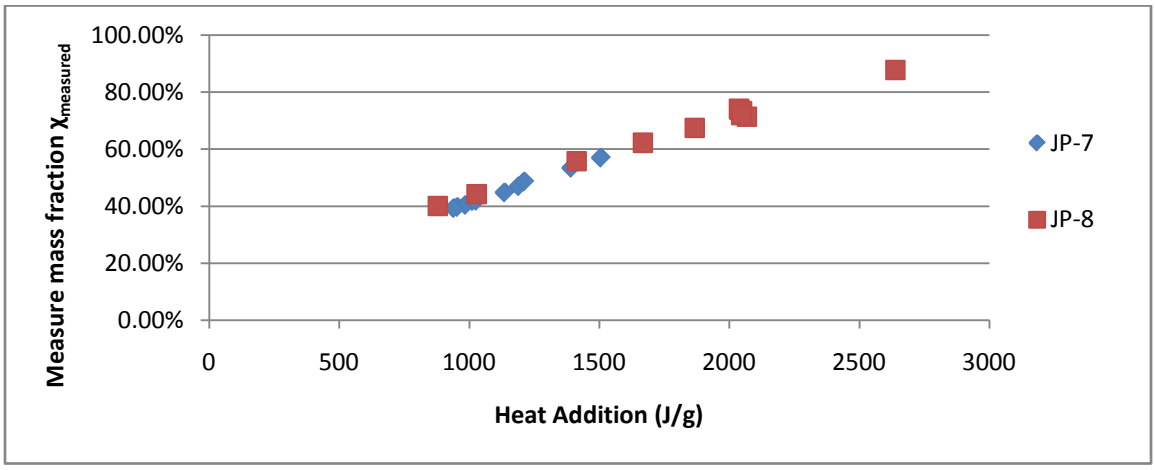

Figure 31. Mass accounting trend

The other factor that contributes to the inaccuracy of the heat addition calculation is the fact that not all of the species included have published values of specific heat. For groups of species, the average of the specific heats of the isomers was used in place of the table values. For individual species, a best guess approximation was made of the specific heat values. As an example there was no specific heat data available in either the NIST webbook or the TRC tables for methyl-cyclohexene. However, data for methyl-cyclopentene, cyclopentene, and cyclohexene were available. The specific heat of methyl-cyclohexene was approximated by adding the difference in specific heat between methyl-cyclopentene and cyclopentene to the specific heat of cyclohexene. This method gives a reasonable approximation of the specific heat of methyl-cyclohexene. Similar methods were used to obtain specific heats for dimethyl-cyclopentene, methyl-hexene, and ethyl-cyclohexene. There was no data available for 1-Octene or benzo-b-fluoranthene so the NIST entries for Octene and benzo-k-fluoranthene were used as substitutes.

Despite the variation in measured mass fraction, the heat addition results show a much greater linearity when plotted against liquid to gas conversion (Fig 31).

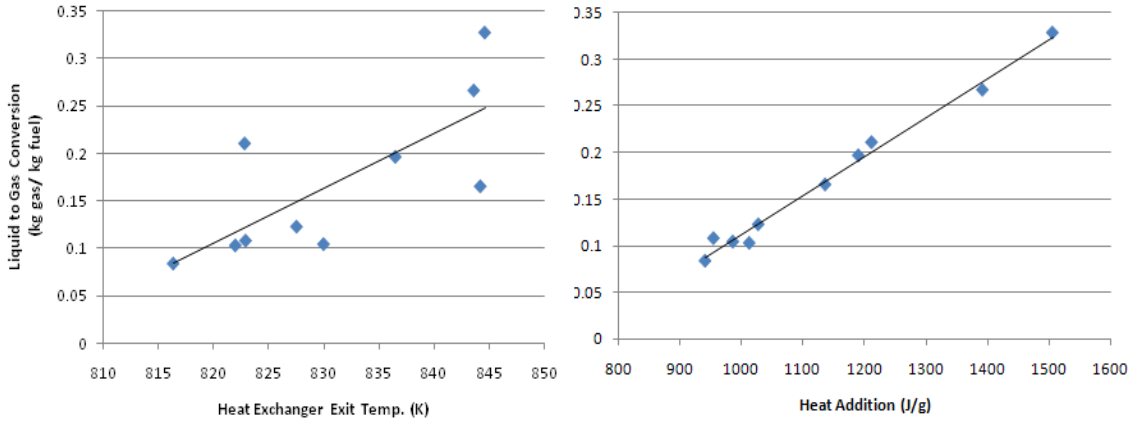

Figure 32. Improvement of linearity when using heat addition

Linear regression of the liquid to gas conversion curves for JP-7 shows that the R^2 increases from 0.5608 to 0.9882 by switching from exit temperature to heat addition. Because heat addition takes into account the changes in chemical composition, the measured mass flow rate of fuel, as well at the fuel temperatures it is a better choice for the independent variable when comparing the performance of the PDE and the fuel heating system than heat exchanger exit temperature.

Error Analysis

Because the goal of this work was to expand on Nagley's work done with JP-8 and much of the same apparatus was used, the experimental uncertainty is identical to that of the JP-8 experiments. The only additional measurement for which experimental uncertainty needs to be examined is for the heat addition described in the last section. As in every case the total uncertainty of a measurement is a combination of the bias limit (B_x) and the precision limit (P_x). Equation 22 shows how the two are combined to give the total uncertainty.

$$U_x = [B_X^2 + P_x^2]^{0.5} \tag{22}$$

Precision error is the effect of random factors that influence the measurement (Colemn, 1989:7). It is sometimes referred to as repeatability or repeatability error. If a measurement were repeated an infinite number of times, the results would fall into a Gaussian or normal distribution. This infinite sampling is referred to as the parent distribution, because any finite set would be contained within the infinite sample. A finite set of repeated samples of a measurement is referred to as a sample population. By examining the sample population and choosing a confidence interval, the precision error

of the sample population can be calculated. The mean of the sample population ($\overline{X}$) is found by evaluating Eq. 23.

$$\overline{X} = \frac{1}{N}\sum_{i=1}^{N} X_i \tag{23}$$

N is the number of readings, X_i, that make up the sample. The standard deviation of the sample (S_s) is found by evaluating Eq. 24.

$$S_x = \left[\frac{1}{N-1}\sum_{i=1}^{N}\left(X_i - \overline{X}\right)^2\right]^{0.5} \tag{24}$$

The confidence interval is a somewhat arbitrary choice of a range in which the mean of the parent population is expected to fall. For Nagley's work a confidence interval of 95% was used, and the same interval was used here. In other words there is a 95% certainty that the mean of the parent population will fall within the uncertainty bounds ($\overline{X}\pm P_X$). Because the sample population does not have a normal distribution, it is necessary to use a t-distribution to define the confidence interval in order to determine the precision limit. Eq. 25 gives the formula for finding the precision limit from the sample standard deviation, t-distribution, and number of readings.

$$P_X = tS_X/\sqrt{N} \tag{25}$$

Bias error is associated with the equipment and methods used to take measurements. Specifically, bias errors occur due to calibration, data acquisition, and data reduction. The elemental bias limit (B_r) is found by calculating the root sum square of the elemental bias limits (B_i) of each of m number of elements (Eq. 26).

$$B_r = \sqrt{\sum_{k=1}^{m}(B_i)_k{}^2} \tag{26}$$

Elemental bias limits propagate through data reduction equations and affect experimental results. The bias limit (B_x) of an experimental result (x) is calculated through Eq. 27.

$$B_X = \sqrt{\sum_{j=1}^{i} \left[\left(\frac{\partial r}{\partial X_j} \right)^2 B_j^2 \right]} \tag{27}$$

Utilizing equations 26 and 27, the bias limits for heat addition ignition time, liquid-to-gas conversion, and mass fraction were found. The average uncertainty for heat addition was 0.0074% with a maximum of 0.0098%. The average uncertainty in ignition time was 21.3% with a maximum of 53.4%. The average uncertainty in liquid to gas conversion was 9.1% with a maximum of 16.7%. The full uncertainties in heat addition, liquid-to-gas conversion, ignition time, and mole fraction are tabulated in Appendix B.

V. Results and Discussion

Overview

This research looked at the performance of fuels when subjected to pyrolysis by the waste heat of a PDE, and at the performance of a PDE running on the stressed fuel. The cracking characteristics of fuels can be established by comparing liquid to gas conversion, production of species with good detonability, and the consumption of the species that make up the raw fuel. The production of gaseous species is an aggregate measure of the extent to which the fuel reacts during heating. High liquid-to-gas conversion ratios indicate that the fuel requires less energy to undergo pyrolysis. A low energy requirement is desirable because the heat loads on the heat exchangers can be reduced. As discussed in chapter two, hydrogen, acetylene, ethylene, and ethane have lower initiation energies than other hydrocarbons. Reacted fuels showing high fractions of these compounds will exhibit better detonation properties than samples with low

concentration. Oppositely, samples containing high concentrations of methane will have increased initiation energies, and, as a result, worse performance. While the consumption of species that make up the raw fuel does not directly contribute to the performance of the fuel, the more of the raw fuel that begins to undergo pyrolysis, the more free radicals are available to produce products that could aid ignition and detonation. In this way the consumption of high molecular weight species during heating is a second measure of the extent of reaction.

There are three important figures of merit for determining the performance of a PDE with an endothermic fuel heating system. Heat capacity measures the ability of the fuel heating system to carry away the heat produced by detonation within the thrust tubes. The heat capacity is determined from the heat added to fuel at a specific heat exchanger exit temperature. Ignition time is a direct measurement of the performance of the PDE while running on pyrolized fuel. The rate at which solid carbon precipitates from the fuel sets the length of time the engine can run before it must be shut down for maintenance. As discussed in chapter two the concentration of polycyclic aromatic hydrocarbons in the reacted fuel provides a relative measure of the solid carbon formation in different samples.

Heat Sink Capacity

Figure 33 shows the heat addition to JP-8 and JP-7 as a function of heat exchanger exit temperature for both sets of heat exchangers. The performance of an endothermic heating system can be compared to a situation where the composition of the fuel remains constant. The extra heat addition that occurs due to the pyrolysis of the fuel is the added benefit of the heat exchanger. A comparison can be drawn between different

fuels and catalysts by looking at the extra heat addition that occurs for similar values of the exit temperature.

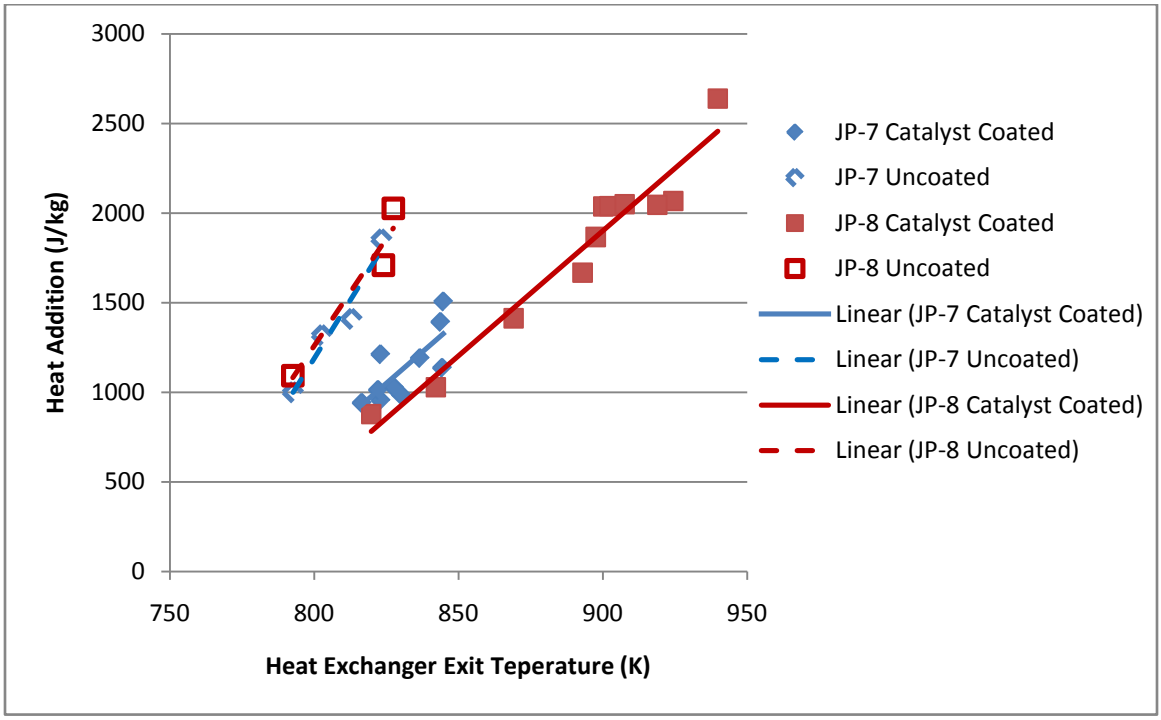

Figure 33. Heat sink capacity of JP-7 and JP-8

The most noticeable trend in Fig 33 is the difference between catalyst coated heat exchangers and uncoated heat exchangers. The heat addition is significantly higher for the untreated tubes suggesting that the catalyst is reducing the heat absorption. One observation that can be made about the catalyst is that it appears to affect the heat addition into JP-8 more than into JP-7.

The additional heat absorbed during experiments with uncoated tubes, and JP-7 resulted in a lower limit to the temperatures that could be attained using waste heat from the PDE. While this is good for the life of the heat exchangers, because of the reduced thermal loading, it meant that the highest temperature that could be reached during testing was 825 K for both fuels in the uncoated heat exchangers, and 845 K for JP-7 in the

coated heat exchangers. The highest temperature attained with JP-8 was 940 K using the catalyst coated heat exchangers.

Ignition Times

Ignition times are the most direct measure of PDE performance available from the data collected. Reductions in ignition time directly affect the length of the fire phase of the PDE cycle. Figure 34 show the ignition time result for all tests with JP-7 and JP-8.

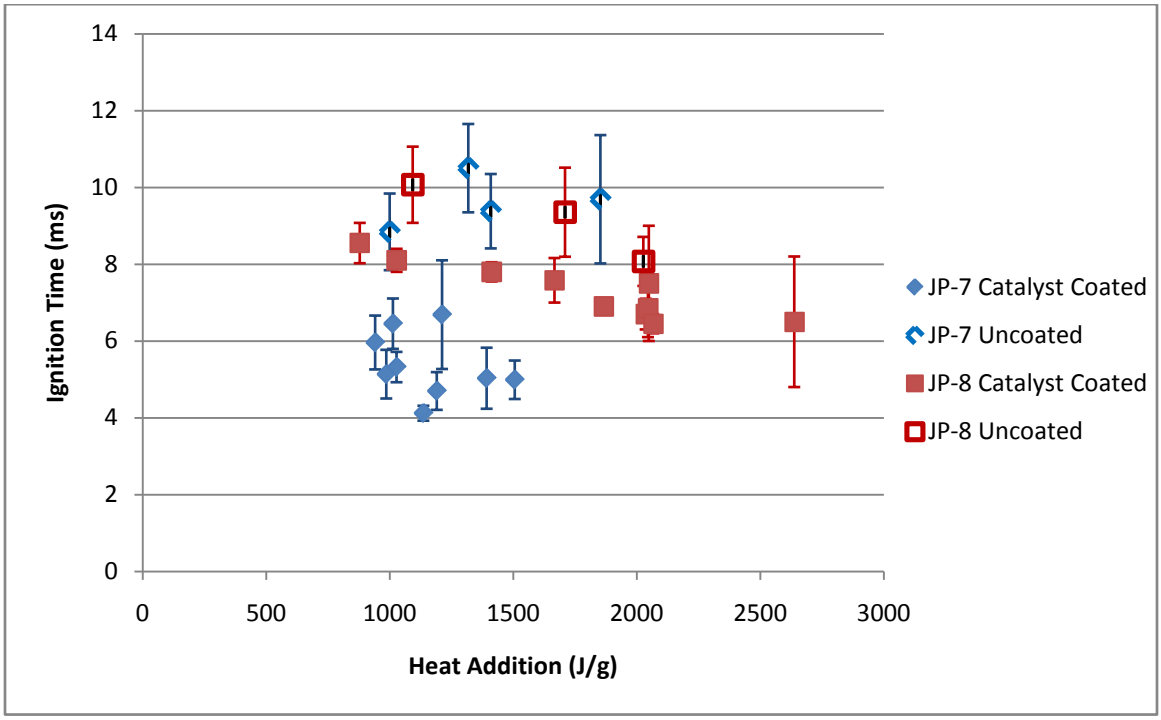

Figure 34. Ignition time results

The ignition times for the catalyst coated heat exchangers is uniformly lower than the ignition times from the uncoated tubes. The catalyst has a positive influence on ignition times for both fuels. The average reduction for JP-7 was 4.23 ms or 44%, and the average reduction for JP-8 was 1.78 ms or 20%.

There was little difference between the ignition times for JP-7 and JP-8 in the uncoated heat exchangers. The standard deviations in the data (plotted as error bars) are too large to make a comparison between the two fuels or to establish temperature trends. The experiments using the catalyst coated tubes had reduced variation, and the trends can be reasonably determined. The catalyst had more influence on the ignition times for JP-7. Figure 35 shows the ignition times recorded from the catalyst coated heat exchangers only.

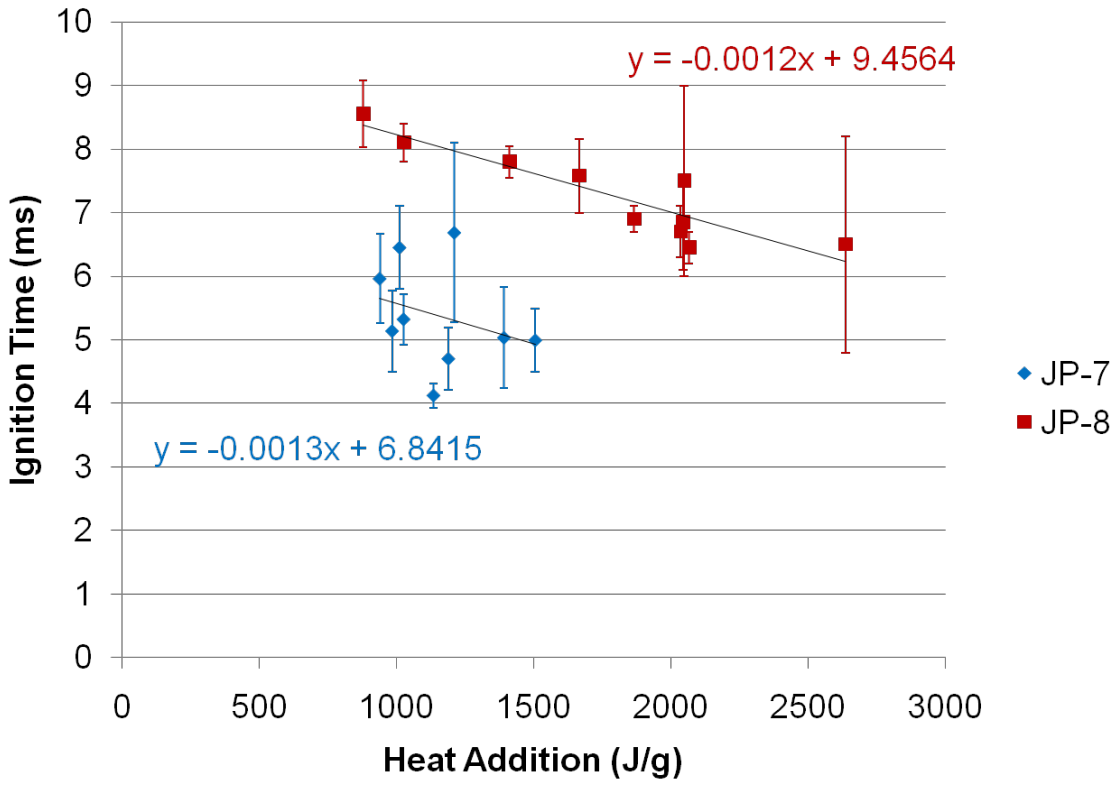

Figure 35. Ignition times as a function of heat addition for ϕ≈1

It is clear from Fig. 35 that JP-7 outperforms JP-8 both in the total ignition time and in the rate of decrease in ignition time as heat addition rises. This result is reinforced by the gas production results presented later in this chapter.

Coking

Coking is a serious problem in running experiments where pyrolysis of fuels occurs. Figure 36 shows the result of coking on a fuel filter.

Figure 36. Photograph of carbon build up on a filter after one run next to a new filter

As explained in Chapter IV, the production of solid carbon during the pyrolysis of the fuel is related to the amount of polycyclic aromatic hydrocarbons (PAH's) present in the collected fuel sample. PAH's are the precursor to the solid carbon that forms. An ideal fuel would produce no PAH's and as a result no solid carbon. Figure 37 is a plot of the PAH mass fraction for JP-7 and JP-8 samples collected from the zeolite coated heat exchangers.

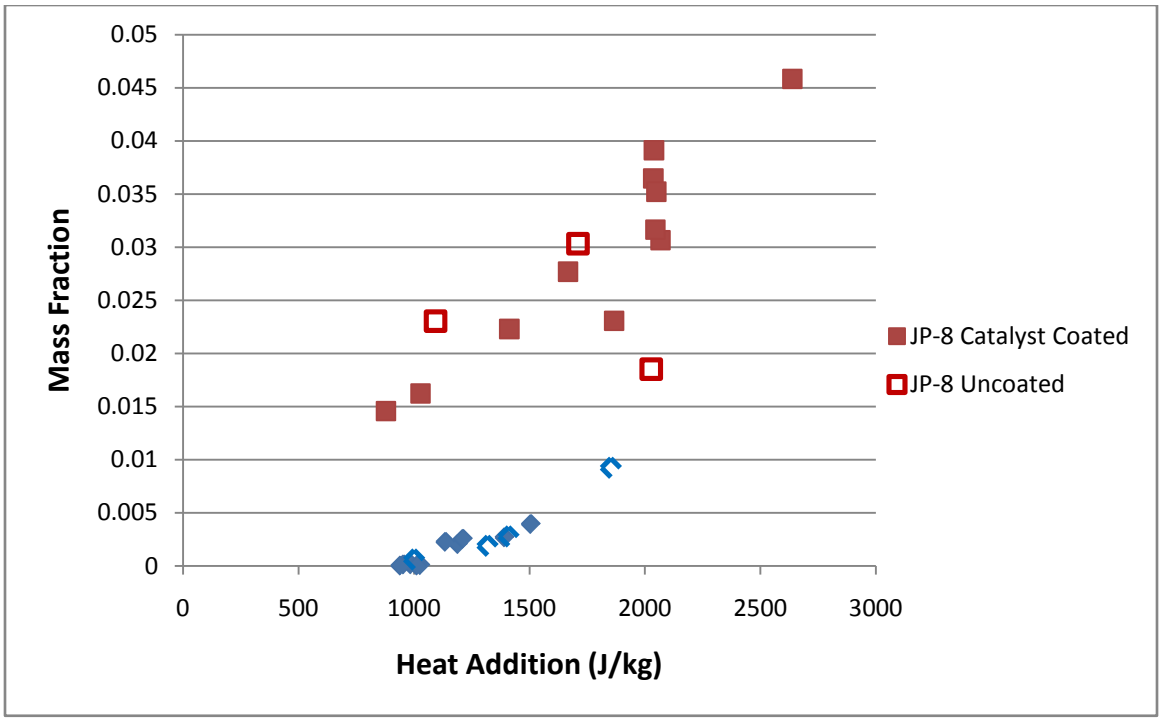

Figure 37. Comparison of PAH concentrations

The figure shows that JP-7 samples have much lower PAH concentrations. This was expected due to the low initial aromatic content of the fuel. The figure does not show any improvement in PAH concentration due to the presence of a catalyst.

Mass Based Liquid to Gas Conversion

The easiest measurement of heat exchanger performance to acquire was the liquid to gas conversion. It only required GC analysis of the gas sample and the density of the liquid sample instead of the full chemical analysis of the liquid sample that was necessary to calculate heat addition. At the beginning of testing, it was not known which fuel would produce the highest gas conversion or what effect the catalyst produced. It was incorrectly assumed that the properties that gave JP-7 high thermal stability (low

aromatic content and high saturation) would reduce the production of gaseous species. After calculating the liquid to gas conversion, it was clear that the opposite was true. JP-7 produced more gas by mass than JP-8 as shown in Fig 38. The gas production of JP-7 was not any greater with the catalyst coated tubes than with the uncoated heat exchangers. JP-8 showed reduced liquid-to-gas conversion in the catalyst coated heat exchangers.

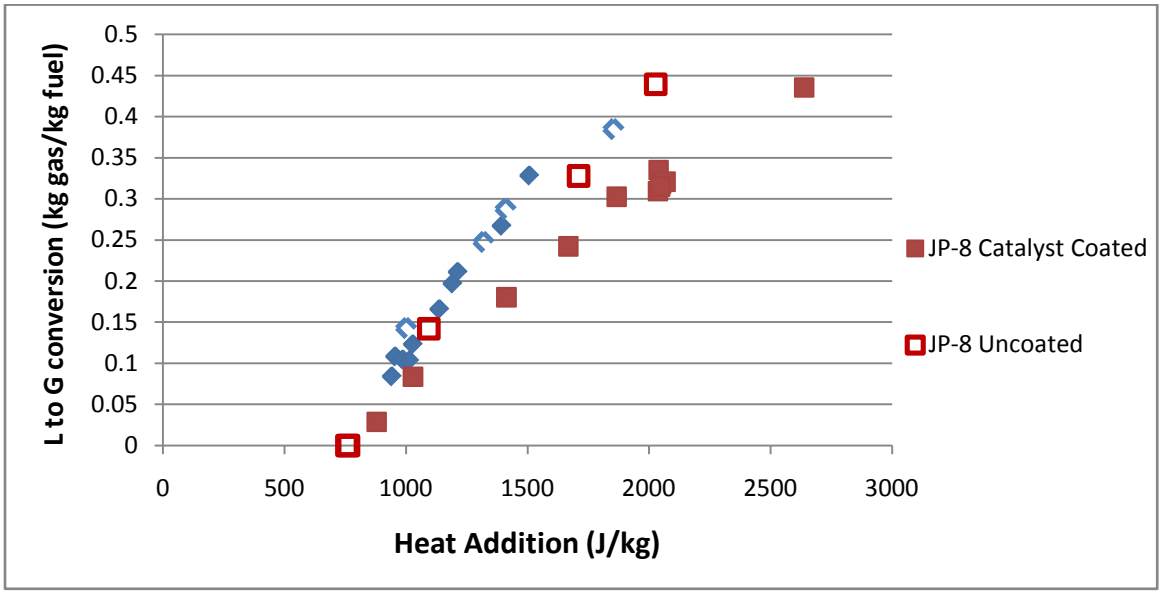

Figure 38. Liquid-to-gas ratio as a function of heat addition

Vapor Composition

Analysis for the gas samples collected showed increased production of all gas species with increased heat addition. The mass fractions of hydrogen produced were an order of magnitude smaller than the mass fraction of other species. This is misleading because the molecular weight of hydrogen is six times smaller than the molecular weight of methane which is the next smallest. Figures 39 through 42 show the mass fractions of the six lightest compounds in the gas samples. In all of the figures, the mass fractions of

propylene, n-propane, and methane are close together, and thy increase at similar rates. Ethylene mass fraction increases at a slower rate, and begins to level out after 1700 J/g.

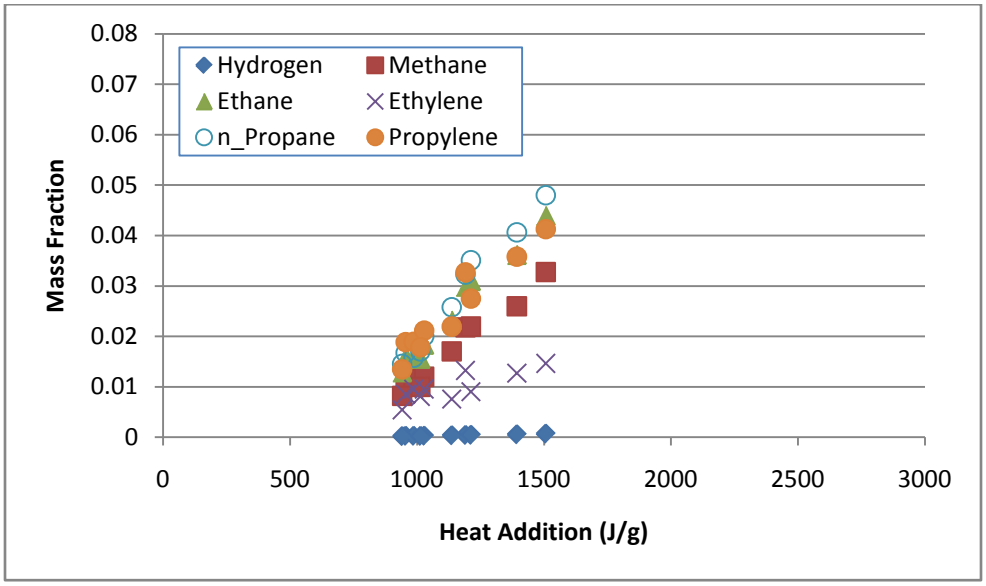

Figure 39. Gas species production: JP-7 in catalyst coated heat exchangers

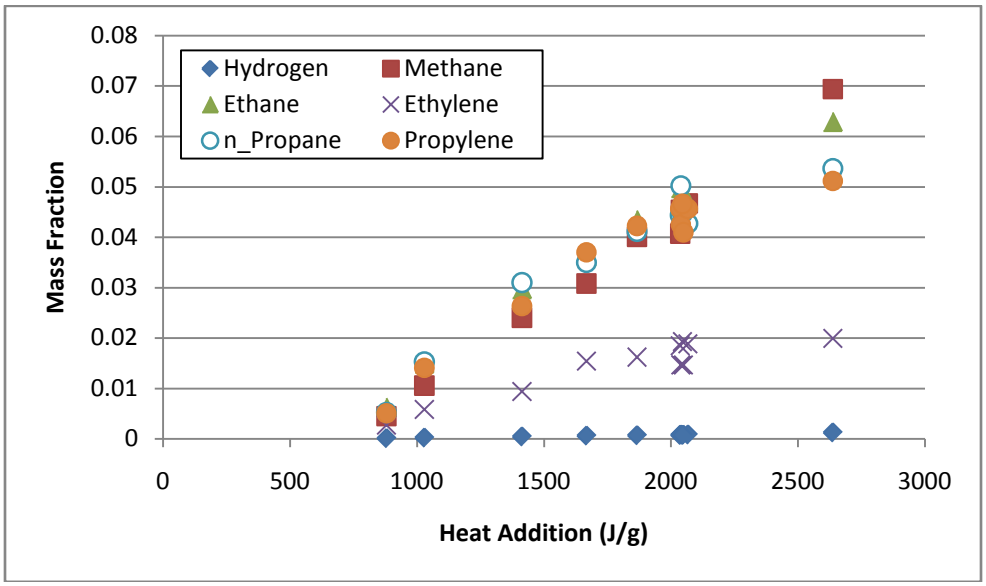

Figure 40. Gas species production: JP-8 in catalyst coated heat exchangers

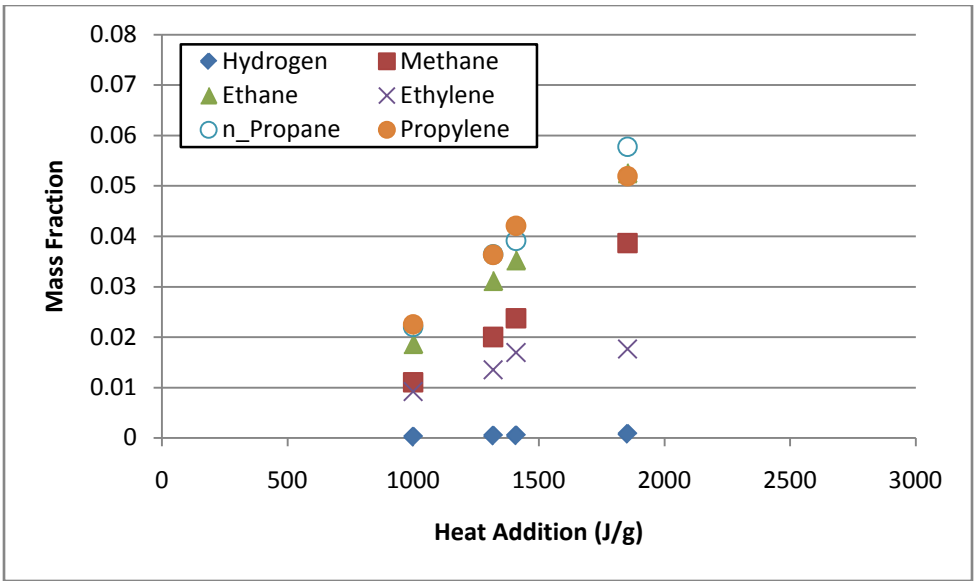

Figure 41. Gas species production: JP-7 in uncoated heat exchangers

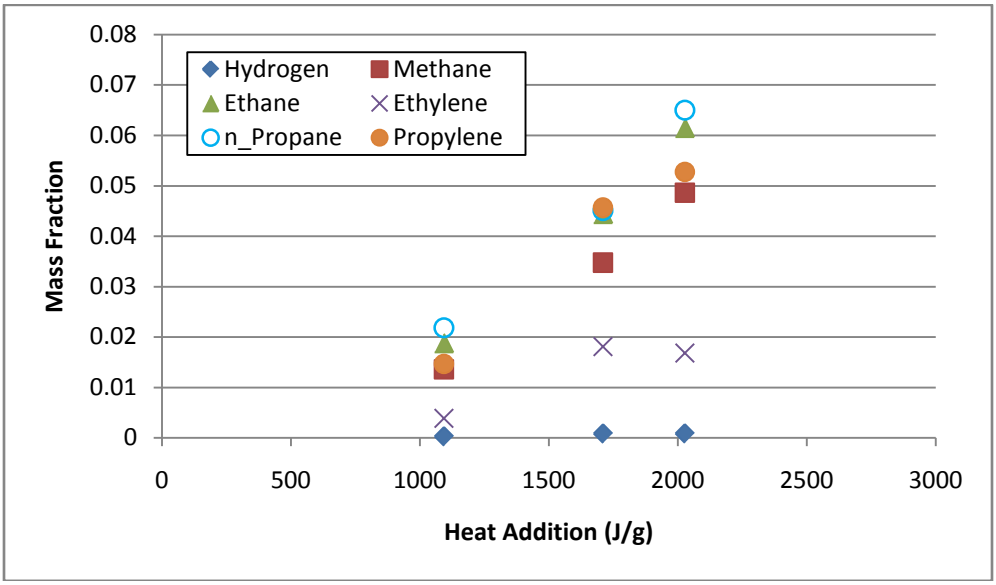

Figure 42. Gas species production: JP-8 in uncoated heat exchangers

Liquid Composition

Because it is known that JP-7 produced more gaseous species during cracking than JP-8, it is expected that JP-7 will also show greater reductions in the concentrations of long chain paraffins. Long chain paraffins are among the first species to be affected by thermal decomposition. As a result they are used up quickly by the initiation reaction.

Figures 43 through 46 show how these compounds are consumed as heat addition increases. As expected, the compounds are consumed faster in JP-7 than JP-8 both with and without the catalyst coating. The more of each species is consumed in JP-7 with the catalyst, but less is consumed inJP-8 with the catalyst. Again the catalyst performs better with JP-7 than with JP-8, but over all the effects are smaller than the differences between the two fuels.

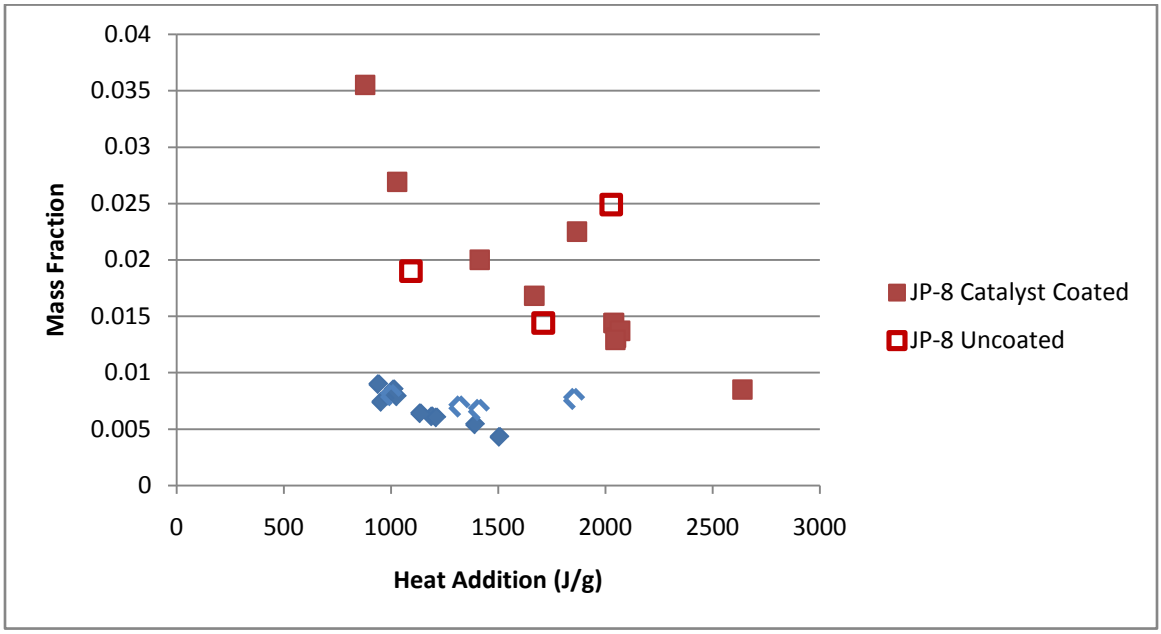

Figure 43. n-Decane consumption

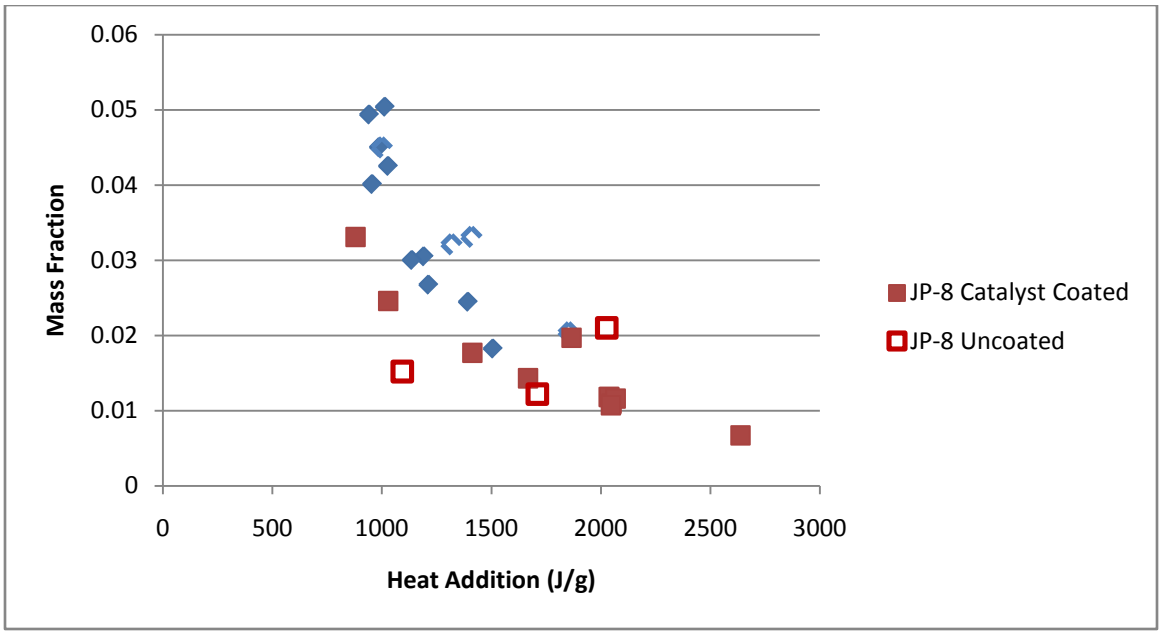

Figure 44. n-Undecane consumption

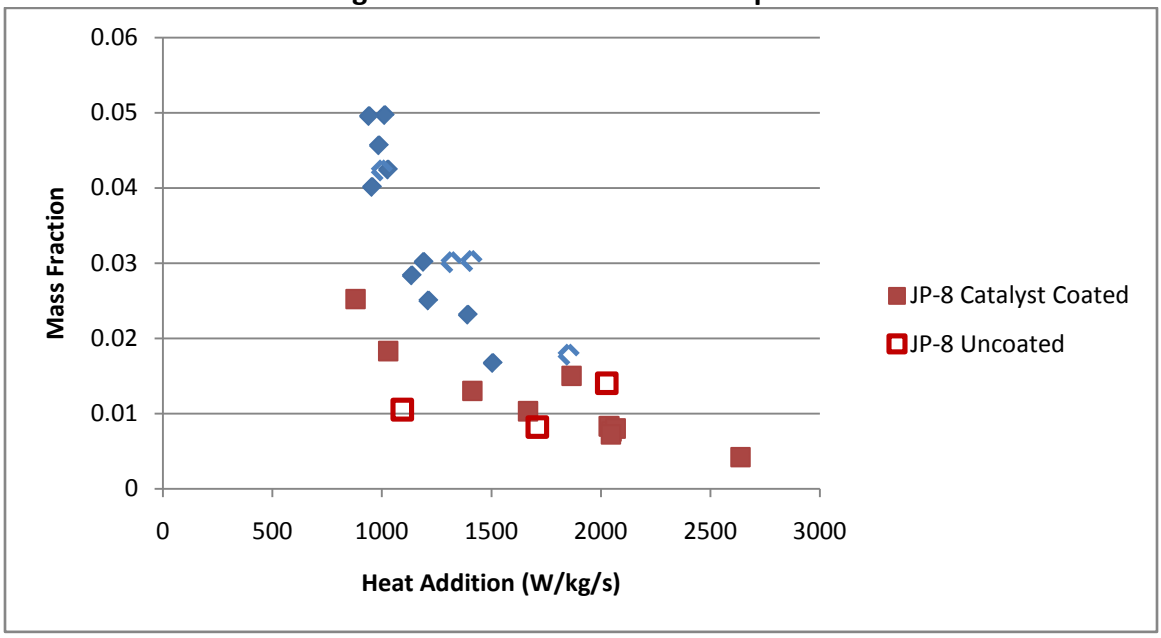

Figure 45. n-Dodecane consumption

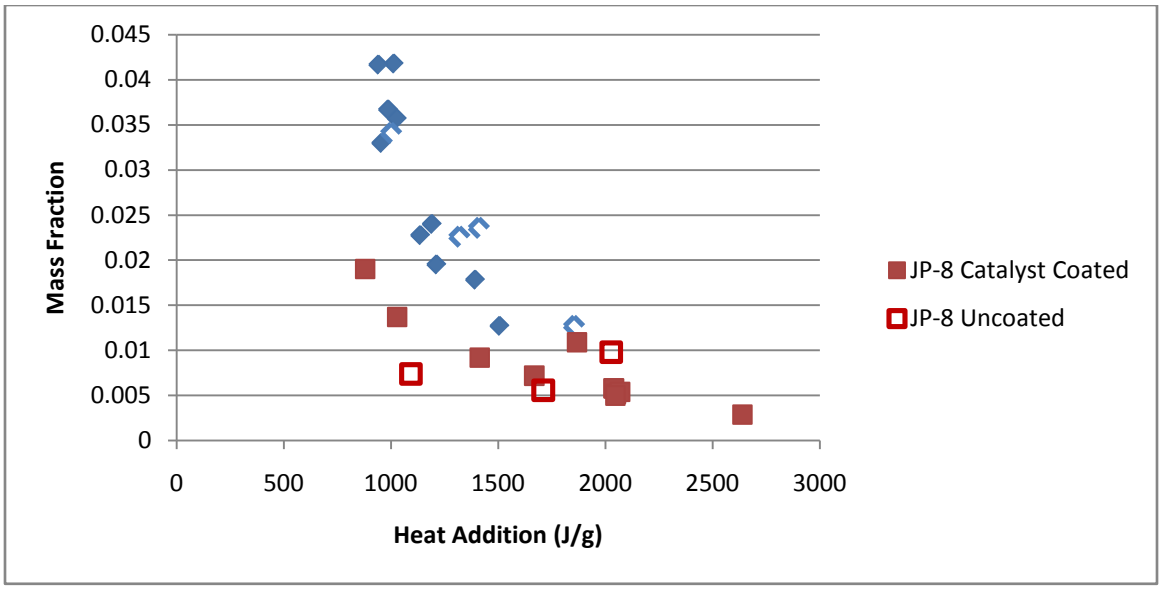

Figure 46. n-Tridecane consumption

Another way to gage the extent of pyrolysis is to look at the overall change in molecular weight of the fuel. This was done by comparing the mass fractions of all the species quantified by chemical analysis and comparing the results as heat addition increased. Figure 47 shows a series of bar graphs that illustrate the changes in mass fraction that occurred between neat fuel and the highest levels of reaction for JP-8.

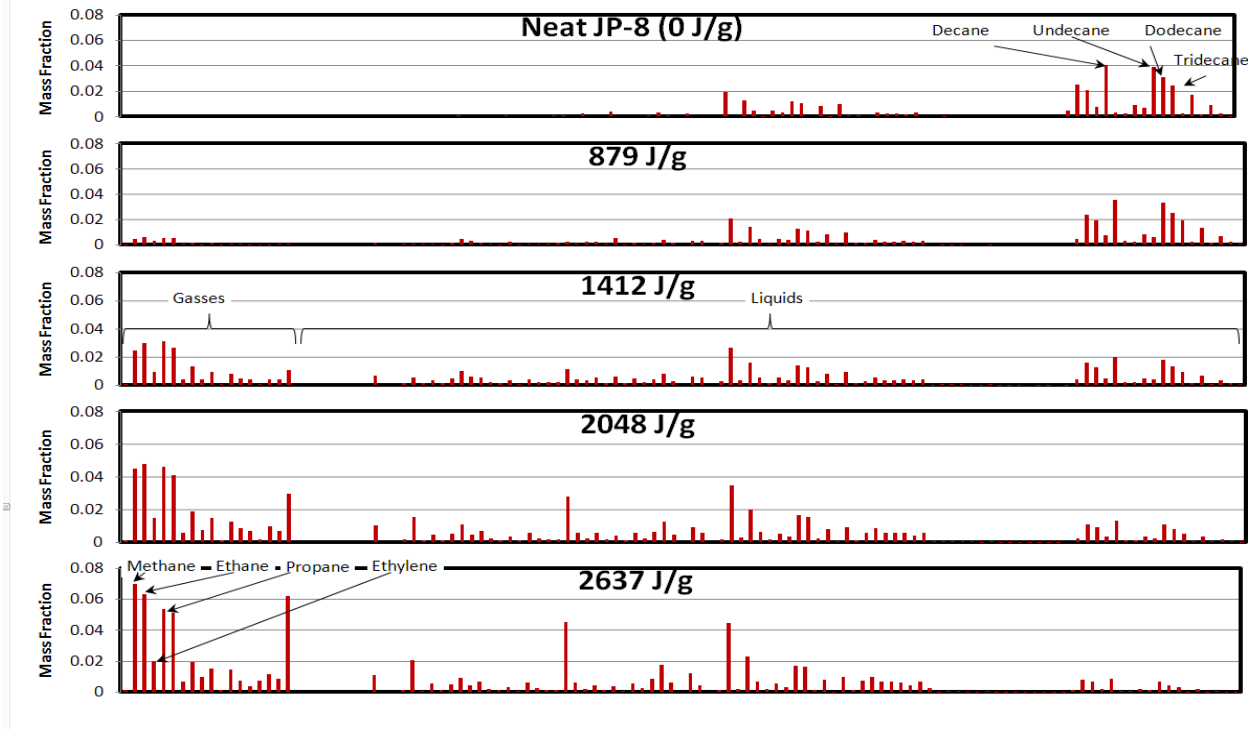

Figure 47. changes in mass fraction with increased heating

Conclusions and Recommendations

Conclusions

The intent of this work was to determine the improvements in PDE performance that could be achieved when a high thermal stability fuel such as JP-7 was substituted for a more common fuel such as JP-8 in a PDE with an endothermic fuel heating system, and to determine the effect of the catalyst wall coating. Experiments were conducted using the sample collection system and analysis techniques developed in earlier work (Nagley, 2008). Data on engine performance and samples of stressed fuel were collected at various heat exchanger exit temperatures. A weakness was identified in the previous analysis. Changes in the fuel flow rate were not accounted for when comparing performance data and the results showed unforeseen variations due to the changing flow rates. A new analysis technique was developed that measured the heat addition to the fuel by comparing the enthalpy of the neat fuel at the test cell temperature to the enthalpy of the

stressed fuel samples at the heat exchanger exit. The heat addition results removed much of the scatter in the engine performance data.

Analysis of the results of experiments performed on JP-8 and JP-7 showed that the higher thermal stability fuel (JP-7) had increased performance in all three metrics of engine performance, heat sink capacity, ignition time, and PAH production. JP-7 also produced more gaseous species during cracking than JP-8 at similar levels of heat addition and showed higher consumption of long chain paraffins. For all of these reasons, a high thermal stability fuel such a JP-7 is better suited for used in a PDE with endothermic fuel heating.

The catalyst improved the performance of the PDE, and the thermal decomposition when used with JP-7 in the thrust tube heat exchangers. For JP-7, the catalyst increased heat addition for a given exit temperature and reduced ignition time. It had no discernable effect on PAH concentration, liquid-to gas-conversion, or ratios of gaseous species produced in JP-7.

The catalyst coating caused similar improvement in performance and thermal decomposition with JP-8. The catalyst caused an increase in heat addition, and a decrease in ignition times. It did not cause changes in PAH concentration, or ratios of gaseous species produced. It did increase the liquid-to-gas conversion in JP-8 which was different than JP-7

Recommendations and Future Work

While this work has shown that a high thermal stability fuel outperformed JP-8 , it only looked at one high stability fuel, JP-7. Future work should perform the same tests on

other fuels such as JP-10 and S-8. Both of these fuels have high thermal stability as well. S-8 is of particular interest because it is a Fischer-Tropsch (F-T) process fuel and is not derived from crude oil.

As in any experimental work there is room for improvement in the equipment used to perform experiments. One of the big drawbacks to the sampling process used in this research was the need to partially disassemble the engine after each test to clean out the nozzles and replace the filters. In the future the fuel system should be redesigned so that less work is required between runs. Another improvement would be more high pressure fuel capacity. Adding one or two more accumulators to the fuel system would greatly increase the run time and the maximum temperatures during experiments.

Third, the heat addition calculation has shown much promise in improving the linearity of the performance data. However the calculation is limited by the number of species quantified by chemical analysis. In the future effort should be made to increase the number of species included in order increase the accuracy of the calculation. Another drawback to the heat addition calculation is that it is done offline. During experiments, the heat exchanger exit temperature is still used as the independent variable. An online measure of heat addition, perhaps utilizing laser fluorimetry, would reduce the guess work involved in sampling.

Appendix A: JP-4 seeded catalyst results

The experiments involving JP-4 and seeded catalysts were not intended to reach endothermic conditions, and for this reason the results of the results of the seeded catalyst experiments are not included with the results of the endothermic experiments involving JP-7 and JP-8. Three tests were performed using different concentrations of the palladium catalyst: 0, 500 ppm, and 1000 ppm. Figure 48 shows the resulting ignition times as a function of equivalence ratio. There is no visible difference in ignition times due to the catalyst.

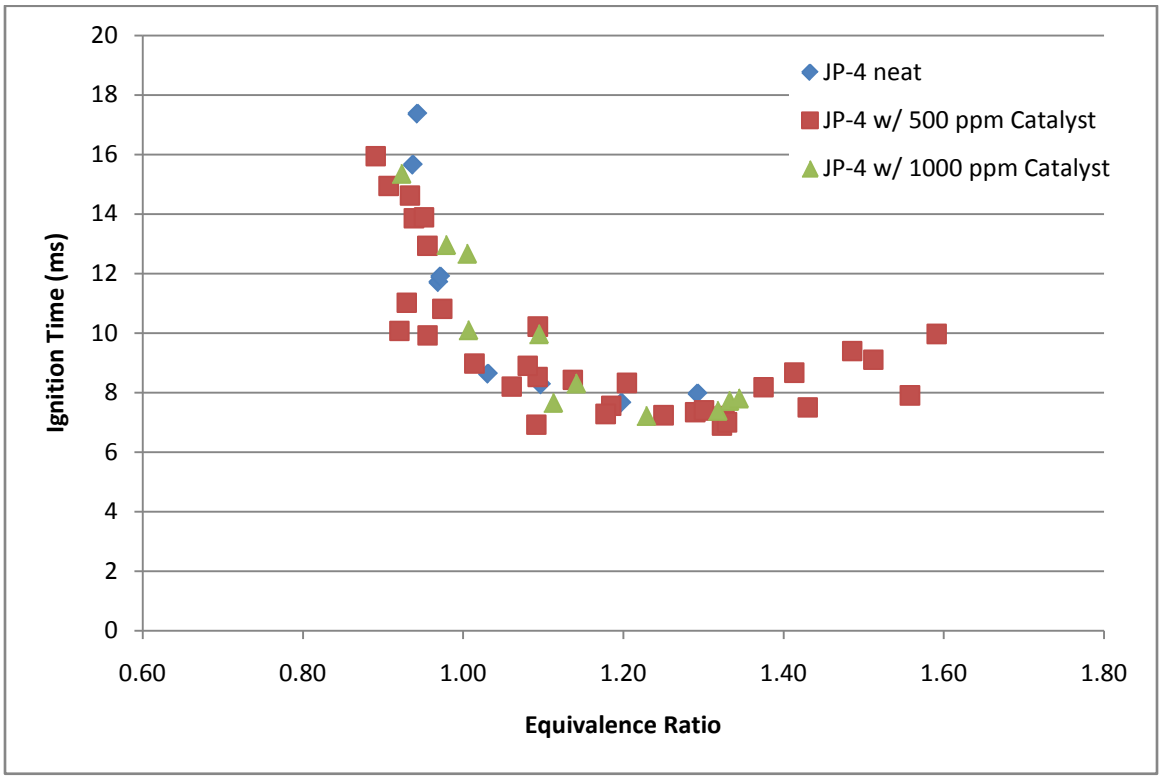

Figure 48. Seeded catalyst ignition times

Appendix B: Uncertainty of measurements

Table B.1. Uncertainty of heat addition

	Heat Addition (J/g)	Uncertainty (J/g)	% Uncertainty
JP-8 Catalyst	1870	0.115	0.0061%
Coated Tubes	1670	0.099	0.0059%
	2040	0.123	0.0060%
	2040	0.123	0.0060%
	879	0.078	0.0089%
	1410	0.086	0.0061%
	1030	0.071	0.0069%
	2050	0.123	0.0060%
	2070	0.122	0.0059%
	2050	0.122	0.0060%
	2640	0.165	0.0063%
JP-7 Catalyst	955	0.081	0.0085%
Coated Tubes	986	0.088	0.0089%
	1190	0.088	0.0074%
	1140	0.080	0.0070%
	1210	0.088	0.0073%
	1030	0.087	0.0084%
	1010	0.087	0.0086%
	941	0.092	0.0098%
	1390	0.101	0.0073%
	1510	0.117	0.0077%
JP-8 Uncoated	1090	0.079	0.0072%
Tubes	1710	0.125	0.0073%
	2030	0.154	0.0076%
JP-7 Uncoated	1410	0.108	0.0077%
Tubes	1320	0.099	0.0075%
	1000	0.089	0.0089%
	1550	0.137	0.0088%

Table B.2. Liquid-to-gas conversion uncertainties

	Liquid-to-gas conversion fraction	Uncertainty	% Uncertainty
JP-8 Catalyst Coated Tubes (Nagley, 2008)	0.30	0.029	9.67%
	0.24	0.017	7.08%
	0.31	0.023	7.42%
	0.33	0.024	7.27%
	0.03	0.005	16.67%
	0.18	0.015	8.33%
	0.08	0.009	11.25%
	0.32	0.048	15.00%
	0.32	0.026	8.13%
	0.31	0.018	5.81%
	0.44	0.028	6.36%
JP-7 Catalyst Coated Tubes	0.11	0.005	4.55%
	0.10	0.011	11.00%
	0.20	0.023	11.50%
	0.17	0.024	14.12%
	0.21	0.030	14.29%
	0.12	0.010	8.33%
	0.10	0.009	9.00%
	0.084	0.007	8.33%
	0.27	0.035	12.96%
	0.33	0.035	10.61%
JP-8 Uncoated Tubes	0.14	0.005	3.57%
	0.33	0.030	9.09%
	0.44	0.011	2.50%
JP-7 Uncoated Tubes	0.29	0.024	8.28%
	0.25	0.022	8.80%
	0.14	0.007	5.00%
	0.38	0.033	8.68%

Table B.3. Ignition time uncertainties

	Average Ignition Time (ms)	Uncertainty (ms)	% Uncertainty
JP-8 Catalyst Coated Tubes (Nagley, 2008)	8.6	1.082404	12.59%
	8.1	0.612682	7.56%
	7.8	0.510568	6.55%
	7.6	1.184518	15.59%
	6.9	0.408454	5.92%
	6.7	0.816909	12.19%
	7.5	3.063409	40.85%
	6.9	1.531704	22.20%
	6.5	0.510568	7.85%
	6.5	3.471863	53.41%
JP-7 Catalyst Coated Tubes	5.1	1.239916	24.31%
	4.7	0.970249	20.64%
	4.1	0.385338	9.40%
	6.7	2.794128	41.70%
	5.3	0.809758	15.28%
	6.5	1.296623	19.95%
	6.0	1.375264	22.92%
	5.0	1.573048	31.46%
	5.0	0.983473	19.67%
JP-8 Uncoated Tubes	10.0	2.02185	20.22%
	9.4	2.369036	25.20%
	8.0	1.307054	16.34%
JP-7 Uncoated Tubes	9.38	1.981004	21.12%
	10.50	2.348613	22.37%
	8.84	2.042272	23.10%
	9.69	3.410595	35.20%

Table B.4. Mass fractions and uncertainties JP-8 in catalyst coated heat exchangers

Heat Addition (J/g)	1866	1667	2036	2038	879	1413	1028	2049	2067	2045	2637
Hydrogen	6.62E-04	5.90E-04	7.32E-04	7.32E-04	8.23E-05	4.13E-04	1.94E-04	7.53E-04	8.07E-04	7.47E-04	1.22E-03
Uncertainty	3.31E-05	2.95E-05	3.66E-05	3.66E-05	4.12E-06	2.07E-05	9.70E-06	3.77E-05	4.04E-05	3.74E-05	6.10E-05
Methane	4.01E-02	3.08E-02	4.07E-02	4.07E-02	4.51E-03	2.40E-02	1.06E-02	4.49E-02	4.67E-02	4.32E-02	6.94E-02
Uncertainty	2.01E-03	1.54E-03	2.04E-03	2.04E-03	2.26E-04	1.20E-03	5.30E-04	2.25E-03	2.34E-03	2.16E-03	3.47E-03
Ethane	4.34E-02	3.60E-02	4.62E-02	4.62E-02	6.18E-03	2.97E-02	1.49E-02	4.49E-02	4.70E-02	4.68E-02	6.29E-02
Uncertainty	2.17E-03	1.80E-03	2.31E-03	2.31E-03	3.09E-04	1.49E-03	7.45E-04	2.25E-03	2.35E-03	2.34E-03	3.15E-03
Ethylene	1.62E-02	1.54E-02	1.84E-02	1.84E-02	2.69E-03	9.37E-03	5.80E-03	1.46E-02	1.88E-02	1.93E-02	1.99E-02
Uncertainty	8.10E-04	7.70E-04	9.20E-04	9.20E-04	1.35E-04	4.69E-04	2.90E-04	7.30E-04	9.40E-04	9.65E-04	9.95E-04
n-Propane	4.11E-02	3.50E-02	4.44E-02	4.44E-02	5.28E-03	3.10E-02	1.53E-02	4.62E-02	4.27E-02	4.47E-02	5.36E-02
Uncertainty	2.06E-03	1.75E-03	2.22E-03	2.22E-03	2.64E-04	1.55E-03	7.65E-04	2.31E-03	2.14E-03	2.24E-03	2.68E-03
Propylene	4.22E-02	3.70E-02	4.56E-02	4.56E-02	5.07E-03	2.63E-02	1.41E-02	4.10E-02	4.56E-02	4.66E-02	5.11E-02
Uncertainty	2.11E-03	1.85E-03	2.28E-03	2.28E-03	2.54E-04	1.32E-03	7.05E-04	2.05E-03	2.28E-03	2.33E-03	2.56E-03
Decane	2.25E-02	1.68E-02	1.44E-02	1.44E-02	3.55E-02	2.00E-02	2.69E-02	1.31E-02	1.37E-02	1.29E-02	8.50E-03
Uncertainty	1.13E-03	8.40E-04	7.20E-04	7.20E-04	1.78E-03	1.00E-03	1.35E-03	6.55E-04	6.85E-04	6.45E-04	4.25E-04
Undecane	1.97E-02	1.43E-02	1.18E-02	1.18E-02	3.31E-02	1.77E-02	2.46E-02	1.09E-02	1.16E-02	1.07E-02	6.70E-03
Uncertainty	9.85E-04	7.15E-04	5.90E-04	5.90E-04	1.66E-03	8.85E-04	1.23E-03	5.45E-04	5.80E-04	5.35E-04	3.35E-04
Dodecane	1.50E-02	1.03E-02	8.30E-03	8.30E-03	2.52E-02	1.30E-02	1.83E-02	7.60E-03	8.00E-03	7.20E-03	4.20E-03
Uncertainty	7.50E-04	5.15E-04	4.15E-04	4.15E-04	1.26E-03	6.50E-04	9.15E-04	3.80E-04	4.00E-04	3.60E-04	2.10E-04
Tridecane	1.09E-02	7.20E-03	5.80E-03	5.80E-03	1.90E-02	9.20E-03	1.37E-02	5.20E-03	5.40E-03	5.00E-03	2.90E-03
Uncertainty	5.45E-04	3.60E-04	2.90E-04	2.90E-04	9.50E-04	4.60E-04	6.85E-04	2.60E-04	2.70E-04	2.50E-04	1.45E-04
Total PAH	2.31E-02	2.77E-02	3.65E-02	3.91E-02	1.46E-02	2.23E-02	1.62E-02	3.52E-02	3.07E-02	3.17E-02	4.58E-02
Uncertainty	4.45E-04	5.30E-04	6.92E-04	6.92E-04	2.84E-04	4.20E-04	3.13E-04	6.48E-04	5.63E-04	5.80E-04	8.06E-04

Table B.5. Mass Fractions and uncertainties JP-7 in catalyst coated heat exchangers

Heat Addition (J/g)	955	986	1190	1136	1212	1028	1013	941	1392	1506
Hydrogen	2.16E-04	2.18E-04	3.88E-04	3.25E-04	4.13E-04	2.38E-04	2.03E-04	1.64E-04	5.15E-04	6.47E-04
Uncertainty	1.08E-05	1.09E-05	1.94E-05	1.63E-05	2.07E-05	1.19E-05	1.02E-05	8.20E-06	2.58E-05	3.24E-05
Methane	1.12E-02	1.15E-02	2.17E-02	1.70E-02	2.19E-02	1.19E-02	9.95E-03	8.19E-03	2.60E-02	3.27E-02
Uncertainty	5.60E-04	5.75E-04	1.09E-03	8.50E-04	1.10E-03	5.95E-04	4.98E-04	4.10E-04	1.30E-03	1.64E-03
Ethane	1.60E-02	1.59E-02	2.99E-02	2.31E-02	3.10E-02	1.83E-02	1.56E-02	1.29E-02	3.62E-02	4.39E-02
Uncertainty	8.00E-04	7.95E-04	1.50E-03	1.16E-03	1.55E-03	9.15E-04	7.80E-04	6.45E-04	1.81E-03	2.20E-03
Ethylene	8.50E-03	9.50E-03	1.32E-02	7.54E-03	8.99E-03	9.55E-03	8.05E-03	5.41E-03	1.27E-02	1.46E-02
Uncertainty	8.00E-04	7.95E-04	1.50E-03	1.16E-03	1.55E-03	9.15E-04	7.80E-04	6.45E-04	1.81E-03	2.20E-03
n-Propane	1.67E-02	1.57E-02	3.22E-02	2.57E-02	3.50E-02	2.00E-02	1.70E-02	1.45E-02	4.06E-02	4.79E-02
Uncertainty	8.35E-04	7.85E-04	1.61E-03	1.29E-03	1.75E-03	1.00E-03	8.50E-04	7.25E-04	2.03E-03	2.40E-03
Propylene	1.88E-02	1.89E-02	3.27E-02	2.19E-02	2.75E-02	2.11E-02	1.78E-02	1.35E-02	3.58E-02	4.12E-02
Uncertainty	9.40E-04	9.45E-04	1.64E-03	1.10E-03	1.38E-03	1.06E-03	8.90E-04	6.75E-04	1.79E-03	2.06E-03
Decane	7.40E-03	7.96E-03	6.12E-03	6.39E-03	6.02E-03	7.89E-03	8.52E-03	8.98E-03	5.41E-03	4.30E-03
Uncertainty	3.70E-04	3.98E-04	3.06E-04	3.20E-04	3.01E-04	3.95E-04	4.26E-04	4.49E-04	2.70E-04	2.15E-04
Undecane	4.01E-02	4.50E-02	3.05E-02	3.00E-02	2.68E-02	4.25E-02	5.04E-02	4.94E-02	2.45E-02	1.83E-02
Uncertainty	2.01E-03	2.25E-03	1.53E-03	1.50E-03	1.34E-03	2.13E-03	2.52E-03	2.47E-03	1.22E-03	9.13E-04
Dodecane	4.01E-02	4.57E-02	3.02E-02	2.84E-02	2.50E-02	4.24E-02	4.97E-02	4.96E-02	2.31E-02	1.67E-02
Uncertainty	2.01E-03	2.28E-03	1.51E-03	1.42E-03	1.25E-03	2.12E-03	2.48E-03	2.48E-03	1.16E-03	8.36E-04
Tridecane	3.30E-02	3.67E-02	2.40E-02	2.28E-02	1.95E-02	3.57E-02	4.18E-02	4.17E-02	1.78E-02	1.27E-02
Uncertainty	1.65E-03	1.84E-03	1.20E-03	1.14E-03	9.77E-04	1.78E-03	2.09E-03	2.08E-03	8.92E-04	6.37E-04
Total PAH	1.44E-04	1.56E-04	2.06E-03	2.27E-03	2.55E-03	8.22E-05	4.45E-05	3.98E-05	2.69E-03	3.94E-03
Uncertainty	3.01E-06	3.19E-06	4.17E-05	4.66E-05	5.44E-05	1.79E-06	1.15E-06	1.03E-06	5.37E-05	7.59E-05

Table B.6. Mass Fractions and uncertainties JP-8 in uncoated heat exchangers

Heat Addition (J/g)	1093	1710	2027
Hydrogen	2.53E-04	8.09E-04	8.22E-04
Uncertainty	1.27E-05	4.05E-05	4.11E-05
Methane	1.35E-02	3.47E-02	4.86E-02
Uncertainty	6.75E-04	1.74E-03	2.43E-03
Ethane	1.88E-02	4.44E-02	6.15E-02
Uncertainty	9.40E-04	2.22E-03	3.08E-03
Ethylene	3.84E-03	1.81E-02	1.68E-02
Uncertainty	1.92E-04	9.05E-04	8.40E-04
n-Propane	2.18E-02	4.50E-02	6.50E-02
Uncertainty	1.09E-03	2.25E-03	3.25E-03
Propylene	1.47E-02	4.57E-02	5.27E-02
Uncertainty	7.35E-04	2.29E-03	2.64E-03
Decane	1.90E-02	1.44E-02	2.49E-02
Uncertainty	9.50E-04	7.20E-04	1.25E-03
Undecane	1.52E-02	1.22E-02	2.10E-02
Uncertainty	7.60E-04	6.10E-04	1.05E-03
Dodecane	1.05E-02	8.20E-03	1.40E-02
Uncertainty	5.25E-04	4.10E-04	7.00E-04
Tridecane	7.40E-03	5.60E-03	9.80E-03
Uncertainty	3.70E-04	2.80E-04	4.90E-04
Total PAH	2.30E-02	3.03E-02	1.85E-02
Uncertainty	5.25E-04	6.74E-04	4.11E-04

Table B.7. Mass Fractions and uncertainties JP-7 in uncoated heat exchangers

Heat Addition (J/g)	1409	1318	1000	1853
Hydrogen	4.68E-04	4.22E-04	2.11E-04	7.75E-04
Uncertainty	2.34E-05	2.11E-05	1.06E-05	3.88E-05
Methane	2.37E-02	2.00E-02	1.10E-02	3.86E-02
Uncertainty	1.19E-03	1.00E-03	5.50E-04	1.93E-03
Ethane	3.53E-02	3.12E-02	1.87E-02	5.26E-02
Uncertainty	1.77E-03	1.56E-03	9.35E-04	2.63E-03
Ethylene	1.69E-02	1.35E-02	9.19E-03	1.76E-02
Uncertainty	8.45E-04	6.75E-04	4.60E-04	8.80E-04
n-Propane	3.91E-02	3.64E-02	2.20E-02	5.77E-02
Uncertainty	1.96E-03	1.82E-03	1.10E-03	2.89E-03
Propylene	4.21E-02	3.63E-02	2.25E-02	5.19E-02
Uncertainty	2.11E-03	1.82E-03	1.13E-03	2.60E-03
Decane	6.70E-03	7.00E-03	8.00E-03	7.66E-03
Uncertainty	3.35E-04	3.50E-04	4.00E-04	3.83E-04
Undecane	3.31E-02	3.21E-02	4.50E-02	2.04E-02
Uncertainty	1.66E-03	1.61E-03	2.25E-03	1.02E-03
Dodecane	3.03E-02	3.01E-02	4.23E-02	1.78E-02
Uncertainty	1.51E-03	1.51E-03	2.12E-03	8.90E-04
Tridecane	2.36E-02	2.26E-02	3.41E-02	1.27E-02
Uncertainty	1.18E-03	1.13E-03	1.71E-03	6.35E-04
Total PAH	2.79E-03	1.91E-03	6.21E-04	9.25E-03
Uncertainty	5.83E-05	4.39E-05	2.56E-05	1.71E-04

Appendix C: Raw Data

Table C.1a. JP-7 in catalyst coated heat exchangers

Heat Exchange Exit Temp (K)	823	830	837	844	823	828	822	816	844	845
Heat Addition (J/g)	955	986	1190	1136	1212	1028	1013	941	1392	1506
L to G conversion	0.108	0.105	0.197	0.166	0.211	0.123	0.103	0.084	0.267	0.328
Average Ignition Time (ms)		5.14	4.70	4.12	6.69	5.32	6.45	5.96	5.03	4.99
Mixture Mass Fractions										
Hydrogen	2.2E-4	2.2E-4	3.9E-4	3.2E-4	4.1E-4	2.4E-4	2.0E-4	1.6E-4	5.1E-4	6.5E-4
Methane	1.1E-2	1.2E-2	2.2E-2	1.7E-2	2.2E-2	1.2E-2	1.0E-2	8.2E-3	2.6E-2	3.3E-2
Ethane	1.6E-2	1.6E-2	3.0E-2	2.3E-2	3.1E-2	1.8E-2	1.6E-2	1.3E-2	3.6E-2	4.4E-2
Ethylene	8.5E-3	9.5E-3	1.3E-2	7.5E-3	9.0E-3	9.5E-3	8.0E-3	5.4E-3	1.3E-2	1.5E-2
n_Propane	1.7E-2	1.6E-2	3.2E-2	2.6E-2	3.5E-2	2.0E-2	1.7E-2	1.4E-2	4.1E-2	4.8E-2
Propylene	1.9E-2	1.9E-2	3.3E-2	2.2E-2	2.7E-2	2.1E-2	1.8E-2	1.3E-2	3.6E-2	4.1E-2
iso_Butane	1.5E-3	1.3E-3	3.1E-3	2.9E-3	4.3E-3	1.9E-3	1.6E-3	1.5E-3	5.2E-3	6.6E-3
n_Butane	6.3E-3	5.5E-3	1.4E-2	1.2E-2	1.6E-2	7.7E-3	6.4E-3	5.9E-3	2.0E-2	2.3E-2
trans_2_Butene	1.9E-3	1.6E-3	3.6E-3	2.9E-3	3.8E-3	1.8E-3	1.5E-3	1.2E-3	5.4E-3	7.0E-3
Butene_1	6.8E-3	6.5E-3	1.2E-2	8.4E-3	1.1E-2	7.6E-3	6.3E-3	4.9E-3	1.5E-2	1.7E-2
iso_Butylene	1.5E-4	1.2E-4	3.6E-4	3.2E-4	4.7E-4	1.8E-4	1.3E-4	1.3E-4	8.2E-4	1.2E-3
cis_2_Butene	4.3E-3	3.9E-3	8.0E-3	5.8E-3	7.6E-3	4.7E-3	3.8E-3	3.1E-3	1.0E-2	1.2E-2
iso_C5	2.1E-3	1.8E-3	4.5E-3	2.8E-3	2.3E-3	8.5E-4	7.0E-4	7.4E-4	3.1E-3	3.9E-3
n_Pentane	1.9E-3	1.6E-3	4.8E-3	3.3E-3	3.0E-3	1.4E-3	1.1E-3	8.7E-4	4.4E-3	5.7E-3
Butadiene	5.9E-4	5.8E-4	9.4E-4	2.1E-3	5.5E-3	2.3E-3	1.8E-3	1.8E-3	7.8E-3	9.4E-3
Methylenes	3.1E-4	2.5E-4	6.8E-4	5.2E-4	4.8E-4	5.4E-4	4.4E-4	2.5E-4	9.0E-4	1.1E-3
Pentene_1	5.8E-4	5.3E-4	8.8E-4	6.2E-4	6.3E-4	3.1E-4	2.2E-4	1.8E-4	1.2E-3	1.6E-3
Undecernable area in gas	1.1E-2	9.4E-3	1.4E-2	2.9E-2	3.1E-2	1.3E-2	1.1E-2	8.9E-3	4.2E-2	5.9E-2
Propene	3.0E-3	2.6E-3	2.6E-3	1.7E-3	2.9E-3	3.1E-3	3.3E-3	2.5E-3	2.5E-3	2.1E-3
methyl_Propene	1.1E-2	1.0E-2	1.1E-2	1.2E-2	1.4E-2	1.2E-2	1.3E-2	1.1E-2	1.2E-2	1.0E-2
methyl_Butane	1.6E-3	1.6E-3	1.9E-3	2.3E-3	2.5E-3	1.9E-3	1.8E-3	2.0E-3	2.1E-3	1.8E-3
Pentene_1	1.1E-2	1.0E-2	1.2E-2	1.2E-2	1.2E-2	1.2E-2	1.1E-2	9.9E-3	1.2E-2	1.1E-2
n_Pentane_a	3.4E-3	3.3E-3	4.7E-3	6.4E-3	6.8E-3	4.5E-3	4.4E-3	4.6E-3	5.7E-3	5.2E-3
Hexene_1	8.4E-3	8.1E-3	9.1E-3	8.7E-3	8.4E-3	8.4E-3	8.0E-3	7.1E-3	8.6E-3	8.2E-3
n_Hexane	2.5E-3	2.3E-3	3.8E-3	5.2E-3	5.4E-3	3.3E-3	3.1E-3	3.5E-3	4.6E-3	4.4E-3
Hexene	1.1E-3	9.9E-4	1.5E-3	1.8E-3	1.9E-3	1.1E-3	1.1E-3	9.3E-4	1.8E-3	2.0E-3
methyl_Cyclopentene	1.4E-3	1.4E-3	1.7E-3	1.9E-3	1.8E-3	1.3E-3	1.2E-3	1.0E-3	2.0E-3	2.0E-3
methyl_Cyclopentane	1.4E-3	1.3E-3	2.0E-3	2.4E-3	2.5E-3	1.4E-3	1.3E-3	1.2E-3	2.5E-3	2.7E-3
methyl_Cyclopentene_a	2.3E-3	2.1E-3	2.9E-3	3.0E-3	3.0E-3	2.2E-3	2.0E-3	1.8E-3	3.3E-3	3.5E-3
methyl_Hexene	6.7E-4	6.2E-4	7.6E-4	7.7E-4	7.2E-4	6.6E-4	6.1E-4	5.5E-4	7.7E-4	7.2E-4
Benzene	2.3E-3	2.0E-3	3.5E-3	3.3E-3	3.5E-3	1.2E-3	9.9E-4	6.5E-4	4.1E-3	5.1E-3
methyl_Hexane	3.6E-4	3.5E-4	5.7E-4	9.0E-4	9.5E-4	4.4E-4	4.5E-4	4.4E-4	7.3E-4	7.4E-4
Cyclohexene	2.8E-3	2.4E-3	3.1E-3	2.9E-3	2.9E-3	2.3E-3	2.0E-3	1.6E-3	3.6E-3	3.6E-3
dimethyl_Cyclopentane	0.0E+0	0.0E+0	3.8E-4	4.7E-4	5.3E-4	3.2E-4	0.0E+0	0.0E+0	4.4E-4	5.4E-4
methyl_Hexene_a	5.2E-3	5.2E-3	5.5E-3	5.8E-3	5.9E-3	5.3E-3	4.8E-3	4.8E-3	6.7E-3	6.7E-3
Heptene_1	8.1E-3	7.7E-3	8.7E-3	8.7E-3	8.0E-3	7.7E-3	7.4E-3	7.0E-3	9.1E-3	8.3E-3
n_Heptane	2.5E-3	2.3E-3	3.6E-3	5.0E-3	5.2E-3	3.2E-3	3.0E-3	3.5E-3	4.7E-3	4.3E-3
dimethyl_Cyclopentene	2.9E-3	2.5E-3	3.5E-3	4.0E-3	4.1E-3	2.6E-3	2.2E-3	2.1E-3	4.4E-3	4.5E-3
Heptene	1.7E-3	1.6E-3	2.2E-3	2.3E-3	2.3E-3	1.7E-3	1.4E-3	1.5E-3	2.5E-3	2.4E-3
Heptene_a	9.2E-4	9.4E-4	1.3E-3	1.3E-3	1.4E-3	9.6E-4	8.1E-4	7.4E-4	1.4E-3	1.4E-3
methyl_Cyclohexane	1.4E-3	1.3E-3	1.8E-3	2.3E-3	2.5E-3	1.4E-3	1.3E-3	1.4E-3	2.3E-3	2.4E-3
ethyl_Cyclopentane	0.0E+0	0.0E+0	4.7E-4	6.0E-4	6.7E-4	3.7E-4	3.1E-4	0.0E+0	5.9E-4	6.5E-4
methyl_Cyclohexene	2.9E-3	2.7E-3	3.4E-3	3.4E-3	3.6E-3	2.6E-3	2.2E-3	2.0E-3	4.0E-3	4.2E-3
ethyl_Cyclopentene	1.1E-3	9.0E-4	1.4E-3	1.5E-3	1.6E-3	9.6E-4	9.0E-4	8.2E-4	1.6E-3	1.7E-3
Octene	1.3E-3	1.3E-3	1.3E-3	1.3E-3	1.2E-3	1.1E-3	1.1E-3	1.0E-3	1.4E-3	1.2E-3
methyl_Heptane	8.5E-4	8.4E-4	1.0E-3	1.2E-3	1.1E-3	8.8E-4	8.1E-4	8.2E-4	1.0E-3	1.0E-3
Toluene	4.0E-3	3.5E-3	6.0E-3	6.5E-3	7.1E-3	2.6E-3	2.0E-3	1.7E-3	8.2E-3	1.1E-2
methyl_Cyclohexene_a	2.9E-3	2.4E-3	3.5E-3	3.6E-3	3.9E-3	2.6E-3	2.2E-3	2.1E-3	4.3E-3	4.3E-3
dimethyl_Cyclohexane	6.6E-4	5.6E-4	9.2E-4	1.2E-3	1.3E-3	7.4E-4	6.0E-4	7.3E-4	1.1E-3	1.1E-3
Octene_1	5.5E-3	5.7E-3	5.8E-3	5.5E-3	5.3E-3	5.5E-3	5.2E-3	4.9E-3	5.4E-3	5.0E-3
dimethyl_Cyclohexene	1.1E-3	9.6E-4	1.2E-3	1.3E-3	1.3E-3	9.6E-4	9.0E-4	8.2E-4	1.2E-3	1.3E-3
n_Octane	1.7E-3	1.6E-3	2.5E-3	3.5E-3	3.6E-3	2.2E-3	2.0E-3	2.4E-3	3.2E-3	2.8E-3

Table C.1b. JP-7 in catalyst coated heat exchangers (continued)

Heat Exchange Exit Temp (K)	823	830	837	844	823	828	822	816	844	845
Heat Addition (J/g)	955	986	1190	1136	1212	1028	1013	941	1392	1506
L to G conversion	0.108	0.105	0.197	0.166	0.211	0.123	0.103	0.084	0.267	0.328
Average Ignition Time (ms)		5.14	4.70	4.12	6.69	5.32	6.45	5.96	5.03	4.99
Mixture Mass Fractions										
Octene_a	5.6E-4	4.9E-4	7.4E-4	8.2E-4	8.5E-4	6.1E-4	4.7E-4	5.1E-4	8.4E-4	7.7E-4
dimethyl_Cyclohexene_a	3.6E-3	3.3E-3	4.0E-3	4.8E-3	4.9E-3	3.3E-3	3.0E-3	2.9E-3	5.3E-3	4.8E-3
ethyl_Cyclohexene	2.0E-3	1.8E-3	2.0E-3	2.4E-3	2.2E-3	1.7E-3	1.7E-3	1.6E-3	2.6E-3	2.4E-3
Ethylbenzene	6.8E-4	5.7E-4	1.1E-3	1.2E-3	1.4E-3	4.8E-4	3.7E-4	3.4E-4	1.5E-3	1.9E-3
p_Xylene	1.1E-3	9.9E-4	1.8E-3	2.1E-3	2.6E-3	8.6E-4	7.1E-4	7.1E-4	2.6E-3	3.4E-3
m_Xylene	5.9E-4	4.4E-4	7.8E-4	9.8E-4	1.0E-3	4.2E-4	3.5E-4	0.0E+0	1.1E-3	1.4E-3
methyl_Octane_3	4.9E-4	5.0E-4	5.6E-4	7.5E-4	7.4E-4	5.2E-4	5.2E-4	6.1E-4	6.5E-4	6.1E-4
o_Xylene	7.2E-4	6.4E-4	1.1E-3	1.3E-3	1.5E-3	5.4E-4	4.4E-4	4.1E-4	1.6E-3	2.0E-3
Nonene_1	7.0E-3	7.0E-3	6.8E-3	6.5E-3	5.8E-3	6.6E-3	6.5E-3	6.3E-3	6.3E-3	5.6E-3
n_Nonane	2.0E-3	2.0E-3	2.4E-3	3.1E-3	3.2E-3	2.5E-3	2.5E-3	2.8E-3	2.7E-3	2.4E-3
Nonene	1.1E-3	8.0E-4	1.3E-3	1.5E-3	1.6E-3	8.4E-4	8.3E-4	1.1E-3	1.5E-3	1.2E-3
C3_Alkylbenzenes	1.6E-3	1.5E-3	2.2E-3	2.6E-3	3.1E-3	1.2E-3	1.2E-3	1.2E-3	3.1E-3	3.7E-3
Decene_1	4.3E-3	4.4E-3	4.2E-3	4.0E-3	3.7E-3	4.4E-3	4.3E-3	3.9E-3	4.0E-3	3.4E-3
trimethyl_Benzene_1_2_4	6.9E-4	6.5E-4	8.5E-4	9.7E-4	1.1E-3	5.8E-4	5.5E-4	5.6E-4	1.1E-3	1.3E-3
C3_Alkylbenzenes_2	0.0E+0	0.0E+0	0.0E+0	0.0E+0	0.0E+0	0.0E+0	0.0E+0	0.0E+0	0.0E+0	0.0E+0
Indane	0.0E+0	0.0E+0	3.0E-4	3.3E-4	3.9E-4	0.0E+0	0.0E+0	0.0E+0	4.3E-4	5.4E-4
C4_Alkylbenzenes	2.1E-3	1.9E-3	2.3E-3	2.8E-3	2.8E-3	2.0E-3	1.8E-3	1.9E-3	2.9E-3	3.2E-3
Butylbenzene	3.3E-4	0.0E+0	4.7E-4	5.2E-4	5.5E-4	3.2E-4	0.0E+0	0.0E+0	5.7E-4	7.1E-4
C4_Alkylbenzenes_2	0.0E+0	0.0E+0	0.0E+0	0.0E+0	0.0E+0	0.0E+0	0.0E+0	0.0E+0	0.0E+0	0.0E+0
C4_Alkylbenzenes_3	0.0E+0	0.0E+0	0.0E+0	0.0E+0	0.0E+0	0.0E+0	0.0E+0	0.0E+0	0.0E+0	0.0E+0
Undecene_1	4.0E-3	3.9E-3	3.5E-3	3.4E-3	3.1E-3	3.7E-3	3.9E-3	3.7E-3	3.3E-3	2.6E-3
C5_Alkylbenzenes	9.8E-4	9.0E-4	1.3E-3	1.5E-3	1.7E-3	0.0E+0	2.6E-4	2.5E-4	7.9E-4	8.9E-4
Pentylbenzene	0.0E+0	0.0E+0	0.0E+0	0.0E+0	0.0E+0	0.0E+0	0.0E+0	0.0E+0	0.0E+0	0.0E+0
C5_Alkylbenzenes_2	0.0E+0	0.0E+0	0.0E+0	0.0E+0	0.0E+0	0.0E+0	0.0E+0	0.0E+0	0.0E+0	0.0E+0
Tetralin	0.0E+0	0.0E+0	0.0E+0	0.0E+0	0.0E+0	0.0E+0	0.0E+0	0.0E+0	3.0E-4	3.7E-4
Naphthalene	0.0E+0	0.0E+0	4.8E-4	4.8E-4	5.3E-4	0.0E+0	0.0E+0	0.0E+0	5.2E-4	7.0E-4
Dodecene_1	0.0E+0	0.0E+0	0.0E+0	0.0E+0	0.0E+0	0.0E+0	0.0E+0	0.0E+0	0.0E+0	0.0E+0
methyl_Naphthalene_2	0.0E+0	0.0E+0	4.4E-4	5.0E-4	5.8E-4	0.0E+0	0.0E+0	0.0E+0	5.5E-4	7.7E-4
methyl_Naphthalene_1	0.0E+0	0.0E+0	2.9E-4	3.3E-4	3.8E-4	0.0E+0	0.0E+0	0.0E+0	3.7E-4	4.9E-4
dimethyl_Naphthalenes	0.0E+0	0.0E+0	4.0E-4	5.0E-4	6.3E-4	0.0E+0	0.0E+0	0.0E+0	5.9E-4	8.7E-4
dimethyl_Naphthalene_1_3	0.0E+0	0.0E+0	0.0E+0	0.0E+0	0.0E+0	0.0E+0	0.0E+0	0.0E+0	0.0E+0	2.4E-4
dimethyl_Naphthalenes_2	0.0E+0	0.0E+0	0.0E+0	0.0E+0	0.0E+0	0.0E+0	0.0E+0	0.0E+0	0.0E+0	0.0E+0
Acenaphthylene	9.5E-6	9.1E-6	1.7E-5	1.2E-5	1.4E-5	0.0E+0	0.0E+0	0.0E+0	1.7E-5	2.7E-5
Acenaphthene	1.5E-5	1.4E-5	3.1E-5	3.5E-5	4.1E-5	9.5E-6	6.6E-6	5.9E-6	3.7E-5	5.6E-5
Fluorene	3.6E-5	3.6E-5	8.3E-5	8.7E-5	9.8E-5	2.1E-5	1.4E-5	1.2E-5	8.7E-5	1.3E-4
Phenanthrene	3.0E-5	3.3E-5	9.3E-5	9.1E-5	7.6E-5	1.7E-5	1.1E-5	9.8E-6	6.5E-5	8.3E-5
Anthracene	9.4E-6	9.8E-6	2.5E-5	2.5E-5	2.5E-5	5.4E-6	0.0E+0	0.0E+0	2.1E-5	3.0E-5
Fluoranthene	7.6E-6	8.4E-6	2.4E-5	2.5E-5	2.2E-5	4.5E-6	0.0E+0	0.0E+0	1.8E-5	2.3E-5
Pyrene	3.1E-5	3.4E-5	9.0E-5	9.1E-5	8.5E-5	1.9E-5	1.3E-5	1.2E-5	6.8E-5	8.7E-5
benz_a_Anthracene	0.0E+0	0.0E+0	1.4E-5	1.5E-5	1.2E-5	0.0E+0	0.0E+0	0.0E+0	9.7E-6	1.1E-5
Chrysene	0.0E+0	0.0E+0	1.3E-5	1.3E-5	8.1E-6	0.0E+0	0.0E+0	0.0E+0	7.6E-6	7.0E-6
benzo_b_Fluoranthene	0.0E+0	0.0E+0	1.0E-5	1.1E-5	8.9E-6	0.0E+0	0.0E+0	0.0E+0	7.3E-6	9.4E-6
benzo_k_Fluoranthene	0.0E+0	0.0E+0	0.0E+0	0.0E+0	0.0E+0	0.0E+0	0.0E+0	0.0E+0	0.0E+0	0.0E+0
benzo_a_Pyrene	0.0E+0	5.1E-6	1.6E-5	1.4E-5	1.2E-5	0.0E+0	0.0E+0	0.0E+0	9.9E-6	1.1E-5
indeno_1_2_3_cd_Pyrene	6.4E-6	6.2E-6	1.6E-5	2.1E-5	1.9E-5	5.2E-6	0.0E+0	0.0E+0	1.5E-5	1.7E-5
dibenz_a_h_Anthracene	0.0E+0	0.0E+0	0.0E+0	0.0E+0	0.0E+0	0.0E+0	0.0E+0	0.0E+0	0.0E+0	0.0E+0
benzo_g_h_i_Perylene	0.0E+0	0.0E+0	1.3E-5	1.5E-5	1.4E-5	0.0E+0	0.0E+0	0.0E+0	1.0E-5	1.2E-5
methyl_Octane_3_2	0.0E+0	0.0E+0	0.0E+0	0.0E+0	0.0E+0	0.0E+0	0.0E+0	0.0E+0	0.0E+0	0.0E+0
n_Nonane_2	0.0E+0	0.0E+0	0.0E+0	0.0E+0	0.0E+0	0.0E+0	0.0E+0	0.0E+0	0.0E+0	0.0E+0
dimethyl_Octane	0.0E+0	0.0E+0	0.0E+0	0.0E+0	0.0E+0	0.0E+0	0.0E+0	0.0E+0	0.0E+0	0.0E+0
methyl_Nonane_2	0.0E+0	0.0E+0	0.0E+0	0.0E+0	0.0E+0	0.0E+0	0.0E+0	0.0E+0	0.0E+0	0.0E+0
n_Decane	7.4E-3	8.0E-3	6.1E-3	6.4E-3	6.0E-3	7.9E-3	8.5E-3	9.0E-3	5.4E-3	4.3E-3
butyl_Cyclohexane	2.4E-3	2.6E-3	1.9E-3	1.9E-3	1.8E-3	2.4E-3	2.6E-3	3.0E-3	1.7E-3	1.2E-3

Table C.1c. JP-7 in catalyst coated heat exchangers (continued)

Heat Exchange Exit Temp (K)	823	830	837	844	823	828	822	816	844	845
Heat Addition (J/g)	955	986	1190	1136	1212	1028	1013	941	1392	1506
L to G conversion	0.108	0.105	0.197	0.166	0.211	0.123	0.103	0.084	0.267	0.328
Average Ignition Time (ms)		5.14	4.70	4.12	6.69	5.32	6.45	5.96	5.03	4.99
Mixture Mass Fractions										
trans_Decalin	3.0E-3	3.1E-3	2.4E-3	2.6E-3	2.4E-3	2.9E-3	3.4E-3	3.3E-3	2.2E-3	1.9E-3
methyl_Decane_2	6.9E-3	7.7E-3	5.4E-3	5.2E-3	4.6E-3	7.2E-3	7.9E-3	8.2E-3	4.3E-3	3.3E-3
methyl_Decane_3	5.8E-3	6.8E-3	4.7E-3	4.7E-3	4.1E-3	6.3E-3	6.8E-3	7.1E-3	3.8E-3	2.8E-3
n_Undecane	4.0E-2	4.5E-2	3.1E-2	3.0E-2	2.7E-2	4.3E-2	5.0E-2	4.9E-2	2.4E-2	1.8E-2
n_Dodecane	4.0E-2	4.6E-2	3.0E-2	2.8E-2	2.5E-2	4.2E-2	5.0E-2	5.0E-2	2.3E-2	1.7E-2
n_Tridecane	3.3E-2	3.7E-2	2.4E-2	2.3E-2	2.0E-2	3.6E-2	4.2E-2	4.2E-2	1.8E-2	1.3E-2
methyl_Tridecane	2.2E-3	2.6E-3	1.6E-3	1.6E-3	1.4E-3	2.3E-3	2.5E-3	2.8E-3	1.2E-3	8.9E-4
n_Tetradecane	1.2E-2	1.3E-2	7.7E-3	7.6E-3	6.6E-3	1.2E-2	1.4E-2	1.4E-2	5.9E-3	4.2E-3
methyl_Tetradecane	5.3E-4	5.8E-4	3.8E-4	3.6E-4	3.5E-4	6.1E-4	5.8E-4	6.7E-4	2.9E-4	0.0E+0
n_Pentadecane	2.4E-3	2.7E-3	1.7E-3	1.8E-3	1.5E-3	2.5E-3	2.9E-3	2.9E-3	1.3E-3	9.4E-4
n_Hexadecane	4.0E-4	4.4E-4	2.9E-4	3.2E-4	2.8E-4	4.4E-4	4.9E-4	5.0E-4	2.2E-4	1.7E-4
n_Heptadecane	1.2E-4	1.2E-4	8.1E-5	8.1E-5	7.1E-5	1.1E-4	9.7E-5	1.3E-4	5.9E-5	3.5E-5

Table C.2a. JP-8 in catalyst coated heat exchangers (Nagley, 2008)

Heat Exchange Exit Temp (K)	898	893	900	902	820	869	842	908	924	919	940
Heat Addition (J/g)	1866	1667	2036	2038	879	1413	1028	2049	2067	2045	2637
L to G conversion	0.302	0.242	0.309	0.335	0.029	0.180	0.084	0.318	0.321	0.315	0.435
Average Ignition Time (ms)	6.90	7.58	6.70		8.55	7.80	8.10	7.50	6.45	6.85	6.50
Mixture Mass Fractions											
Hydrogen	6.6E-4	5.9E-4	7.3E-4	7.3E-4	8.2E-5	4.1E-4	1.9E-4	7.5E-4	8.1E-4	7.5E-4	1.2E-3
Methane	4.0E-2	3.1E-2	4.1E-2	4.1E-2	4.5E-3	2.4E-2	1.1E-2	4.5E-2	4.7E-2	4.3E-2	6.9E-2
Ethane	4.3E-2	3.6E-2	4.6E-2	4.6E-2	6.2E-3	3.0E-2	1.5E-2	4.8E-2	4.7E-2	4.7E-2	6.3E-2
Ethylene	1.6E-2	1.5E-2	1.8E-2	1.8E-2	2.7E-3	9.4E-3	5.8E-3	1.5E-2	1.9E-2	1.9E-2	2.0E-2
n_Propane	4.1E-2	3.5E-2	4.4E-2	4.4E-2	5.3E-3	3.1E-2	1.5E-2	4.6E-2	4.3E-2	4.5E-2	5.4E-2
Propylene	4.2E-2	3.7E-2	4.6E-2	4.6E-2	5.1E-3	2.6E-2	1.4E-2	4.1E-2	4.6E-2	4.7E-2	5.1E-2
iso_Butane	4.9E-3	3.9E-3	5.1E-3	5.1E-3	3.7E-4	3.6E-3	1.4E-3	5.7E-3	5.0E-3	5.1E-3	7.0E-3
n_Butane	1.6E-2	1.4E-2	1.8E-2	1.8E-2	1.4E-3	1.3E-2	5.2E-3	1.9E-2	1.6E-2	1.7E-2	1.9E-2
trans_2_Butene	7.0E-3	5.3E-3	6.9E-3	6.9E-3	2.7E-4	3.7E-3	1.2E-3	7.0E-3	7.5E-3	6.8E-3	9.8E-3
Butene_1	1.6E-2	1.3E-2	1.6E-2	1.6E-2	1.2E-3	9.3E-3	4.1E-3	1.4E-2	1.6E-2	1.5E-2	1.5E-2
iso_Butylene	6.4E-4	7.7E-4	6.3E-4	6.3E-4	1.1E-5	2.6E-4	7.2E-5	8.2E-4	7.1E-4	6.1E-4	1.3E-3
cis_2_Butene	1.2E-2	1.0E-2	1.3E-2	1.3E-2	8.7E-4	7.4E-3	3.1E-3	1.2E-2	1.3E-2	1.3E-2	1.5E-2
iso_C5	7.9E-3	6.2E-3	8.0E-3	8.0E-3	3.3E-4	4.6E-3	1.5E-3	8.5E-3	8.5E-3	5.4E-3	7.5E-3
n_Pentane	5.9E-3	4.4E-3	6.0E-3	6.0E-3	2.9E-4	3.9E-3	1.3E-3	6.5E-3	5.7E-3	2.9E-3	4.0E-3
Butadiene	1.6E-3	1.3E-3	1.6E-3	1.6E-3	4.7E-5	5.6E-4	2.0E-4	1.4E-3	1.8E-3	5.5E-3	7.6E-3
Methylenes	1.1E-2	6.0E-3	8.3E-3	8.3E-3	2.3E-4	4.0E-3	1.4E-3	9.8E-3	9.6E-3	8.3E-3	1.1E-2
Pentene_1	7.5E-3	5.2E-3	6.5E-3	6.5E-3	3.4E-4	3.6E-3	1.4E-3	6.7E-3	8.1E-3	6.3E-3	8.6E-3
Undecernable area in gas	3.1E-2	2.0E-2	2.6E-2	2.6E-2	6.0E-4	1.0E-2	4.3E-3	3.0E-2	3.0E-2	2.7E-2	6.2E-2
Propene	0.0E+0	0.0E+0	0.0E+0	0.0E+0	0.0E+0	0.0E+0	0.0E+0	0.0E+0	0.0E+0	0.0E+0	0.0E+0
methyl_Propene	0.0E+0	0.0E+0	0.0E+0	0.0E+0	0.0E+0	0.0E+0	0.0E+0	0.0E+0	0.0E+0	0.0E+0	0.0E+0
methyl_Butane	0.0E+0	0.0E+0	0.0E+0	0.0E+0	0.0E+0	0.0E+0	0.0E+0	0.0E+0	0.0E+0	0.0E+0	0.0E+0
Pentene_1	0.0E+0	0.0E+0	0.0E+0	0.0E+0	0.0E+0	0.0E+0	0.0E+0	0.0E+0	0.0E+0	0.0E+0	0.0E+0
n_Pentane_a	0.0E+0	0.0E+0	0.0E+0	0.0E+0	0.0E+0	0.0E+0	0.0E+0	0.0E+0	0.0E+0	0.0E+0	0.0E+0
Hexene_1	0.0E+0	0.0E+0	0.0E+0	0.0E+0	0.0E+0	0.0E+0	0.0E+0	0.0E+0	0.0E+0	0.0E+0	0.0E+0
n_Hexane	0.0E+0	0.0E+0	0.0E+0	0.0E+0	0.0E+0	0.0E+0	0.0E+0	0.0E+0	0.0E+0	0.0E+0	0.0E+0
Hexene	0.0E+0	0.0E+0	0.0E+0	0.0E+0	0.0E+0	0.0E+0	0.0E+0	0.0E+0	0.0E+0	0.0E+0	0.0E+0
methyl_Cyclopentene	5.4E-3	8.1E-3	1.1E-2	1.1E-2	1.4E-3	6.1E-3	3.8E-3	1.0E-2	9.5E-3	9.8E-3	1.1E-2
methyl_Cyclopentane	0.0E+0	0.0E+0	0.0E+0	0.0E+0	0.0E+0	0.0E+0	0.0E+0	0.0E+0	0.0E+0	0.0E+0	0.0E+0
methyl_Cyclopentene_a	0.0E+0	0.0E+0	0.0E+0	0.0E+0	0.0E+0	0.0E+0	0.0E+0	0.0E+0	0.0E+0	0.0E+0	0.0E+0
methyl_Hexene	1.3E-3	1.7E-3	1.8E-3	1.8E-3	5.0E-4	1.3E-3	1.0E-3	1.6E-3	1.8E-3	1.6E-3	1.3E-3
Benzene	5.0E-3	8.5E-3	1.3E-2	1.3E-2	4.0E-4	4.8E-3	1.3E-3	1.5E-2	1.4E-2	1.3E-2	2.1E-2
methyl_Hexane	7.0E-4	9.0E-4	1.2E-3	1.2E-3	6.0E-4	1.2E-3	9.0E-4	9.0E-4	9.0E-4	1.1E-3	1.0E-3
Cyclohexene	2.8E-3	3.9E-3	5.1E-3	5.1E-3	6.0E-4	2.9E-3	1.6E-3	4.6E-3	5.0E-3	4.9E-3	5.5E-3
dimethyl_Cyclopentane	8.0E-4	1.0E-3	1.3E-3	1.3E-3	3.0E-4	1.0E-3	6.0E-4	1.1E-3	1.0E-3	1.1E-3	1.1E-3
methyl_Hexene_a	3.8E-3	4.2E-3	5.5E-3	5.5E-3	1.7E-3	4.5E-3	3.7E-3	5.0E-3	4.6E-3	5.7E-3	4.8E-3
Heptene_1	8.2E-3	1.1E-2	1.2E-2	1.2E-2	4.1E-3	9.9E-3	6.9E-3	1.1E-2	1.1E-2	1.1E-2	9.2E-3
n_Heptane	3.4E-3	4.4E-3	5.7E-3	5.7E-3	2.8E-3	5.7E-3	4.5E-3	4.3E-3	3.9E-3	5.1E-3	4.6E-3
dimethyl_Cyclopentene	3.9E-3	5.3E-3	7.4E-3	7.4E-3	1.2E-3	4.8E-3	3.1E-3	6.5E-3	6.1E-3	6.7E-3	6.8E-3
Heptene	1.6E-3	2.0E-3	2.5E-3	2.5E-3	5.0E-4	2.0E-3	1.3E-3	2.1E-3	2.2E-3	2.4E-3	2.2E-3
Heptene_a	9.0E-4	1.3E-3	1.5E-3	1.5E-3	3.0E-4	1.1E-3	7.0E-4	1.2E-3	1.3E-3	1.4E-3	1.4E-3
methyl_Cyclohexane	2.5E-3	3.0E-3	3.7E-3	3.7E-3	1.8E-3	3.1E-3	2.6E-3	3.1E-3	2.8E-3	3.2E-3	3.3E-3
ethyl_Cyclopentane	5.0E-4	7.0E-4	9.0E-4	9.0E-4	3.0E-4	7.0E-4	5.0E-4	7.0E-4	7.0E-4	8.0E-4	1.0E-3
methyl_Cyclohexene	3.4E-3	4.5E-3	6.0E-3	6.0E-3	9.0E-4	3.6E-3	2.3E-3	5.6E-3	5.5E-3	5.9E-3	6.2E-3
ethyl_Cyclopentene	1.3E-3	1.8E-3	2.1E-3	2.1E-3	4.0E-4	1.5E-3	1.0E-3	2.0E-3	1.9E-3	2.1E-3	2.3E-3
Octene	1.3E-3	1.4E-3	1.5E-3	1.5E-3	6.0E-4	1.5E-3	1.4E-3	1.4E-3	1.5E-3	1.7E-3	1.1E-3
methyl_Heptane	1.6E-3	1.6E-3	1.7E-3	1.7E-3	1.2E-3	1.8E-3	1.5E-3	1.7E-3	1.6E-3	1.7E-3	1.4E-3
Toluene	9.8E-3	1.6E-2	2.5E-2	2.5E-2	1.8E-3	1.1E-2	4.2E-3	2.8E-2	2.3E-2	2.4E-2	4.5E-2
methyl_Cyclohexene_a	3.3E-3	4.4E-3	5.8E-3	5.8E-3	9.0E-4	3.7E-3	2.3E-3	5.4E-3	5.1E-3	5.6E-3	6.1E-3
dimethyl_Cyclohexane	2.5E-3	2.4E-3	2.7E-3	2.7E-3	2.4E-3	2.8E-3	2.7E-3	2.4E-3	2.2E-3	2.5E-3	2.2E-3
Octene_1	4.8E-3	5.2E-3	6.1E-3	6.1E-3	2.4E-3	5.3E-3	4.3E-3	5.5E-3	5.8E-3	5.8E-3	4.5E-3
dimethyl_Cyclohexene	1.1E-3	1.4E-3	1.7E-3	1.7E-3	5.0E-4	1.4E-3	9.0E-4	1.6E-3	1.5E-3	1.6E-3	1.5E-3
n_Octane	4.3E-3	4.3E-3	4.9E-3	4.9E-3	5.1E-3	5.6E-3	5.4E-3	4.0E-3	3.9E-3	4.4E-3	3.7E-3

Table C.2b. JP-8 in catalyst coated heat exchangers (Nagley, 2008) (continued)

Heat Exchange Exit Temp (K)	898	893	900	902	820	869	842	908	924	919	940
Heat Addition (J/g)	1866	1667	2036	2038	879	1413	1028	2049	2067	2045	2637
L to G conversion	0.302	0.242	0.309	0.335	0.029	0.180	0.084	0.318	0.321	0.315	0.435
Average Ignition Time (ms)	6.90	7.58	6.70		8.55	7.80	8.10	7.50	6.45	6.85	6.50
Mixture Mass Fractions											
Octene_a	7.0E-4	8.0E-4	1.1E-3	1.1E-3	3.0E-4	1.0E-3	7.0E-4	9.0E-4	9.0E-4	1.0E-3	9.0E-4
dimethyl_Cyclohexene_a	3.8E-3	4.6E-3	6.2E-3	6.2E-3	1.3E-3	4.1E-3	3.0E-3	5.5E-3	4.8E-3	5.9E-3	5.5E-3
ethyl_Cyclohexene	1.6E-3	2.3E-3	2.6E-3	2.6E-3	5.0E-4	1.8E-3	1.3E-3	2.3E-3	2.2E-3	2.5E-3	2.6E-3
Ethylbenzene	3.0E-3	4.1E-3	5.9E-3	5.9E-3	1.5E-3	3.5E-3	1.9E-3	6.0E-3	5.1E-3	5.6E-3	8.5E-3
p_Xylene	7.0E-3	9.0E-3	1.3E-2	1.3E-2	3.9E-3	7.6E-3	4.7E-3	1.2E-2	1.1E-2	1.2E-2	1.7E-2
m_Xylene	2.6E-3	3.5E-3	4.3E-3	4.3E-3	1.4E-3	2.6E-3	1.8E-3	4.4E-3	4.1E-3	4.1E-3	6.0E-3
methyl_Octane_3	0.0E+0	0.0E+0	0.0E+0	0.0E+0	0.0E+0	0.0E+0	0.0E+0	0.0E+0	0.0E+0	0.0E+0	0.0E+0
o_Xylene	5.3E-3	6.7E-3	9.1E-3	9.1E-3	3.1E-3	5.7E-3	3.8E-3	9.0E-3	7.9E-3	8.7E-3	1.2E-2
Nonene_1	5.9E-3	5.6E-3	5.8E-3	5.8E-3	3.1E-3	5.2E-3	4.6E-3	5.3E-3	5.5E-3	5.3E-3	4.1E-3
n_Nonane	0.0E+0	0.0E+0	0.0E+0	0.0E+0	0.0E+0	0.0E+0	0.0E+0	0.0E+0	0.0E+0	0.0E+0	0.0E+0
Nonene	1.7E-3	1.9E-3	2.0E-3	2.0E-3	1.2E-3	2.1E-3	1.8E-3	1.8E-3	1.7E-3	1.9E-3	1.4E-3
C3_Alkylbenzenes	2.6E-2	2.9E-2	3.6E-2	3.6E-2	2.1E-2	2.6E-2	2.2E-2	3.5E-2	3.1E-2	3.4E-2	4.5E-2
Decene_1	3.0E-3	2.9E-3	3.0E-3	3.0E-3	1.8E-3	2.9E-3	2.7E-3	2.7E-3	3.0E-3	2.9E-3	2.0E-3
trimethyl_Benzene_1_2_4	1.6E-2	1.7E-2	2.1E-2	2.1E-2	1.4E-2	1.6E-2	1.4E-2	2.0E-2	1.8E-2	2.0E-2	2.3E-2
C3_Alkylbenzenes_2	5.4E-3	5.5E-3	6.6E-3	6.6E-3	4.6E-3	5.2E-3	4.8E-3	6.2E-3	5.8E-3	6.0E-3	7.0E-3
Indane	1.0E-3	1.2E-3	1.5E-3	1.5E-3	6.0E-4	1.0E-3	7.0E-4	1.6E-3	1.3E-3	1.5E-3	2.0E-3
C4_Alkylbenzenes	4.9E-3	4.8E-3	5.6E-3	5.6E-3	4.6E-3	4.8E-3	4.5E-3	5.1E-3	4.8E-3	5.1E-3	5.7E-3
Butylbenzene	3.1E-3	3.0E-3	3.2E-3	3.2E-3	3.4E-3	3.0E-3	2.8E-3	3.2E-3	2.8E-3	3.3E-3	3.2E-3
C4_Alkylbenzenes_2	1.4E-2	1.5E-2	1.6E-2	1.6E-2	1.3E-2	1.4E-2	1.3E-2	1.7E-2	1.4E-2	1.5E-2	1.7E-2
C4_Alkylbenzenes_3	1.3E-2	1.3E-2	1.6E-2	1.6E-2	1.1E-2	1.2E-2	1.1E-2	1.5E-2	1.4E-2	1.5E-2	1.7E-2
Undecene_1	2.8E-3	2.5E-3	2.4E-3	2.4E-3	2.0E-3	2.6E-3	2.7E-3	2.4E-3	2.3E-3	2.4E-3	1.4E-3
C5_Alkylbenzenes	7.6E-3	7.3E-3	8.1E-3	8.1E-3	8.0E-3	7.6E-3	7.5E-3	7.6E-3	7.2E-3	7.5E-3	7.8E-3
Pentylbenzene	4.0E-4	3.0E-4	4.0E-4	4.0E-4	5.0E-4	4.0E-4	5.0E-4	4.0E-4	4.0E-4	3.0E-4	4.0E-4
C5_Alkylbenzenes_2	9.2E-3	8.8E-3	9.7E-3	9.7E-3	9.5E-3	9.1E-3	8.9E-3	9.2E-3	8.7E-3	8.8E-3	9.6E-3
Tetralin	1.2E-3	1.1E-3	1.3E-3	1.3E-3	1.3E-3	1.2E-3	1.2E-3	1.2E-3	1.1E-3	1.2E-3	1.2E-3
Naphthalene	2.7E-3	3.5E-3	5.0E-3	5.0E-3	1.4E-3	2.7E-3	1.7E-3	5.4E-3	4.6E-3	4.8E-3	7.1E-3
Dodecene_1	1.7E-3	1.5E-3	1.3E-3	1.3E-3	3.3E-3	5.0E-3	3.7E-3	8.3E-3	7.1E-3	7.3E-3	1.0E-2
methyl_Naphthalene_2	4.9E-3	6.0E-3	7.9E-3	7.9E-3	2.1E-3	3.4E-3	2.5E-3	5.4E-3	4.7E-3	4.8E-3	6.7E-3
methyl_Naphthalene_1	3.3E-3	4.0E-3	5.2E-3	5.2E-3	2.1E-3	3.4E-3	2.5E-3	5.4E-3	4.7E-3	4.8E-3	6.7E-3
dimethyl_Naphthalenes	3.6E-3	4.1E-3	5.2E-3	5.2E-3	2.7E-3	3.6E-3	2.9E-3	5.3E-3	4.6E-3	4.8E-3	6.3E-3
dimethyl_Naphthalene_1_3	2.7E-3	3.1E-3	3.9E-3	3.9E-3	2.0E-3	3.1E-3	2.1E-3	4.0E-3	3.5E-3	3.5E-3	4.6E-3
dimethyl_Naphthalenes_2	3.9E-3	4.5E-3	5.7E-3	5.7E-3	2.9E-3	4.0E-3	3.1E-3	5.8E-3	5.1E-3	5.3E-3	7.0E-3
Acenaphthylene	5.0E-5	1.0E-4	1.2E-4	1.2E-4	0.0E+0	4.0E-5	1.0E-5	1.7E-4	1.5E-4	1.3E-4	2.5E-3
Acenaphthene	9.0E-5	1.5E-4	2.1E-4	2.1E-4	2.0E-5	1.1E-4	4.0E-5	2.6E-4	2.1E-4	2.0E-4	3.5E-4
Fluorene	2.0E-4	3.3E-4	4.6E-4	4.6E-4	5.0E-5	2.4E-4	9.0E-5	5.0E-4	4.7E-4	4.6E-4	7.7E-4
Phenanthrene	1.3E-4	2.6E-4	4.8E-4	4.8E-4	1.0E-5	1.6E-4	4.0E-5	6.7E-4	5.6E-4	5.3E-4	9.4E-4
Anthracene	4.0E-5	8.0E-5	1.4E-4	1.4E-4	0.0E+0	5.0E-5	1.0E-5	1.8E-4	1.4E-4	1.3E-4	2.2E-4
Fluoranthene	3.0E-5	5.0E-5	9.0E-5	9.0E-5	0.0E+0	3.0E-5	1.0E-5	1.2E-4	1.1E-4	1.1E-4	1.9E-4
Pyrene	1.4E-4	2.5E-4	4.1E-4	4.1E-4	1.0E-5	1.7E-4	4.0E-5	4.7E-4	3.9E-4	3.8E-4	5.9E-4
benz_a_Anthracene	2.0E-5	3.0E-5	6.0E-5	6.0E-5	0.0E+0	2.0E-5	0.0E+0	7.0E-5	6.0E-5	7.0E-5	1.0E-4
Chrysene	1.0E-5	3.0E-5	5.0E-5	5.0E-5	0.0E+0	1.0E-5	0.0E+0	6.0E-5	5.0E-5	6.0E-5	9.0E-5
benzo_b_Fluoranthene	1.0E-5	2.0E-5	5.0E-5	5.0E-5	0.0E+0	1.0E-5	0.0E+0	5.0E-5	5.0E-5	7.0E-5	1.1E-4
benzo_k_Fluoranthene	0.0E+0	0.0E+0	1.0E-5	1.0E-5	0.0E+0	0.0E+0	0.0E+0	1.0E-5	1.0E-5	1.0E-5	1.0E-5
benzo_a_Pyrene	2.0E-5	3.0E-5	7.0E-5	7.0E-5	0.0E+0	2.0E-5	0.0E+0	7.0E-5	6.0E-5	7.0E-5	1.1E-4
indeno_1_2_3_cd_Pyrene	2.0E-5	4.0E-5	6.0E-5	6.0E-5	0.0E+0	3.0E-5	0.0E+0	8.0E-5	6.0E-5	8.0E-5	1.3E-4
dibenz_a_h_Anthracene	0.0E+0	0.0E+0	1.0E-5	1.0E-5	0.0E+0	0.0E+0	0.0E+0	1.0E-5	1.0E-5	1.0E-4	2.0E-5
benzo_g_h_i_Perylene	1.0E-5	3.0E-5	6.0E-5	6.0E-5	0.0E+0	2.0E-5	0.0E+0	0.0E+0	4.0E-5	6.0E-5	1.0E-4
methyl_Octane_3_2	3.0E-3	2.4E-3	2.4E-3	2.4E-3	4.1E-3	3.9E-3	3.5E-3	2.1E-3	2.2E-3	2.2E-3	1.6E-3
n_Nonane_2	1.6E-2	1.3E-2	1.2E-2	1.2E-2	2.3E-2	1.6E-2	2.0E-2	1.1E-2	1.1E-2	1.1E-2	7.8E-3
dimethyl_Octane	1.4E-2	1.1E-2	9.9E-3	9.9E-3	1.9E-2	1.2E-2	1.6E-2	9.2E-3	9.7E-3	9.2E-3	6.5E-3
methyl_Nonane_2	4.9E-3	3.6E-3	3.2E-3	3.2E-3	7.1E-3	4.5E-3	5.5E-3	3.0E-3	3.1E-3	3.0E-3	2.1E-3
n_Decane	2.3E-2	1.7E-2	1.4E-2	1.4E-2	3.6E-2	2.0E-2	2.7E-2	1.3E-2	1.4E-2	1.3E-2	8.5E-3
butyl_Cyclohexane	1.8E-3	1.4E-3	1.3E-3	1.3E-3	2.9E-3	1.7E-3	2.3E-3	1.2E-3	1.2E-3	1.2E-3	8.0E-4

Table C.2c. JP-8 in catalyst coated heat exchangers (Nagley, 2008) (continued)

Heat Exchange Exit Temp (K)	898	893	900	902	820	869	842	908	924	919	940
Heat Addition (J/g)	1866	1667	2036	2038	879	1413	1028	2049	2067	2045	2637
L to G conversion	0.302	0.242	0.309	0.335	0.029	0.180	0.084	0.318	0.321	0.315	0.435
Average Ignition Time (ms)	6.90	7.58	6.70		8.55	7.80	8.10	7.50	6.45	6.85	6.50
Mixture Mass Fractions											
trans_Decalin	1.8E-3	1.4E-3	1.4E-3	1.4E-3	2.3E-3	1.8E-3	2.0E-3	1.2E-3	1.2E-3	1.3E-3	9.0E-4
methyl_Decane_2	5.1E-3	3.7E-3	3.2E-3	3.2E-3	7.8E-3	4.5E-3	6.1E-3	3.0E-3	3.1E-3	2.8E-3	2.0E-3
methyl_Decane_3	4.0E-3	2.9E-3	2.5E-3	2.5E-3	6.1E-3	3.5E-3	4.8E-3	2.3E-3	2.5E-3	2.3E-3	1.5E-3
n_Undecane	2.0E-2	1.4E-2	1.2E-2	1.2E-2	3.3E-2	1.8E-2	2.5E-2	1.1E-2	1.2E-2	1.1E-2	6.7E-3
n_Dodecane	1.5E-2	1.0E-2	8.3E-3	8.3E-3	2.5E-2	1.3E-2	1.8E-2	7.6E-3	8.0E-3	7.2E-3	4.2E-3
n_Tridecane	1.1E-2	7.2E-3	5.8E-3	5.8E-3	1.9E-2	9.2E-3	1.4E-2	5.2E-3	5.4E-3	5.0E-3	2.9E-3
methyl_Tridecane	1.2E-3	8.0E-4	6.0E-4	6.0E-4	2.1E-3	1.1E-3	1.4E-3	6.0E-4	7.0E-4	6.0E-4	4.0E-4
n_Tetradecane	7.2E-3	4.6E-3	3.4E-3	3.4E-3	1.3E-2	6.2E-3	9.1E-3	3.4E-3	3.4E-3	3.2E-3	1.7E-3
methyl_Tetradecane	7.0E-4	4.3E-3	4.0E-4	4.0E-4	1.1E-3	6.0E-4	8.0E-4	3.0E-4	3.0E-4	3.0E-4	2.0E-4
n_Pentadecane	3.4E-3	2.4E-3	1.5E-3	1.5E-3	6.8E-3	3.2E-3	4.6E-3	1.5E-3	1.7E-3	1.4E-3	7.0E-4
n_Hexadecane	9.0E-4	6.0E-4	4.0E-4	4.0E-4	1.8E-3	8.0E-4	1.2E-4	4.0E-4	4.0E-4	4.0E-4	2.0E-4
n_Heptadecane	2.0E-4	1.5E-4	1.1E-4	1.1E-4	4.0E-4	2.0E-4	3.0E-4	1.0E-4	1.0E-4	1.0E-4	1.0E-4

Table C.3a. JP-8 in uncoated heat exchangers

Heat Exchange Exit Temp (K)	793	824	827
Heat Addition (J/g)	1093	1710	2027
L to G conversion (kg gas/kg fuel)	0.142	0.328	0.439
Average Ignition Time (ms)	10.068	9.354	8.072
Mass Fractions			
Hydrogen	2.5E-4	8.1E-4	8.2E-4
Methane	1.4E-2	3.5E-2	4.9E-2
Ethane	1.9E-2	4.4E-2	6.2E-2
Ethylene	3.8E-3	1.8E-2	1.7E-2
n_Propane	2.2E-2	4.5E-2	6.5E-2
Propylene	1.5E-2	4.6E-2	5.3E-2
iso_Butane	2.9E-3	5.0E-3	8.4E-3
n_Butane	1.1E-2	1.8E-2	2.8E-2
trans_2_Butene	2.9E-3	6.7E-3	1.0E-2
Butene_1	5.6E-3	1.5E-2	1.9E-2
iso_Butylene	2.5E-3	6.4E-4	9.6E-3
cis_2_Butene	3.9E-3	1.3E-2	1.2E-2
iso_C5	2.2E-3	6.2E-3	5.6E-3
n_Pentane	3.1E-3	4.5E-3	8.6E-3
Butadiene	2.3E-3	3.9E-3	5.1E-3
Methylenes	2.7E-4	1.2E-3	1.8E-3
Pentene_1	5.0E-4	1.4E-3	1.5E-3
Undecernable area in gas	1.9E-2	4.0E-2	5.7E-2
Propene	0.0E+0	3.6E-4	8.6E-4
methyl_Propene	3.1E-3	6.7E-3	9.0E-3
methyl_Butane	1.3E-3	1.2E-3	1.5E-3
Pentene_1	3.4E-3	4.2E-3	3.5E-3
n_Pentane_a	5.8E-3	4.8E-3	5.2E-3
Hexene_1	7.8E-3	1.0E-2	8.1E-3
n_Hexane	7.8E-3	4.9E-3	4.5E-3
Hexene	2.3E-3	2.9E-3	2.2E-3
methyl_Cyclopentene	2.0E-3	2.8E-3	2.1E-3
methyl_Cyclopentane	3.5E-3	3.8E-3	3.2E-3
methyl_Cyclopentene_a	3.5E-3	4.6E-3	3.6E-3
methyl_Hexene	1.4E-3	1.9E-3	1.6E-3
Benzene	2.5E-3	8.1E-3	5.9E-3
methyl_Hexane	1.7E-3	1.1E-3	1.0E-3
Cyclohexene	2.9E-3	4.9E-3	3.6E-3
dimethyl_Cyclopentane	1.1E-3	1.2E-3	9.0E-4
methyl_Hexene_a	4.2E-3	4.8E-3	4.1E-3
Heptene_1	8.8E-3	1.1E-2	9.3E-3
n_Heptane	7.6E-3	5.1E-3	4.8E-3
dimethyl_Cyclopentene	6.0E-3	7.0E-3	5.2E-3
Heptene	2.3E-3	2.5E-3	1.9E-3
Heptene_a	1.4E-3	1.5E-3	1.1E-3
methyl_Cyclohexane	4.1E-3	3.6E-3	3.3E-3
ethyl_Cyclopentane	1.0E-3	9.0E-4	8.0E-4
methyl_Cyclohexene	4.9E-3	7.0E-3	5.2E-3
ethyl_Cyclopentene	2.0E-3	2.2E-3	1.7E-3
Octene	1.2E-3	1.4E-3	1.2E-3
methyl_Heptane	1.9E-3	1.7E-3	1.8E-3
Toluene	8.2E-3	1.9E-2	1.1E-2
methyl_Cyclohexene_a	4.6E-3	5.9E-3	4.1E-3
dimethyl_Cyclohexane	3.6E-3	3.0E-3	3.2E-3
Octene_1	4.5E-3	5.8E-3	5.1E-3
dimethyl_Cyclohexene	2.4E-3	3.1E-3	2.5E-3
n_Octane	6.6E-3	4.7E-3	5.5E-3

Table C.3b JP-8 in uncoated heat exchangers (continued)

Heat Exchange Exit Temp (K)	793	824	827
Heat Addition (J/g)	1093	1710	2027
L to G conversion (kg gas/kg fuel)	0.142	0.328	0.439
Average Ignition Time (ms)	10.068	9.354	8.072
Mass Fractions			
Octene_a	1.2E-3	1.1E-3	9.0E-4
dimethyl_Cyclohexene_a	7.8E-3	8.6E-3	6.4E-3
ethyl_Cyclohexene	2.2E-3	2.8E-3	2.0E-3
Ethylbenzene	2.9E-3	4.7E-3	3.2E-3
p_Xylene	6.8E-3	1.0E-2	7.2E-3
m_Xylene	2.5E-3	4.0E-3	2.6E-3
methyl_Octane_3	2.8E-3	2.2E-3	3.3E-3
o_Xylene	5.4E-3	7.8E-3	5.7E-3
Nonene_1	4.8E-3	5.5E-3	4.9E-3
n_Nonane	1.5E-2	1.2E-2	1.9E-2
Nonene	2.0E-3	2.0E-3	1.7E-3
C3_Alkylbenzenes	3.0E-2	3.5E-2	3.1E-2
Decene_1	2.5E-3	2.8E-3	2.5E-3
trimethyl_Benzene_1_2_4	1.5E-2	1.9E-2	1.6E-2
C3_Alkylbenzenes_2	0.0E+0	0.0E+0	0.0E+0
Indane	9.0E-4	1.4E-3	1.0E-3
C4_Alkylbenzenes	3.1E-2	3.5E-2	3.0E-2
Butylbenzene	3.1E-3	3.3E-3	3.4E-3
C4_Alkylbenzenes_2	0.0E+0	0.0E+0	0.0E+0
C4_Alkylbenzenes_3	0.0E+0	0.0E+0	0.0E+0
Undecene_1	2.6E-3	2.7E-3	2.6E-3
C5_Alkylbenzenes	1.7E-2	1.8E-2	1.5E-2
Pentylbenzene	0.0E+0	0.0E+0	0.0E+0
C5_Alkylbenzenes_2	0.0E+0	0.0E+0	0.0E+0
Tetralin	1.1E-3	1.2E-3	1.1E-3
Naphthalene	3.1E-3	4.2E-3	2.7E-3
Dodecene_1	0.0E+0	0.0E+0	0.0E+0
methyl_Naphthalene_2	4.9E-3	6.6E-3	3.8E-3
methyl_Naphthalene_1	3.2E-3	4.4E-3	2.6E-3
dimethyl_Naphthalenes	7.6E-3	9.4E-3	5.8E-3
dimethyl_Naphthalene_1_3	2.7E-3	3.3E-3	2.1E-3
dimethyl_Naphthalenes_2	0.0E+0	0.0E+0	0.0E+0
Acenaphthylene	2.0E-5	9.1E-5	2.5E-5
Acenaphthene	7.5E-5	1.7E-4	6.0E-5
Fluorene	1.6E-4	3.6E-4	1.4E-4
Phenanthrene	6.0E-5	1.9E-4	6.8E-5
Anthracene	2.2E-5	6.7E-5	2.5E-5
Fluoranthene	9.4E-6	3.6E-5	1.4E-5
Pyrene	6.4E-5	2.0E-4	9.0E-5
benz_a_Anthracene	0.0E+0	1.9E-5	7.0E-6
Chrysene	0.0E+0	1.6E-5	5.6E-6
benzo_b_Fluoranthene	0.0E+0	1.1E-5	1.4E-5
benzo_k_Fluoranthene	0.0E+0	0.0E+0	0.0E+0
benzo_a_Pyrene	0.0E+0	1.8E-5	0.0E+0
indeno_1_2_3_cd_Pyrene	0.0E+0	3.0E-5	6.9E-6
dibenz_a_h_Anthracene	0.0E+0	0.0E+0	0.0E+0
benzo_g_h_i_Perylene	0.0E+0	1.6E-5	0.0E+0
methyl_Octane_3_2	7.5E-3	7.2E-3	1.1E-2
n_Nonane_2	0.0E+0	0.0E+0	0.0E+0
dimethyl_Octane	0.0E+0	0.0E+0	0.0E+0
methyl_Nonane_2	3.4E-3	3.2E-3	5.0E-3
n_Decane	1.9E-2	1.4E-2	2.5E-2
butyl_Cyclohexane	1.4E-3	1.2E-3	1.9E-3

Table C.3c. JP-8 in uncoated heat exchangers (continued)

Heat Exchange Exit Temp (K)	793	824	827
Heat Addition (J/g)	1093	1710	2027
L to G conversion (kg gas/kg fuel)	0.142	0.328	0.439
Average Ignition Time (ms)	10.068	9.354	8.072
Mass Fractions			
trans_Decalin	1.7E-3	1.3E-3	1.8E-3
methyl_Decane_2	3.8E-3	3.2E-3	5.1E-3
methyl_Decane_3	2.9E-3	2.5E-3	4.1E-3
n_Undecane	1.5E-2	1.2E-2	2.1E-2
n_Dodecane	1.1E-2	8.2E-3	1.4E-2
n_Tridecane	7.4E-3	5.6E-3	9.8E-3
methyl_Tridecane	9.0E-4	6.0E-4	1.0E-3
n_Tetradecane	4.7E-3	3.2E-3	6.0E-3
methyl_Tetradecane	4.0E-4	4.0E-4	5.0E-4
n_Pentadecane	2.3E-3	1.5E-3	2.8E-3
n_Hexadecane	7.0E-4	4.0E-4	7.0E-4
n_Heptadecane	1.4E-4	1.0E-4	1.0E-4

Table C.4a. JP-7 in uncoated heat exchangers

Heat Exchange Exit Temp (K)	813	803	793	823
Heat Addition (J/g)	1409	1318	1000	1853
L to G conversion (kg gas/kg fuel)	0.288	0.248	0.143	0.385
Average Ignition Time (ms)	9.38	10.50	8.84	9.69
Mass Fractions				
Hydrogen	4.7E-4	4.2E-4	2.1E-4	7.7E-4
Methane	2.4E-2	2.0E-2	1.1E-2	3.9E-2
Ethane	3.5E-2	3.1E-2	1.9E-2	5.3E-2
Ethylene	1.7E-2	1.3E-2	9.2E-3	1.8E-2
n_Propane	3.9E-2	3.6E-2	2.2E-2	5.8E-2
Propylene	4.2E-2	3.6E-2	2.3E-2	5.2E-2
iso_Butane	3.8E-3	3.5E-3	1.8E-3	6.6E-3
n_Butane	1.7E-2	1.7E-2	9.1E-3	2.7E-2
trans_2_Butene	5.5E-3	4.5E-3	2.0E-3	8.7E-3
Butene_1	1.6E-2	1.4E-2	8.4E-3	1.9E-2
iso_Butylene	4.5E-4	3.6E-4	5.4E-3	1.6E-2
cis_2_Butene	1.1E-2	9.5E-3	1.4E-3	6.3E-3
iso_C5	3.7E-3	2.8E-3	1.0E-3	4.6E-3
n_Pentane	2.7E-3	2.7E-3	2.7E-3	5.5E-3
Butadiene	6.0E-3	5.4E-3	4.6E-4	5.8E-3
Methylenes	1.6E-3	1.2E-3	2.8E-4	1.4E-3
Pentene_1	1.1E-3	5.9E-4	7.1E-4	1.8E-3
Undecernable area in gas	4.0E-2	3.2E-2	1.4E-2	5.6E-2
Propene	8.6E-4	1.4E-3	1.9E-3	2.3E-3
methyl_Propene	8.8E-3	1.3E-2	1.2E-2	2.0E-2
methyl_Butane	9.7E-4	1.6E-3	1.2E-3	2.8E-3
Pentene_1	5.0E-3	6.4E-3	5.4E-3	9.1E-3
n_Pentane_a	5.5E-3	7.3E-3	5.6E-3	1.0E-2
Hexene_1	1.2E-2	1.3E-2	1.1E-2	1.4E-2
n_Hexane	4.9E-3	6.1E-3	4.1E-3	8.6E-3
Hexene	2.6E-3	2.6E-3	1.4E-3	4.1E-3
methyl_Cyclopentene	2.4E-3	2.4E-3	1.7E-3	4.1E-3
methyl_Cyclopentane	3.1E-3	3.3E-3	1.8E-3	6.0E-3
methyl_Cyclopentene_a	4.1E-3	4.2E-3	2.5E-3	6.8E-3
methyl_Hexene	1.7E-3	1.8E-3	1.3E-3	2.0E-3
Benzene	4.6E-3	3.4E-3	1.1E-3	1.1E-2
methyl_Hexane	7.1E-4	9.0E-4	5.3E-4	1.4E-3
Cyclohexene	5.0E-3	4.6E-3	2.8E-3	7.0E-3
dimethyl_Cyclopentane	9.6E-4	9.9E-4	6.2E-4	1.6E-3
methyl_Hexene_a	4.4E-3	5.0E-3	3.7E-3	5.7E-3
Heptene_1	1.2E-2	1.2E-2	9.2E-3	1.3E-2
n_Heptane	4.5E-3	5.5E-3	3.9E-3	7.1E-3
dimethyl_Cyclopentene	6.1E-3	6.0E-3	3.5E-3	9.5E-3
Heptene	2.4E-3	2.5E-3	1.5E-3	3.1E-3
Heptene_a	1.3E-3	1.4E-3	8.9E-4	1.9E-3
methyl_Cyclohexane	2.8E-3	3.2E-3	2.1E-3	4.4E-3
ethyl_Cyclopentane	7.1E-4	7.7E-4	4.2E-4	1.3E-3
methyl_Cyclohexene	7.3E-3	6.9E-3	4.4E-3	9.8E-3
ethyl_Cyclopentene	2.3E-3	2.3E-3	1.3E-3	3.2E-3
Octene	1.5E-3	1.5E-3	1.2E-3	1.6E-3
methyl_Heptane	1.3E-3	1.4E-3	1.1E-3	1.5E-3
Toluene	9.8E-3	7.5E-3	2.6E-3	7.8E-3
methyl_Cyclohexene_a	6.0E-3	6.0E-3	3.4E-3	4.4E-3
dimethyl_Cyclohexane	1.5E-3	1.9E-3	1.1E-3	2.6E-3
Octene_1	7.5E-3	7.9E-3	6.5E-3	7.1E-3
dimethyl_Cyclohexene	3.2E-3	3.3E-3	2.5E-3	4.2E-3
n_Octane	3.2E-3	3.9E-3	2.7E-3	4.6E-3
Octene_a	9.8E-4	9.9E-4	7.1E-4	1.3E-3

Table C.4b. JP-7 in uncoated heat exchangers (continued)

Heat Exchange Exit Temp (K)	813	803	793	823
Heat Addition (J/g)	1409	1318	1000	1853
L to G conversion (kg gas/kg fuel)	0.288	0.248	0.143	0.385
Average Ignition Time (ms)	9.38	10.50	8.84	9.69
Mass Fractions				
dimethyl_Cyclohexene_a	9.3E-3	9.5E-3	6.0E-3	1.3E-2
ethyl_Cyclohexene	3.5E-3	3.4E-3	2.3E-3	4.1E-3
Ethylbenzene	1.7E-3	1.3E-3	4.4E-4	3.9E-3
p_Xylene	2.6E-3	2.4E-3	8.9E-4	6.9E-3
m_Xylene	1.2E-3	1.1E-3	3.5E-4	3.0E-3
methyl_Octane_3	4.9E-4	6.3E-4	4.4E-4	7.0E-4
o_Xylene	1.8E-3	1.4E-3	5.3E-4	4.1E-3
Nonene_1	8.6E-3	8.4E-3	7.7E-3	7.4E-3
n_Nonane	2.9E-3	3.4E-3	2.7E-3	3.5E-3
Nonene	1.7E-3	1.6E-3	1.2E-3	2.1E-3
C3_Alkylbenzenes	3.6E-3	3.0E-3	1.4E-3	7.5E-3
Decene_1	4.9E-3	5.5E-3	4.7E-3	4.4E-3
trimethyl_Benzene_1_2_4	1.3E-3	1.2E-3	6.0E-4	2.5E-3
C3_Alkylbenzenes_2	0.0E+0	0.0E+0	0.0E+0	0.0E+0
Indane	5.3E-4	5.0E-4	0.0E+0	1.2E-3
C4_Alkylbenzenes	3.5E-3	3.3E-3	1.9E-3	5.9E-3
Butylbenzene	7.0E-4	6.0E-4	4.0E-4	1.4E-3
C4_Alkylbenzenes_2	0.0E+0	0.0E+0	0.0E+0	0.0E+0
C4_Alkylbenzenes_3	0.0E+0	0.0E+0	0.0E+0	0.0E+0
Undecene_1	4.4E-3	5.1E-3	4.6E-3	4.1E-3
C5_Alkylbenzenes	2.2E-3	2.3E-3	8.0E-4	4.4E-3
Pentylbenzene	0.0E+0	0.0E+0	0.0E+0	0.0E+0
C5_Alkylbenzenes_2	0.0E+0	0.0E+0	0.0E+0	0.0E+0
Tetralin	4.0E-4	0.0E+0	0.0E+0	7.0E-4
Naphthalene	4.0E-4	4.0E-4	0.0E+0	1.3E-3
Dodecene_1	0.0E+0	0.0E+0	0.0E+0	0.0E+0
methyl_Naphthalene_2	5.0E-4	0.0E+0	0.0E+0	1.4E-3
methyl_Naphthalene_1	0.0E+0	4.0E-4	0.0E+0	9.0E-4
dimethyl_Naphthalenes	6.0E-4	5.0E-4	5.0E-4	1.7E-3
dimethyl_Naphthalene_1_3	0.0E+0	0.0E+0	0.0E+0	5.0E-4
dimethyl_Naphthalenes_2	6.5E-4	4.4E-4	1.1E-4	1.9E-3
Acenaphthylene	2.1E-5	1.2E-5	0.0E+0	6.6E-5
Acenaphthene	3.8E-5	2.6E-5	0.0E+0	1.3E-4
Fluorene	7.5E-5	4.8E-5	9.9E-6	2.5E-4
Phenanthrene	3.7E-5	2.3E-5	0.0E+0	1.3E-4
Anthracene	1.6E-5	1.0E-5	0.0E+0	5.3E-5
Fluoranthene	9.1E-6	5.7E-6	0.0E+0	3.2E-5
Pyrene	4.2E-5	2.7E-5	0.0E+0	1.3E-4
benz_a_Anthracene	0.0E+0	0.0E+0	0.0E+0	1.5E-5
Chrysene	0.0E+0	0.0E+0	0.0E+0	9.6E-6
benzo_b_Fluoranthene	0.0E+0	0.0E+0	0.0E+0	1.0E-5
benzo_k_Fluoranthene	0.0E+0	0.0E+0	0.0E+0	0.0E+0
benzo_a_Pyrene	0.0E+0	5.7E-6	0.0E+0	1.5E-5
indeno_1_2_3_cd_Pyrene	7.2E-6	6.9E-6	0.0E+0	2.8E-5
dibenz_a_h_Anthracene	0.0E+0	0.0E+0	0.0E+0	0.0E+0
benzo_g_h_i_Perylene	0.0E+0	0.0E+0	0.0E+0	1.5E-5
methyl_Octane_3_2	0.0E+0	0.0E+0	0.0E+0	0.0E+0
n_Nonane_2	0.0E+0	0.0E+0	0.0E+0	0.0E+0
dimethyl_Octane	0.0E+0	0.0E+0	0.0E+0	0.0E+0
methyl_Nonane_2	0.0E+0	0.0E+0	0.0E+0	0.0E+0
n_Decane	6.7E-3	7.0E-3	8.0E-3	7.7E-3
butyl_Cyclohexane	2.0E-3	2.0E-3	2.3E-3	2.2E-3
trans_Decalin	2.8E-3	3.0E-3	3.1E-3	2.3E-3
methyl_Decane_2	5.6E-3	5.6E-3	6.9E-3	3.8E-3

Table C.4c. Jp-7 in uncoated heat exchangers (continued)

Heat Exchange Exit Temp (K)	813	803	793	823
Heat Addition (J/g)	1409	1318	1000	1853
L to G conversion (kg gas/kg fuel)	0.288	0.248	0.143	0.385
Average Ignition Time (ms)	9.38	10.50	8.84	9.69
Mass Fractions				
methyl_Decane_3	5.0E-3	5.0E-3	6.1E-3	3.3E-3
n_Undecane	3.3E-2	3.2E-2	4.5E-2	2.0E-2
n_Dodecane	3.0E-2	3.0E-2	4.2E-2	1.8E-2
n_Tridecane	2.4E-2	2.3E-2	3.4E-2	1.3E-2
methyl_Tridecane	1.8E-3	1.6E-3	2.4E-3	9.0E-4
n_Tetradecane	7.7E-3	7.5E-3	1.1E-2	4.0E-3
methyl_Tetradecane	3.8E-4	3.6E-4	5.3E-4	2.0E-4
n_Pentadecane	1.5E-3	1.4E-3	2.2E-3	8.0E-4
n_Hexadecane	2.5E-4	2.7E-4	3.5E-4	1.0E-4
n_Heptadecane	5.3E-5	6.3E-5	8.9E-5	0.0E+0

Table C.5a. Specific heat curve fit coefficients

Species	MW	a	b	c	d	e
Hydrogen	2.01588	-2.1E-11	6.33E-08	-6.5E-05	0.029234	24.43238
Methane	16.0425	8.35E-11	-2.7E-07	0.000289	-0.07138	37.88583
Ethane	30.069	2.22E-10	-5.9E-07	0.0005	-0.0474	35.99083
Ethylene	28.0532	2.52E-10	-6.5E-07	0.000552	-0.09584	37.7479
n_Propane	44.0956	2.63E-10	-6.7E-07	0.000508	0.038457	32.95333
Propylene	42.0797	2.19E-10	-5.6E-07	0.000428	0.021761	33.05083
iso_Butane	58.1222	2.73E-10	-6.8E-07	0.000455	0.147651	28.68667
n_Butane	58.1222	2.87E-10	-7.3E-07	0.000543	0.088371	41.90167
trans_2_Butene	56.1063	1.15E-10	-3.1E-07	0.000214	0.146583	33.02667
Butene_1	56.1063	3.06E-10	-7.7E-07	0.000566	0.05156	37.8775
iso_Butylene	56.1063	1.33E-10	-3.3E-07	0.000187	0.176686	26.7375
cis_2_Butene	56.1063	4.32E-10	-1.1E-06	0.000908	-0.08724	51.64917
iso_C5	72.1488	1.84E-10	-4.3E-07	0.000203	0.31752	16.425
n_Pentane	72.1488	4.9E-10	-1.3E-06	0.00101	-0.0159	65.40167
Butadiene	54.0904	4.61E-10	-1.1E-06	0.000711	0.032978	31.295
Methylenes	70.1329	1.01E-10	-2.1E-07	1.32E-05	0.334844	13.75401
Pentene_1	70.1329	3.53E-10	-8.8E-07	0.00063	0.102469	42.90556
Undecernable_Area	86.1754	5.65E-10	-1.5E-06	0.001133	0.01297	73.01944
Propene	42.0797	2.19E-10	-5.6E-07	0.000428	0.021761	33.05083
methyl_Propene	56.1063	1.33E-10	-3.3E-07	0.000187	0.176686	26.7375
methyl_Butane	72.1488	1.84E-10	-4.3E-07	0.000203	0.31752	16.425
Pentene_1	70.1329	3.53E-10	-8.8E-07	0.00063	0.102469	42.90556
n_Pentane_a	72.1488	4.9E-10	-1.3E-06	0.00101	-0.0159	65.40167
Hexene_1	84.1595	1.13E-10	-2.3E-07	-2.3E-05	0.4285	11.80955
n_Hexane	86.1754	5.65E-10	-1.5E-06	0.001133	0.01297	73.01944
Hexene	84.1595	2.69E-11	-5.5E-08	-5.5E-06	0.102416	2.822295
methyl_Cyclopentene	82.1436	2.22E-10	-5.2E-07	0.000227	0.349136	-12.0543
methyl_Cyclopentane	84.1595	8.26E-10	-2.1E-06	0.001623	-0.12065	50.3
methyl_Cyclopentene_a	82.1436	2.22E-10	-5.2E-07	0.000227	0.349136	-12.0543
methyl_Hexene	98.1861	8.99E-11	-1.5E-07	-0.00016	0.578314	4.246513
Benzene	78.1118	6.64E-10	-1.6E-06	0.001144	-0.03603	28.05083
methyl_Hexane	100.2019	3.39E-10	-8.1E-07	0.000439	0.389429	28.82222
Cyclohexene	82.14136	6.45E-10	-1.6E-06	0.001195	0.00339	31.78333
dimethyl_Cyclopentane	98.1861	7.81E-10	-1.9E-06	0.001431	0.033351	42.85667
methyl_Hexene_a	98.1861	8.99E-11	-1.5E-07	-0.00016	0.578314	4.246513
Heptene_1	98.1861	1.39E-10	-2.8E-07	-2.1E-05	0.502938	13.47422
n_Heptane	100.2019	-1.1E-09	3.34E-06	-0.00382	2.260311	-267.557
dimethyl_Cyclopentene	96.1702	2.3E-10	-5.1E-07	0.00016	0.456737	-13.3398
Heptene	98.1861	1.39E-10	-2.8E-07	-2.1E-05	0.502938	13.47422
Heptene_a	98.1861	1.39E-10	-2.8E-07	-2.1E-05	0.502938	13.47422

Table C.5b. Specific heat curve fit coefficients (continued)

Species	MW	a	b	c	d	e
methyl_Cyclohexane	98.1861	6.88E-10	-1.7E-06	0.001197	0.141891	27.1
ethyl_Cyclopentane	98.1861	9E-10	-2.2E-06	0.001726	-0.08186	57.64167
methyl_Cyclohexene	96.1702	1.12E-10	-1.4E-07	-0.00028	0.679451	-44.9695
ethyl_Cyclopentene	96.1702	1.92E-10	-4.6E-07	0.000234	0.269408	-15.3769
Octene	112.2126	1.51E-10	-3E-07	-4.6E-05	0.586778	14.02644
methyl_Heptane	114.2285	-4.9E-10	9.32E-07	-0.00076	0.739753	10.913
Toluene	92.1384	3.53E-10	-8.3E-07	0.000475	0.253203	5.944444
methyl_Cyclohexene_a	96.1702	1.12E-10	-1.4E-07	-0.00028	0.679451	-44.9695
dimethyl_Cyclohexane	110.1968	8.74E-10	-2.2E-06	0.001644	0.048805	45.1
Octene_1	112.2126	1.51E-10	-3E-07	-4.6E-05	0.586778	14.02644
dimethyl_Cyclohexene	110.1968	1.2E-10	-1.3E-07	-0.00034	0.787015	-46.249
n_Octane	110.1968	7.43E-10	-1.9E-06	0.001454	0.04428	91.26611
Octene_a	114.2285	1.51E-10	-3E-07	-4.6E-05	0.586778	14.02644
dimethyl_Cyclohexene_a	112.2126	1.2E-10	-1.3E-07	-0.00034	0.787015	-46.249
ethyl_Cyclohexene	110.1988	-4.7E-10	1.48E-06	-0.00191	1.424216	-137.275
Ethylbenzene	106.165	-6.7E-09	1.24E-05	-0.00763	2.14226	-102.295
p_Xylene	106.165	5.78E-10	-1.4E-06	0.000965	0.134839	32.71667
m_Xylene	106.165	3.85E-10	-9.2E-07	0.000549	0.280214	15.63889
methyl_Octane_3	128.2551	2.28E-10	-6.1E-07	0.000236	0.599866	24.28333
o_Xylene	106.165	3.69E-10	-9E-07	0.000564	0.245494	30.71111
Nonene_1	126.2392	1.63E-10	-3.2E-07	-7E-05	0.669968	14.62012
n_Nonane	128.2551	8.65E-10	-2.2E-06	0.001671	0.042211	102.2822
Nonene	126.2392	1.63E-10	-3.2E-07	-7E-05	0.669968	14.62012
C3_Alkylbenzenes	120.1916	3.64E-10	-9E-07	0.000559	0.295468	42.81929
Decene_1	140.2658	2.03E-10	-4.1E-07	-4.1E-05	0.734804	17.51536
trimethyl_Benzene_1_2_4	120.1916	4.36E-10	-1.1E-06	0.000672	0.288472	27.23333
C3_Alkylbenzenes_2	120.1916	3.64E-10	-9E-07	0.000559	0.295468	42.81929
Indane	118.1757	8.53E-10	-2E-06	0.001441	0.066525	30.45917
C4_Alkylbenzenes	134.2182	4.16E-10	-1E-06	0.000676	0.299254	58.79722
Butylbenzene	134.2182	-4.6E-09	1.04E-05	-0.00865	3.172918	-375.76
C4_Alkylbenzenes_2	134.2182	4.16E-10	-1E-06	0.000676	0.299254	58.79722
C4_Alkylbenzenes_3	134.2182	4.16E-10	-1E-06	0.000676	0.299254	58.79722
Undecene_1	154.2924	2.08E-10	-4.1E-07	-8.4E-05	0.825917	17.03616
C5_Alkylbenzenes	148.2447	3.72E-10	-9.2E-07	0.000561	0.388282	68.83333
Pentylbenzene	148.2447	1.73E-10	-2.9E-07	-0.00021	0.820473	-21.3449
C5_Alkylbenzenes_2	148.2447	1.73E-10	-2.9E-07	-0.00021	0.820473	-21.3449
Tetralin	132.2023	8.1E-10	-1.9E-06	0.001328	0.177267	25.505
Naphthalene	128.1705	7.6E-10	-1.8E-06	0.001144	0.177436	19.035
Dodecene_1	168.319	-5E-09	1.38E-05	-0.01385	6.423438	-739.472
methyl_Naphthalene_2	142.1971	7.92E-10	-1.9E-06	0.001245	0.186901	31.71667

Table C.5c. Specific heat curve fit coefficients (continued)

Species	MW	a	b	c	d	e
methyl_Naphthalene_1	142.1971	6.66E-10	-1.5E-06	0.000907	0.319103	18.80833
dimethyl_Naphthalenes	156.2237	-1.9E-10	3.09E-07	-0.00037	0.677705	8.11
dimethyl_Naphthalene_1_3	156.2237	1.01E-10	-2.4E-07	-7.4E-05	0.632536	10.475
dimethyl_Naphthalenes_2	156.2237	-1.9E-10	3.09E-07	-0.00037	0.677705	8.11
Acenaphthylene	152.1919	6.89E-10	-1.6E-06	0.000876	0.356362	6.046
Acenaphthene	154.2078	3.46E-09	-7.5E-06	0.004912	-0.54239	66.5275
Fluorene	166.2185	9.28E-10	-2.1E-06	0.001329	0.295884	15.92667
Phenanthrene	178.2292	4.18E-10	-1.6E-06	0.001541	0.018615	54.19667
Anthracene	178.2292	8.7E-10	-2E-06	0.001169	0.382466	12.335
Fluoranthene	202.2506	9.06E-10	-2.1E-06	0.001162	0.46572	8.3825
Pyrene	202.2506	8.56E-10	-1.9E-06	0.001025	0.521706	1.125833
benz_a_Anthracene	228.2879	1.06E-09	-2.4E-06	0.001388	0.514454	12.69083
Chrysene	228.2879	-7.1E-10	3.9E-06	-0.00499	2.556263	-154.072
benzo_b_Fluoranthene	226.272	1.11E-09	-2.5E-06	0.001416	0.588209	8.986667
benzo_k_Fluoranthene	226.272	1.11E-09	-2.5E-06	0.001416	0.588209	8.986667
benzo_a_Pyrene	252.3093	1.03E-09	-2.3E-06	0.00122	0.659463	2.359167
indeno_1_2_3_cd_Pyrene	276.3307	1.27E-09	-2.9E-06	0.001731	0.553695	11.47667
dibenz_a_h_Anthracene	278.3466	1.25E-09	-2.8E-06	0.001613	0.644675	13.32167
benzo_g_h_i_Perylene	276.3307	1.07E-09	-2.4E-06	0.001215	0.744937	-4.97917
methyl_Octane_3_2	128.2551	2.28E-10	-6.1E-07	0.000236	0.599866	24.28333
n_Nonane_2	128.2551	8.65E-10	-2.2E-06	0.001671	0.042211	102.2822
dimethyl_Octane	142.2817	2.82E-10	-5.5E-07	-4.1E-05	0.860463	-7.73879
methyl_Nonane_2	142.2817	1.65E-09	-4.4E-06	0.003567	-0.48882	158.3745
n_Decane	142.2817	1.5E-09	-3.9E-06	0.003145	-0.39925	162.3656
butyl_Cyclohexane	140.2658	-2.1E-10	4.03E-07	-0.00033	0.27073	-10.9549
trans_Decalin	138.2499	3.43E-09	-7.6E-06	0.005154	-0.58784	69.30389
methyl_Decane_2	156.3083	9.91E-10	-2.3E-06	0.001523	0.328455	77.05667
methyl_Decane_3	156.3083	6.98E-10	-1.7E-06	0.00102	0.492284	56.61667
n_Undecane	156.3083	3.69E-09	-7.9E-06	0.005678	-0.9678	220.2349
n_Dodecane	170.3348	1.17E-09	-3E-06	0.00223	0.06547	132.1989
n_Tridecane	184.3614	1.28E-09	-3.2E-06	0.002419	0.072086	142.2961
methyl_Tridecane	198.388	8.94E-10	-2.2E-06	0.001362	0.583418	79.62778
n_Tetradecane	198.388	1.39E-09	-3.5E-06	0.002642	0.065219	154.0544
methyl_Tetradecane	212.4146	1.1E-09	-2.7E-06	0.001744	0.529488	95.9
n_Pentadecane	212.4146	1.52E-09	-3.8E-06	0.002845	0.07169	163.8378
n_Hexadecane	226.4412	1.23E-09	-3.1E-06	0.002192	0.365703	143.7544
n_Heptadecane	240.4677	1.68E-09	-4.2E-06	0.00315	0.10723	181.7822

Bibliography

Bartok, W. and Sarofim, A. F. *Fossil Fuel Combustion: A Source Book*. New York. John Wiley & Sons, Inc., 1991.

Coleman, Hugh W. and Steele, W. Glenn. *Experimentation and Uncertainty Analysis for Engineers*. New York. JohnWiley & Sons, 1989.

Cooper, M and Shepherd, J.E. "Experiments Studying Thermal Cracking, Catalytic Cracking, and Pre-Mixed Partial Oxidation of JP-10," *39th AIAA/ASME/SAE/ASEE Joint Propulsion Conference and Exhibit*. Hunstville, AL. AIAA 2003-4687, 20-23 July 2003.

DeWitt, Matthew J. "Overview of Pyrolysis." PowerPoint Presentation. University of Dayton Research Institute, Dayton, OH, 16 July 2007.

Edwards, Tim. "Liquid Fuels and Propellants for Aerospace Propulsion: 1903-2003," *Journal of Propulsion and Power*, Vol. 19, No. 6: 1089-1107 (Nov-Dec 2003).

Edwards, Tim, DeWitt, Matthew J., Shafer, Linda M., Brooks, David, Huang, He, Bagley, Sean P., Ona, Jorge O., Wornat, Mary J. "Fuel Composition Influence on Deposition in Endothermic Fuels," *14th AIAA/AHI Space Planes and Hypersonic Systems and Technologies Conference.* Canberra, Australia. AIAA 2006-7973, 6-9 November 2006.

Fickett, W. and Davis, W. C. *Detonation: Theory and Experiment*. New York. Dover Publications Inc., 1979.

Ford, Thomas J. "Liquid-Phase Thermal Decomposition of Hexadecane: Reaction Mechanisms," *Journal of Industrial & Engineering Chemistry Fundamentals*, Vol. 25, No. 2. 240-243 (May 1986)

Galligan, Carrie. *Catalytic Cracking of Jet Propellant-10 for Pulse Detonation Engine Applications*, MS thesis, Université Laval, Quebec City, Quebec. March 2005.

Helfrich, Tim M. *Cycle performance of a Pulse Detonation Engine with Supercritical Fuel Injection*, MS thesis, AFIT/GAE/ENY/06-M14. Graduate School of Engineering and Management, Air Force Institute of Technology, Wright-Patterson AFB, OH. March 2006.

Helfrich, Tim M., King, Paul I., Hoke, John L., Schauer, Frederick. "Effect of Supercritical Fuel Injection on Cycle Performance of Pulsed Detonation Engines" *Journal of Propulsion and Power*, Vol. 23, No.4: 0748-4658 (July-August 2007)

Huang, He, Spadaccini, Louis J., Sobel, David R. "Fuel-Cooled Thermal Management for Advanced Aeroengines," *Journal of Engineering for Gas Turbines and Power*, Vol. 126. 284-293 (Apr 2004).

Huang, He, Sobel, David R.., and Spadaccini, Louis J. "Endothermic Heat-Sink of Hydrocarbon Fuels for Scramjet Cooling," *38th AIAA/AMSE/SAE/ASEE Joint Propulsion Conference and Exhibit*. Indianapolis, IN. AIAA 2002-3871, 7-10 July 2002.

Kaneshige, M. and Shepherd, J. E. *Detonation Database*. Technical Report FM97-8, GALCIT, July 1997.

Knystautas, R., Guirao, C., Lee, J. H., and Sulmistras, A. "Measurement of Cell Size in Hydrocarbon-Air Mixtures and Predictions of Critical Tube Diameter, Critical Initiation Energy, and Detonability Limits." *Progress in Aeronautics and Astronautics, AIAA*, Vol. 94. 23-37 (1984).

Kossiakoff, A. and Rice, F.O. Journal of American Chemical Society, Vol. 65. 590-595 (1943).

Kuo, Kenneth K. *Principles of Combustion*, 2nd ed. Hoboken. John Wiley and Sons Inc., 2005.

Littlewood, A. *Gas Chromatography*, 2nd ed. New York, Academic Press, 1970.

Miser, Christen L. *Pulse Detonation Engine Thrust Tube Heat Exchanger for Flash Vaporization and Supercritical Heating of JP-8*, MS thesis, AFIT/GAE/ENY/05-M11. Graduate School of Engineering and Management, Air Force Institute of Technology, Wright-Patterson AFB, OH. March 2005.

Nagley, E *Fuel Composition Analysis of Endothermically Heated JP-8 Fuel for Use in a Pulse Detonation Engine.* MS thesis. AFIT/GAE/ENY/08-J08, Graduate School of Engineering and Management, Air Force Institute of Technology, Wright-Patterson AFB, OH, June 2008

Panzenhagen, Kristin L. *Detonation Branching in a PDE with Liquid Hydrocarbon Fuel*. MS thesis, AFIT/GAE/ENY/04-M14. Graduate School of Engineering and Management, Air Force Institute of Technology, Wright-Patterson AFB,OH. March 2004.

Rice, F.O. *Journal of the American Chemical Society*, Vol. 55. 3035-3040 (1933).

Schauer, Frederick R., Stutrud, Jeffery, and Bradley, Royce P. "Detonation Initiation Studies and Performance Results for Pulse Detonation Engine Applications," *39th AIAA Aerospace Sciences Meeting and Exhibit.* Reno, NV: AIAA 2001-129, 8-11 January 2001.

Schauer, Frederick R., Miser, Christen. L., Tucker, K. Colin., Bradley, Royce. P., and Hoke, John. L. "Detonation Initiation Hydrocarbon-Air Mixtures in a Pulsed Detonation Engine," *43rd AIAA Aerospace Sciences Meeting and Exhibit*. Reno, NV. AIAA 2005-1343, 10-13 January 2005.

Shchelkin, K. L. *Soviet Journal of Technical Physics*, Vol. 10. 823-827 (1940).

Slack, J. David. *Branch Detonation of a Pulse Detonation Engine with Flash Vaporized JP-8*, MS thesis, AFIT/GAE/ENY/07-D04. Graduate School of Engineering and Management, Air Force Institute of Technology, Wright-Patterson AFB, OH. Dec 2006.

Turns, Stephen R. *An Introduction to Combustion: Concepts and Applications*, 2nd ed. Boston. McGraw Hill, 2000.

Vita

Christopher Stevens was born in Springfield, Ohio. He graduated from Kenton Ridge High School in June of 2002. He attended Rose-Hulman Institute of Technology in Terre Haute, IN where he graduated with a Bachelor of Science in Mechanical Engineering in May 0f 2006. In September 2007 he enter the Air Force Institute of Technology Graduate School of Engineering and Management to pursue a Masters of Science in Aeronautical Engineering. His emphasis was in air breathing propulsion and finite element analysis. After graduating in March 2009, he will remain at the Air Force Institute of Technology to pursue a Doctorate of Philosophy in Aeronautical Engineering

REPORT DOCUMENTATION PAGE

Form Approved
OMB No. 0704–0188

The public reporting burden for this collection of information is estimated to average 1 hour per response, including the time for reviewing instructions, searching existing data sources, gathering and maintaining the data needed, and completing and reviewing the collection of information. Send comments regarding this burden estimate or any other aspect of this collection of information, including suggestions for reducing this burden to Department of Defense, Washington Headquarters Services, Directorate for Information Operations and Reports (0704–0188), 1215 Jefferson Davis Highway, Suite 1204, Arlington, VA 22202–4302. Respondents should be aware that notwithstanding any other provision of law, no person shall be subject to any penalty for failing to comply with a collection of information if it does not display a currently valid OMB control number. PLEASE DO NOT RETURN YOUR FORM TO THE ABOVE ADDRESS.

1. REPORT DATE (DD–MM–YYYY)	2. REPORT TYPE	3. DATES COVERED *(From — To)*
26-03-2009	Master's Thesis	Jun 2008 – Mar 2009

4. TITLE AND SUBTITLE
Fuel Composition and Performance Analysis of Endothermically Heated Fuels for Pulse Detonation Engines

5a. CONTRACT NUMBER

5b. GRANT NUMBER

5c. PROGRAM ELEMENT NUMBER

6. AUTHOR(S)
Christopher A Stevens, CTR

5d. PROJECT NUMBER

5e. TASK NUMBER

5f. WORK UNIT NUMBER

7. PERFORMING ORGANIZATION NAME(S) AND ADDRESS(ES)
Air Force Institute of Technology
Graduate School of Engineering and Management (AFIT/ENY)
2950 Hobson Way
WPAFB OH 45433-7765

8. PERFORMING ORGANIZATION REPORT NUMBER
AFIT/GAE/ENY/09-M21

9. SPONSORING / MONITORING AGENCY NAME(S) AND ADDRESS(ES)
Air Force Research Labs, Propulsion Directorate, Turbine Engine Division, Combustion Branch

Dr. Frederick Schauer Civ.
1950 5th Street
WPAFB, OH 45433

10. SPONSOR/MONITOR'S ACRONYM(S)
AFRL/RZTC

11. SPONSOR/MONITOR'S REPORT NUMBER(S)

12. DISTRIBUTION / AVAILABILITY STATEMENT
APPROVED FOR PUBLIC RELEASE; DISTRIBUTION UNLIMITED

13. SUPPLEMENTARY NOTES

14. ABSTRACT

Waste heat from a pulse detonation engine (PDE) was extracted via concentric, counter flow heat exchangers to produce supercritical pyrolytic conditions for JP-7 and JP-8 fuels. A sampling system and method was utilized to collect samples of reacted fuel to be extracted during steady state operation. Samples were collected over a range of heat exchanger exit temperatures from 820 K (1016 °F) to 940 K (1232 °F) and for two sets of heat exchangers, one set coated with zeolite catalyst and one set left uncoated. Variation in fuel mass flow rate required the calculation of heat addition as an alternate to heat exchanger exit temperature as the independent variable when comparing fuel decomposition and engine performance. Offline chemical analysis of liquid and vapor portions of each sample indicated fuel decomposition via pyrolytic pathways. The analyses showed the formation of hydrogen, unsaturated hydrocarbons (aromatics and alkenes), and smaller alkanes in both fuels. The high thermal stability and low aromatic content of neat JP-7 resulted in the formation of more gaseous products and fewer poly-aromatic compounds than was produced by JP-8. The additional concentrations of lighter hydrocarbons reduced the ignition times by an average of 15.6%, and the reduced poly-aromatic concentrations decreased the bulk carbon deposits formed during pyrolysis by 92.5% on average.

15. SUBJECT TERMS
Pulse Detonation Engine, Fuel Chemistry, Endothermic Reactions

16. SECURITY CLASSIFICATION OF:			17. LIMITATION OF ABSTRACT	18. NUMBER OF PAGES	19a. NAME OF RESPONSIBLE PERSON
a. REPORT	b. ABSTRACT	c. THIS PAGE			Full name and title of Research Advisor
U	U	U	UU	130	19b. TELEPHONE NUMBER (Include Area Code) 255-3636 x4628 Paul.King@afit.edu